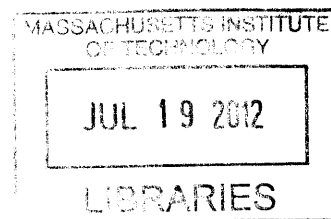


# ANTI-INFLAMMATORY DRUGS FOR MODULATION OF HOST RESPONSE TO BIOMATERIALS AND APPLICATION IN DIABETES THERAPY

ARCHIVES

By  
**THUY TRAM DANG**

B.Sc. Chemical Engineering, 2006  
University of Illinois, Urbana-Champaign




Submitted to the Department of Chemical Engineering in  
Partial Fulfillment of the Requirements for the Degree of  
**Doctor of Philosophy**  
At the  
**Massachusetts Institute of Technology**  
September 2012

© 2012 Massachusetts Institute of Technology. All rights reserved.


Signature of Author:

.....

  
Thuy Tram Dang  
Department of Chemical Engineering  
July 10<sup>th</sup>, 2012

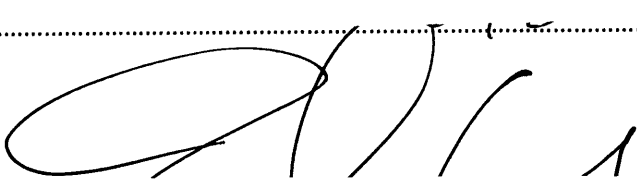
\_\_\_\_ Certified by:

.....

  
Robert S. Langer, Sc.D.  
Institute Professor  
Thesis Supervisor


\_\_\_\_ Certified by:

.....

  
Daniel G. Anderson, Ph.D.  
Professor of Chemical Engineering  
& Division of Health Sciences and Technology  
Thesis Supervisor

\_\_\_\_ Accepted by:

.....

  
Patrick Doyle, Ph.D.  
Professor of Chemical Engineering  
Chairman, Committee for Graduate Students

# Anti-inflammatory drugs for modulation of host response to biomaterials and application in diabetes therapy

By

**THUY TRAM DANG**

Submitted to the Department of Chemical Engineering on July 11, 2012 in partial fulfillment of the requirements for the degree of Doctor of Philosophy in Chemical Engineering

## ABSTRACT

Host response to implanted biomaterials and medical devices poses tremendous challenges to their clinical applications. Today, the quest to mitigate this immunological attack for improved longevity of these devices remains daunting. This thesis aims to explore the use of anti-inflammatory drugs in minimizing the host response and improve the efficacy of implantable and transplantable therapeutics.

Firstly, we developed a new non-invasive *in vivo* imaging technique to study the activity of early immune cells in the host response to implanted biomaterials. A fluorescent imaging probe (Prosense680<sup>®</sup>, Perkin Elmer) activatable by cathepsins, a class of inflammatory proteases secreted from immune cells, was used for simultaneous biocompatibility screening of up to 8 different materials per animal in immunocompetent hairless SKH1E mice. In this assay, the different biocompatibility properties of polystyrene beads, alginate and saline were correlated with varying levels of cathepsin activities as acquired by imaging. Comparison of the imaging results with traditional histological analysis validated that this new fluorescent imaging technique can be used to assess material biocompatibility efficiently and rapidly.

We applied this new fluorescent imaging technique to investigate the *in vivo* spatial and temporal host response to a subcutaneously-injected, controlled-release anti-inflammatory drug formulation. Poly-lactic-co-glycolic (PLGA) microparticles with low loading (1.3wt%) of dexamethasone locally inhibited the activity of cathepsin enzymes from immune cells, while high drug loading formulation (26wt%) resulted in systemic immunosuppression. We also showed that incorporation of dexamethasone at a low loading (1.3wt%) attenuated the coverage of polymeric microparticles by immune cell layers. Temporal monitoring of the drug effect confirmed that incorporation of dexamethasone decreased early enzymatic activity and long-term cellular infiltration to implanted materials.

Next, we performed *in vivo* subcutaneous screening of 16 small molecule anti-inflammatory drugs (NSAIDs, polyphenols, glucocorticoids and other non-steroidal immunosuppressants) encapsulated in PLGA microparticles in immunocompetent hairless SKH-1E mice. Using non-invasive fluorescent imaging coupled with parallel bioluminescent imaging, we identified dexamethasone and curcumin as the most effective drugs in inhibiting the activities of inflammatory proteases and reactive oxygen species respectively. Histological analysis also showed that dexamethasone and curcumin encapsulated in PLGA microparticles decreased subsequent cellular infiltration and fibrosis formation surrounding the subcutaneously injected PLGA microparticles for up to 4 weeks and 2 weeks respectively.

Lastly, we designed hybrid alginate hydrogel microcapsules co-encapsulating pancreatic rat islets and dexamethasone or curcumin. Uniform spherical microcapsules containing homogeneously distributed dexamethasone (2mg/ml) or curcumin (1mg/ml) were transplanted into streptozotocin-induced C57B6/J diabetic mice. Using a marginal islet mass of 250 islet equivalents, curcumin-loaded capsules effectively improved glycemic control by increasing the graft survival time to 30 days compared to 15 and 21 days by control and dexamethasone-containing capsules respectively. Curcumin also significantly reduced fibrotic overgrowth on the encapsulated islets explanted on day 60 as evidenced by DNA fluorescent staining of the fibrotic cell layers on the surface of the retrieved capsules.

Taken together, the results of this thesis demonstrate that anti-inflammatory drugs have the potential to minimize the attack by host immune system and improve the efficacy or functional longevity of cell-based therapeutics and possibly other implantable medical devices.

**Thesis Advisor : Robert S. Langer, Sc.D**

**Title : Institute Professor**

**Thesis Advisor : Daniel G. Anderson, Ph.D**

**Title: Associate Professor of Chemical Engineering**

This doctoral thesis was successfully defended in public on Tuesday, July 10<sup>th</sup> 2012 at 1:00PM at the Koch Institute in partial fulfillment of the degree of Doctor of Philosophy in Chemical Engineering at the Massachusetts Institute of Technology. This thesis has been examined by the following Thesis Committee:

Thesis Advisors

**Robert S. Langer, Sc.D.**  
Institute Professor  
Massachusetts Institute of Technology

**Daniel G. Anderson, Ph.D.**  
Associate Professor of Chemical Engineering  
Massachusetts Institute of Technology

Thesis Committee

**Gordon Weir, M.D.**  
Professor of Medicine  
Harvard Medical School

**Michael Strano, Ph.D.**  
Associate Professor of Chemical Engineering  
Massachusetts Institute of Technology

## **ACKNOWLEDGEMENTS**

I would like to take this opportunity to express my profound gratitude to my advisors, Professor Robert Langer and Professor Daniel Anderson. It is through their constant support and guidance that this work can finally be accomplished. Their research vision, high standards and great enthusiasm have been the source of motivation during my study.

I am grateful to Professor Gordon Weir and Professor Michael Strano who kindly served in my thesis committee and provided insightful suggestions and feedbacks.

I would also like to thank all my colleagues in Professor Langer and Professor Anderson's Groups. Though I cannot mention all of their names, I would like to thank all of them for their valuable help and intellectually stimulating scientific discussions. I thank Dr. Qiaobing Xu, Dr. Kaitlin Bratlie, Dr. Minglin Ma, Dr. Wendy Liu, Dr. Arturo Vegas, Dr. Todd Hoare, Dr. Zhen Gu, Dr. Hao Cheng, Dr. Yair Levy, Dr. Christopher Levins, Dr. Christian Kastrup, Dr. Daniel Siegwart, Dr. Weiwei Gao, Dr. Juliana Chan, Dr. Paulina Hill, Dr. Omar Fisher, Dr. Manos Karagiannis, Dr. Daniel Heller, Said Boratyrev and Yadira Soto.

I am indebted to my team of excellent students including my research technicians, Anh Thai and Jeremy Slosberg and my undergraduate research assistants (UROPS), Ivy Xiao Chen, Catherine Fan, Diviya Chhabra, and Evgeny Kiner. They have been one of the most wonderful highlights of my graduate study at MIT and fuelled my passion in mentoring students.

I am extremely grateful to my collaborators in Professor Gordon Weir's group at the Joslin Diabetes Centers, especially Dr. Esther O'Sullivan, Dr. Jennifer Hollister-Lock, Karolina Siniakowicz, Josh Cohen, Dr. Francisco Caballero-Gonzalez, Dr. Amedeo Vetere and Professor Dale Greiner's team at University of Massachusetts Medical School, especially Dr. Rita Bortell and Elaine Norowski, as well as Professor Stephan Lyle at University of Massachusetts.

The staff at various MIT's core facilities has also been instrumental in my successful completion of this doctoral thesis. My sincere appreciation goes to the dedicated staff at MIT Division of Comparative Medicine, the Koch Institute's Swanson Biotechnology Center, the Institute of Soldier Nanotechnology and the Keck Microscopy Facility at the Whitehead Institute.

I also gratefully acknowledge the Singapore A\*STAR National Science Graduate Fellowship (NSS-PhD), the MIT Edward Clark Walsh Presidential Fellowship and the Juvenile Diabetes Research Foundation for research funding.

Most importantly, I would like to show my deepest gratitude to my parents, Dang Ngoc Dong and Phan Thi Hong Anh, to my sister, Dang Thao Huong for their love and support throughout my life and especially to my husband, Nguyen Hong Tam, to whom I owe the most for his endless understanding, support and encouragement. I am also extremely grateful to receive the most beautiful gift of life, my newborn daughter - Nguyen Marie Minh Chau, during my last year of graduate study. Finally, I would like to dedicate my work to the lasting memory of my grandmother, Nguyen Thi Phung, who had always believed that I would achieve my dreams.

# TABLE OF CONTENTS

<b>ACKNOWLEDGEMENTS .....</b>	<b>4</b>
<b>TABLE OF CONTENTS .....</b>	<b>5</b>
<b>LIST OF TABLES .....</b>	<b>9</b>
<b>LIST OF FIGURES .....</b>	<b>10</b>
<b>INTRODUCTION.....</b>	<b>12</b>
<b>CHAPTER 1 – BACKGROUND.....</b>	<b>14</b>
<b>1.1. HOST RESPONSE TO BIOMATERIALS AND MEDICAL DEVICES .....</b>	<b>14</b>
1.1.1. Biological mechanisms underlying the host response.....	14
1.1.2. Existing techniques to characterize host response.....	14
<b>1.2. FAILURE OF IMPLANTABLE MEDICAL DEVICES DUE TO HOST RESPONSE .....</b>	<b>15</b>
1.2.1. Encapsulated islets in diabetes therapy.....	15
1.2.3. Other implantable biomedical devices .....	16
<b>1.3. ANTI-INFLAMMATORY DRUGS TO IMPROVE DURABILITY OF IMPLANTABLE DEVICES</b> <b>.....</b>	<b>17</b>
<b>CHAPTER 2 – NON-INVASIVE IMAGING OF EARLY HOST RESPONSE .....</b>	<b>19</b>
<b>2.1. ABSTRACT .....</b>	<b>19</b>
<b>2.2. INTRODUCTION.....</b>	<b>19</b>
<b>2.3. MATERIALS AND METHODS.....</b>	<b>20</b>
2.3.1. Molar Absorptivity.....	20
2.3.2. Ethics Statement.....	20
2.3.3. Animals. ....	21
2.3.4. Injections.....	21
2.3.5. Imaging. ....	21
2.3.6. Histology.....	22
2.3.7. Statistical Analysis. ....	22
<b>2.4. RESULTS .....</b>	<b>22</b>
2.4.1. Linearity of Fluorescence Response to Dose Concentration.....	22
2.4.2. <i>In Vivo</i> Imaging of Cathepsin Activity and Macrophages.....	23

2.4.3. Histology .....	24
2.5. DISCUSSION .....	25
2.6. CONCLUSION.....	26

**CHAPTER 3 – IMAGING SPATIO-TEMPORAL EFFECTS OF A CONTROLLED-RELEASE ANTI-INFLAMMATORY DRUG .....33**

3.1. ABSTRACT .....	33
3.2. INTRODUCTION.....	33
3.3. MATERIALS AND METHODS.....	35
3.3.1. Fabrication and characterization of PLGA microparticles .....	35
3.3.2. <i>In vitro</i> drug release kinetics.....	35
3.3.3. Animal care .....	36
3.3.4. Subcutaneous injection of polymeric microparticles .....	36
3.3.5. <i>In vivo</i> fluorescent imaging of whole animals .....	36
3.3.6. Tissue harvest and histology processing .....	37
3.3.7. Histology analysis by laser scanning cytometry .....	37
3.3.8. Statistical analysis.....	37
3.4. RESULTS AND DISCUSSION .....	38
3.4.1. Spatial effect of a controlled-release anti-inflammatory drug.....	38
3.4.1.1. <i>Effect of drug loading on controlled-release properties</i> .....	38
3.4.1.2. <i>Anti-inflammatory drug attenuated coverage of implanted polymer by immune cell layers</i> .....	39
3.4.2 Temporal effect of a controlled-release anti-inflammatory drug.....	40
3.4.2.1. <i>Time-evolution of cathepsin activity</i> .....	40
3.4.2.2. <i>Time-evolution of cellular infiltration</i> .....	41
3.5. CONCLUSION.....	42
3.6. SUPPLEMENTAL INFORMATION.....	47

**CHAPTER 4 – ANTI-INFLAMMATORY DRUGS FOR IMPROVED EFFICACY OF ENCAPSULATED ISLETS .....49**

4.1. ABSTRACT .....	49
4.2. INTRODUCTION.....	49
4.3. MATERIALS AND METHODS.....	51
4.3.1. Animal care and use .....	51

4.3.2. Fabrication and characterization of PLGA microparticles .....	52
4.3.3. Subcutaneous injection of PLGA microparticles.....	52
4.3.4. Non-invasive fluorescent and bioluminescent imaging of SKH-1E mice .....	53
4.3.5. Tissue retrieval and histology processing of subcutaneously injected PLGA microparticles .....	53
4.3.6. Isolation of rat pancreatic islets.....	53
4.3.7. Fabrication of hybrid alginate microcapsules co-encapsulating drug and islets.....	54
4.3.8. Transplantation of encapsulated islets into STZ-induced diabetic C57B6/J mice .....	55
4.3.9. Blood glucose monitoring and Intraperitoneal Glucose Tolerance Test .....	55
4.3.9.1. Daily blood glucose monitoring :.....	55
4.3.9.2. Intraperitoneal glucose tolerance test (IPGTT):.....	55
4.3.10. Retrieval of transplanted capsules from the intraperitoneal cavity.....	55
4.3.11. Quantification of fibrosis by DNA fluorescent staining.....	56
4.3.12. Statistical analysis.....	56
<b>4.4. RESULTS .....</b>	<b>56</b>
4.4.1. <i>In vivo</i> subcutaneous screening of small molecule anti-inflammatory drugs .....	56
4.4.2. Effect of selected drugs on the subcutaneous cellular dynamics and fibrosis formation .....	57
4.4.3. Improved glycemic control by alginate microcapsules co-encapsulating drug and islets in diabetic mice .....	59
4.4.4. Reduced fibrotic overgrowth on explanted hybrid drug-islet capsules.....	61
<b>4.5. DISCUSSION .....</b>	<b>62</b>
<b>4.6. CONCLUSION.....</b>	<b>65</b>
<b>4.7. SUPPLEMENTARY INFORMATION .....</b>	<b>72</b>
4.7.1. Supplementary results.....	72
4.7.1.1. Subcutaneous screening of different formulations of anti-inflammatory drugs .....	72
4.7.1.2. Temporal evolution of inflammation markers in the host response.....	73
4.7.1.3. Analysis of excised PLGA microparticles to determine the presence of residual drugs .....	74
4.7.1.4. Determination of marginal islet mass for transplantation in diabetic mice .....	75
4.7.1.5. Establishing DNA fluorescent staining as a quantitative method for fibrosis assessment .....	76
4.7.1.6. Residual drugs from hybrid islet-drug capsules explanted after two months .....	77
4.7.2. Supplementary materials and methods.....	78
4.7.2.1. Detection of residual drug in ex-vivo tissue by HPLC analysis .....	78

<b>CHAPTER 5 – MICROFABRICATION OF CELL-LADEN, ASYMMETRIC HYDROGEL MICROCAPSULES .....</b>	<b>79</b>
<b>5.1. ABSTRACT .....</b>	<b>79</b>

<b>5.2. INTRODUCTION .....</b>	<b>79</b>
<b>5.3. MATERIALS AND METHODS.....</b>	<b>80</b>
5.3.1. Fabrication of alginate hydrogel capsules .....	80
5.3.2. Asymmetric surface modification of hydrogel capsules.....	81
5.3.3. Cell culture .....	81
5.3.4. Viability analysis of encapsulated cells .....	81
5.3.5. Static glucose-stimulated insulin secretion .....	82
<b>5.4. RESULTS AND DISCUSSION .....</b>	<b>82</b>
5.4.1. Properties of template meshes for successful capsule fabrication .....	82
5.4.2. Fabrication of hydrogel capsules with different shapes and asymmetrically modified surfaces	83
5.4.3. Fabrication of hydrogel capsules containing insulin-secreting cells .....	84
5.4.4. Assessment of viability, proliferation and function of encapsulated cells .....	84
5.4.3.1. Fabrication of hydrogel capsules containing insulin-secreting cells .....	84
5.4.3.2. Static glucose-stimulated insulin secretion .....	85
<b>5.5. CONCLUSION.....</b>	<b>85</b>
<b>CHAPTER 6 – CONCLUSION AND RECOMMENDATION FOR FUTURE WORK .....</b>	<b>93</b>
6.1. CONCLUSION.....	93
6.2. RECOMMENDATION FOR FUTURE WORK.....	93
<b>REFERENCES .....</b>	<b>95</b>
<b>APPENDIX A – ABBREVIATIONS .....</b>	<b>105</b>
<b>APPENDIX B – CURICULLUM VITAE .....</b>	<b>106</b>



## **LIST OF TABLES**

<b>Table 4.1: Small molecule anti-inflammatory drugs investigated in the <i>in vivo</i> subcutaneous screening .....</b>	<b>66</b>
<b>Table 5.1: Relationship between the feasibility of microcapsule formation and the properties of a variety of thermoplastic meshes.....</b>	<b>87</b>

## **LIST OF FIGURES**

Figure 1.1: Temporal variation of tissue response to implanted biodegradable microspheres . .....	14
Figure 1.2: Immuno-isolation of islets and fibrosis response after transplantation. ....	16
Figure 1.3: Schematic illustration of an amperometric glucose sensor and potential sources of declining sensor signals . ....	17
Figure 2.1: Subcutaneous Injection arrays.....	28
Figure 2.2: Time evolution of cathepsin activity in response to injected materials fluorescently imaged.....	29
Figure 2.3: Time evolution of macrophage response to injected materials fluorescently imaged.....	30
Figure 2.4: Histological scores of materials subcutaneously injected. ....	31
Figure 2.5: H&E staining of representative sections subcutaneously injected materials. ....	32
Figure 3.1: Effect of drug loading on the localization of anti-inflammatory properties. ....	43
Figure 3.2: Anti-inflammatory drug attenuated coverage of implanted polymer by immune cell layers.....	44
Figure 3.3: Quantitative temporal monitoring of cathepsin activity.....	45
Figure 3.4: Quantitative monitoring of cellular infiltration to the inter-particle spaces. ....	46
Figure 3.5: <i>In vitro</i> and <i>in vivo</i> fluorescent images of PLGA microparticles with different glycolide monomer contents. ....	47
Figure 3.6: Incorporation of dexamethasone did not alter the physical properties of the microparticles. ....	48
Figure 4.1: <i>In vivo</i> subcutaneous screening of anti-inflammatory drugs encapsulated in PLGA microparticles. ....	67
Figure 4.2: Effects of selected drugs on the peak activities of cathepsin enzymes and ROS in the subcutaneous host response to PLGA microparticles. ....	68
Figure 4.3: Histology analysis of subcutaneously injected PLGA microparticles with and without drugs excised from SKH-1E mice at different time points over a period of 28 days. ..	69

<b>Figure 4.4: Effects of hybrid drug-islet capsules on glycemic control of STZ-induced diabetic mice transplanted with a marginal islet mass of 250 IE. ....</b>	<b>70</b>
<b>Figure 4.5: Characterization of fibrotic pericapsular overgrowth on microcapsules retrieved 60 days after transplantation into STZ-induced C57B6J diabetic mice. ....</b>	<b>71</b>
<b>Figure 4.6: <i>In vivo</i> subcutaneous screening of anti-inflammatory drugs encapsulated in PLGA microparticles. ....</b>	<b>72</b>
<b>Figure 4.7: Temporal evolution of cathepsin enzymes and ROS in the host response to PLGA microparticles with and without drugs. ....</b>	<b>73</b>
<b>Figure 4.8: <i>Ex-vivo</i> analysis of PLGA microparticles excised from SKH1E mice at day 28. ....</b>	<b>74</b>
<b>Figure 4.9: Blood glucose concentrations in STZ-induced diabetic C57B6/J mice depended on the transplanted mass of encapsulated Sprague–Dawley rat islets.....</b>	<b>75</b>
<b>Figure 4.10: DNA fluorescent staining correlated with fibrosis scoring by observation.....</b>	<b>76</b>
<b>Figure 4.11: Comparison of alginate capsules containing islets before transplantation and after retrieval from C57B6/J diabetic mice on day 60.....</b>	<b>77</b>
<b>Figure 5.1: Schematic illustration of the procedure to fabricate alginate microcapsules .....</b>	<b>88</b>
<b>Figure 5.2: Images of polypropylene meshes used for microcapsule fabrication. ....</b>	<b>89</b>
<b>Figure 5.3: Microcapsules with different geometries and asymmetric modification.....</b>	<b>90</b>
<b>Figure 5.4: Light and fluorescent microscopy images of alginate microcapsules containing INS-1 cells.....</b>	<b>91</b>
<b>Figure 5.5: Viability and homogeneous distribution of cell clusters in a single microcapsule..</b>	<b>92</b>
<b>Figure 5.6: Insulin secretion of encapsulated INS-1 cells over a period of ten days. ....</b>	<b>92</b>

## INTRODUCTION

The fields of material biocompatibility and drug-device combination have progressed rapidly in the past decades. However, with the exception of the steroid-eluting pacemaker leads and the drug-eluting stents, no other clinical success has been achieved for medical devices utilizing controlled drug release technology to improve device biocompatibility. This thesis research aims to address several challenges that remain the bottlenecks for achieving further understanding and improved performance of medical devices.

The commentary in **Chapter 1** discusses the background on the host response to implanted biomaterials and medical devices. This chapter outlines the biological mechanisms underlying the host response to implanted foreign objects, existing techniques to characterize this phenomenon and examples of medical device failures due to this host reaction. Existing studies on the incorporation of controlled-release anti-inflammatory drugs as a strategy to improve device performance and durability were also reviewed.

**Chapter 2** reports the development of a new non-invasive imaging technique to study the activity of early immune cells in the early host response to implanted biomaterials. Fluorescent imaging probes activatable by inflammatory proteases secreted from immune cells were used for simultaneous biocompatibility screening of multiple materials in an immune-competent mouse model. Comparison of the imaging results with traditional histological analysis validated that the new fluorescent imaging technique can be used to assess material biocompatibility efficiently and rapidly.

The new fluorescent imaging technique in Chapter 2 was applied to study the spatio-temporal effects of a controlled release anti-inflammatory drug as outlined in **Chapter 3**. Subcutaneously injected poly (lactic-co-glycolic) (PLGA) microparticles with and without dexamethasone were investigated in hairless immunocompetent SKH-1E mice. The influence of drug loading and release kinetics on the local and systemic inhibition of inflammatory cellular activities was investigated by fluorescent imaging and parallel semi-quantitative histology analysis. Temporal monitoring of host response showed that the inhibition of inflammatory proteases in the early phase correlated with decreased cellular infiltration in the later phase of this reaction.

Built on the understanding of drug release kinetics and the dynamics of cellular activity in the early host response from chapter 3, *in vivo* subcutaneous screening of several classes of small molecule anti-inflammatory drugs encapsulated in PLGA microparticles were performed as described in the first part of **chapter 4**. Acquired by parallel non-invasive fluorescent and bioluminescent imaging during the acute inflammation phase, the results from this chapter demonstrated that dexamethasone most

effectively inhibited the activities of inflammatory proteases while curcumin, a polyphenol drug, significantly decreased the presence of reactive oxygen species secreted by early immune cells. These drugs also decreased subsequent cellular infiltration and fibrosis formation surrounding subcutaneously injected polymeric microparticles.

The second part of **chapter 4** focuses on applying the favorable finding from the subcutaneous drug screening in a medically relevant context with a focus on improving the treatment of type I diabetes by immuno-isolated islets. Hybrid alginate hydrogel microcapsules co-encapsulating pancreatic rat islets and selected drugs were developed and optimized to achieve good capsule morphology and drug loading. Curcumin effectively reduced the fibrotic response against encapsulated islets and improved their efficacy with better glycemic control in a mouse model of chemically-induced type I diabetes.

In a different effort to improve the design and production of islet-encapsulating microcapsules, **Chapter 5** introduces a new fabrication method that allows for rapid, homogenous microencapsulation of insulin-secreting cells with varying microscale geometries and asymmetrically modified surfaces. Micromolding systems were developed using polypropylene mesh, and the material/surface properties associated with efficient encapsulation were identified. Cells encapsulated using these methods maintain desirable viability and preserve their ability to proliferate and secrete insulin in a glucose-responsive manner. This new cell encapsulation approach enables a practical route to an inexpensive and convenient process for the generation of cell-laden microcapsules without requiring any specialized equipment or microfabrication process.

Lastly, the commentary in **Chapter 6** summarizes the collective finding from this thesis research and recommends directions for future research.

# CHAPTER 1 – BACKGROUND

## 1.1. HOST RESPONSE TO BIOMATERIALS AND MEDICAL DEVICES

### 1.1.1. Biological mechanisms underlying the host response

During the implantation of a biomaterial or biomedical device, tissue injury activates the inflammation cascade which leads to migration of inflammatory cells to the wound site, release of cytokines and growth factors that promote cell proliferation and protein synthesis as well as activation of complements, blood clotting and fibrinolytic cascades [1]. Typical events following the implantation of a material or device are depicted in Figure 1.1 below [2, 3]. The acute and chronic inflammatory responses are of short duration occurring over the first several weeks post-implantation[2]. Eosinophils and polymorphonuclear cells are typically present during the acute phase while macrophages and fibroblasts are observed during the chronic phase [4]. If not controlled, this sequence of inflammatory events can trigger the proliferation of fibroblasts which synthesize and deposit extracellular matrix to form granulation tissues and subsequently fibrous scars surrounding the implanted subject[5]. The duration of granulation tissue development, foreign body reaction, and fibrosis formation varies depending upon the characteristics of the implanted materials [2]

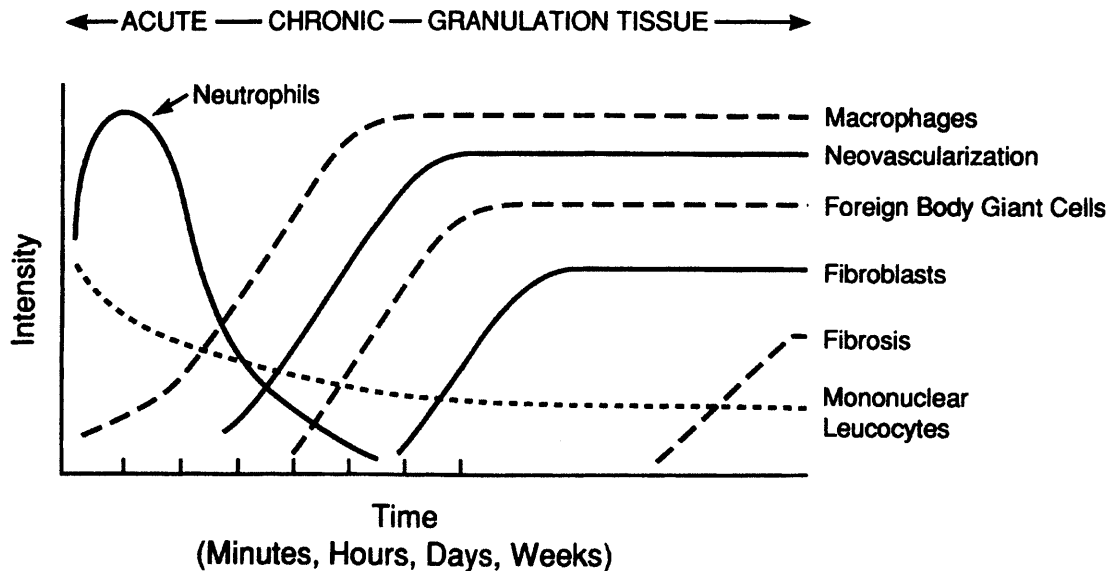


**Figure 1.1: Temporal variation of tissue response to implanted biodegradable microspheres [2].** Patterns of cellular recruitment change dynamically during the acute inflammatory response, chronic inflammatory response, granulation tissue development, and foreign body reaction [2].

### 1.1.2. Existing techniques to characterize host response

Traditionally, host response to biomaterial is characterized via histology analysis of excised samples *ex vivo*. This approach has primarily relied on visual evaluation by trained pathologists[6]. Computer-aided image analysis systems and immunohistochemical staining techniques have also been introduced to gain semi-quantitative information and improve data consistency and accuracy [7-9]. These histological approaches provide an informative end-point assessment with useful static information on cell types, quantity and distribution. However, the quality of data acquisition and interpretation remained variable [10].

Host response is a dynamic process involving the constant migration and recruitment of different population of immune cells whose secretion of active biomolecules such as cytokines and enzymes play an important role in determining the immunological response to an implanted object [2, 3]. For example, when evaluating a polymer system encapsulating a therapeutic drug, *in vivo* cellular secretory products such as inflammatory enzymes or cell signaling molecules might affect the degradation rate of the polymeric matrix [11-13] used to encapsulate drugs, and are partly responsible for the discrepancy between *in vitro* and *in vivo* release kinetics [14].

There remains a substantial need for new methods to provide more information in the characterization of biocompatibility phenomena, especially quantitative approaches that acquire kinetic information on the dynamic activities of the immune cell populations participating in the host response.

## **1.2. FAILURE OF IMPLANTABLE MEDICAL DEVICES DUE TO HOST RESPONSE**

### **1.2.1. Encapsulated islets in diabetes therapy**

Implantable biomedical devices often suffer from loss of function *in vivo* due to changes caused in the tissue surrounding the devices caused by surgical injuries during implantation [15]. For example, immuno-isolated islets suffer transplanted capsules. Encapsulated islets as shown schematically in Figure 1.2A have been investigated as a technology which allows transplantation of non-autologous insulin-secreting cells into diabetic patients in the absence of long-term systemic administration of immunosuppressants [16-19]. The semi-permeable alginate hydrogel membrane surrounding the islets allows the diffusion of nutrients, oxygen and glucose while excluding antibodies and immune cells[20].

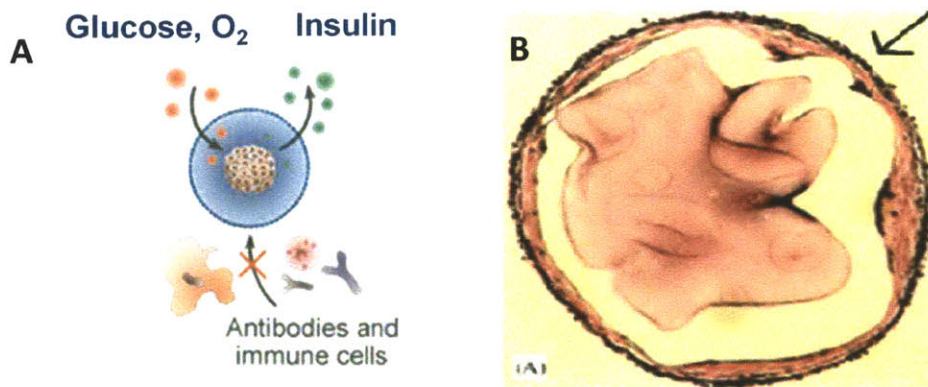


**Figure 1.2: Immuno-isolation of islets and fibrosis response after transplantation.**

**(A)** Schematic illustration of microencapsulated islets in alginate hydrogel membrane[20]. **(B)** Deposition of fibroblastic overgrowth on an alginate microcapsules retrieved from rat[21].

However, current development of islet encapsulation is still facing the problem of graft rejection and the lack of long-term survival of the islet grafts[22]. The capsules suffer from attachment by the components of the immune system such as antibodies and inflammatory cells which may induce capsular overgrowth as shown in Figure 1.2B , especially in the case of xenografts [23, 24]. This cellular layer can block the transport of nutrients and oxygen resulting in islet starvation. In addition, it was also suggested that non-specific inflammation caused by surgical trauma can lead to further recruitment of immune cells which secrete soluble cytokines[25]. These cytokines might be able to penetrate the alginate layers causing early mass loss and impaired function of the transplanted beta cells[26].

### 1.2.3. Other implantable biomedical devices

Glucose biosensors are also typical examples of biomedical devices whose functions are adversely affected by such tissue responses. Figure 1.3 illustrates a subcutaneously implanted amperometric glucose sensor with several potential sources of declining sensor signals [15]. Glucose diffuses through the sensor's outer membrane and is enzymatically converted to species that are detected by the electrode. Sensors fail due to host tissue response includes membrane biofouling, fibrous encapsulation and membrane biodegradation as well as electrode passivation due to protein adsorption and cell attachment [15].



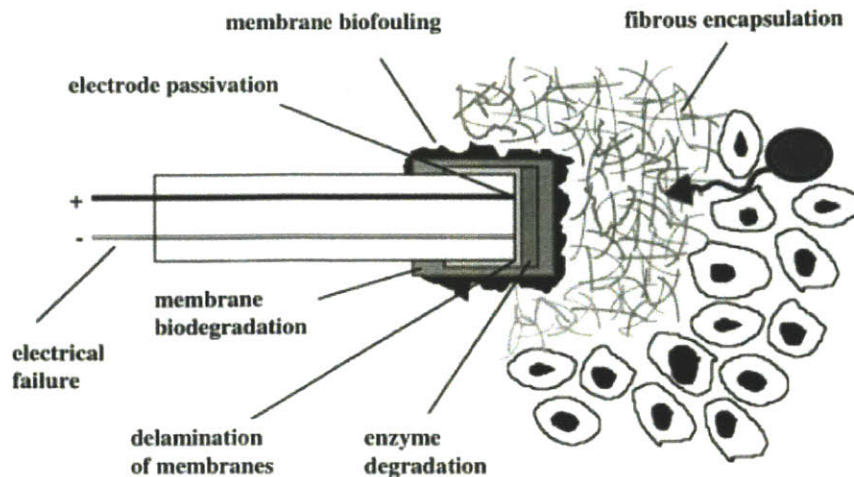


Figure 1.3: Schematic illustration of an amperometric glucose sensor and potential sources of declining sensor signals [15].

Causes of device failure includes membrane biofouling, fibrous encapsulation and membrane biodegradation as well as electrode passivation due to protein adsorption and cell attachment [15].

### 1.3. ANTI-INFLAMMATORY DRUGS TO IMPROVE DURABILITY OF IMPLANTABLE DEVICES

Administration of inhibitory therapeutics such as anti-inflammatory drugs can help to improve device performance by mitigating early tissue response and subsequent fibrosis [27]. Drug-incorporated medical devices represent an emerging trend to localized delivery of therapeutics specifically to the site of implantation [27]. This strategy promises to avoid the side effects of systemic administration, minimize the effective dosage and ensure continuous drug release over a prolonged period of time [27]. However, development of devices incorporating anti-inflammatory therapeutics has mostly focused on one or two model drugs with success in some devices but failure in others [28, 29]. The lack of an efficient and systematic approach to characterize and compare drug efficacy *in vivo* hinders progress in selecting optimal drug dosages and formulations for applications to specific devices.

Host response as discussed above significantly impairs the functions of devices that require specific electrochemical or biochemical communication with the host microenvironment. Potent steroidal anti-inflammatory drugs have been incorporated in medical devices to inhibit acute inflammation and attenuate recruitment of fibroblasts and collagen production [28, 30, 31]. The success of this strategy has been reported for cardiac pacing electrode tips in pacemakers by Medtronic in the late 1980s. The implantation of a pacemaker lead on to the surface of the heart produces a local inflammatory response

at the electrode-tissue interface[28]. This response can be attenuated by local delivery of glucocorticosteroids from the steroid-eluting tip of the electrode. Clinical studies comparing identical electrode configurations with and without local release of dexamethasone showed the superior performance of steroid-eluting pacemaker leads [32]. These steroid-eluting pacemaker leads are now widely used for patients with slow heart rates, abnormal rhythms or heart failure.

Recently, several groups have attempted to adapt this approach to improve the performance of glucose sensors. A composite of dexamethasone-loaded PLGA microparticles with poly-vinyl alcohol hydrogel has been reported to demonstrate some ability to modulate acute and chronic inflammation *in vivo* and was proposed to be used as a coating for implantable biosensors[33]. However, most of the recent research on combining anti-inflammatory drugs and medical devices has focused on a limited number of model drugs. Dexamethasone has been most widely used in attempts to improve biosensor performance, possibly due to its high potency and historical success with pacemaker leads. However, no significant improvement in sensor performance has been demonstrated. Ward *et al* reported that the lifetime of amperometric glucose sensor subcutaneously implanted in dogs for several weeks was not improved by localized delivery of dexamethasone[29]. Given the difference in the modes of communication (electric vs electrochemical) and the sites of implantation (heart muscle vs subcutaneous or intradermal) of the pacemaker lead and the glucose sensor, it is possible that an even stronger inhibitory agent or a combination of several drugs is needed to minimize tissue response and ensure acceptable communication between the sensor and the host environment. On the other hand, dexamethasone and other potent synthetic steroids are known to have diabetogenic effect and inhibit insulin secretion in islets[34]. Even though these potent glucocorticoids might be effective in mitigating the host response, they might not be the most efficacious for incorporation into cell-based therapeutics as they might adversely affect cell viability and function [35, 36]. Other classes of anti-inflammatory drugs such as Non-steroidal Anti-inflammatory Drugs (NSAIDs), polyphenols or non-steroidal immunosuppressants might be useful in inhibiting fibrosis while supporting cellular functionality and survival.

## **CHAPTER 2 – NON-INVASIVE IMAGING OF EARLY HOST RESPONSE**

The work reported in this chapter was conducted in collaboration primarily with Dr Kaitlin M. Bratlie. The content of this chapter has been published in whole or in part in the following peer-reviewed journal article:

Bratlie KM, Dang TT, Lyle S, Nahrendorf M, Weissleder R, Langer R, Anderson DG. "Rapid biocompatibility analysis of materials by *in vivo* fluorescent imaging of inflammatory response". **PLoS ONE** 2010; 5(4): e10032. doi:10.1371/ journal.pone.0010032

### **2.1. ABSTRACT**

Many materials are unsuitable for medical use because of poor biocompatibility. Recently, advances in the high throughput synthesis of biomaterials has significantly increased the number of potential biomaterials, however current biocompatibility analysis methods are slow and require histological analysis. Here we develop rapid, non-invasive methods for *in vivo* quantification of the inflammatory response to implanted biomaterials. Materials were placed subcutaneously in an array format and monitored for host responses. Host cell activity in response to these materials was imaged kinetically, *in vivo* using fluorescent whole animal imaging. Data captured using whole animal imaging displayed similar temporal trends in cellular recruitment of phagocytes to the biomaterials compared to histological analysis. Histological analysis similarity validates this technique as a novel, rapid approach for screening biocompatibility of implanted materials. Through this technique there exists the possibility to rapidly screen large libraries of polymers *in vivo*.

### **2.2. INTRODUCTION**

To our knowledge, there are no methods for *in vivo* visualization of biocompatibility or inflammatory responses to implanted biomaterials. Traditionally, biocompatibility is determined via histology. Histology allows for the determination of cell type and number near the implant, including those belonging to the immune system. However, histology is an endpoint measurement, allowing examination of only one time point per animal. Fluorescence imaging represents a set of powerful techniques that have traditionally been employed as a method for examining tumor models[37-42], along with inflammation resulting from arthritis[43, 44], pulmonary inflammation[45, 46], and transplant rejection models[47].

When a biomaterial is implanted, the healing response is initiated by monocytes and neutrophils, followed by propagation of fibroblasts and vascular endothelial cells[48]. Infiltration of inflammatory

cells can lead to such complications as: bio-instability of glucose sensors[49]; overgrowth of encapsulated pancreatic islets for diabetes therapy causing ischemia and, eventually, necrosis of the islets[50]; and constrictive fibrosis following silicone implants in mammary augmentation[51]. Granulation tissue will then be formed and may appear as early as 3 to 5 days following implantation[48]. In general, granulation tissue will ultimately form a fibrous capsule surrounding the implant[48].

Immunological responses are dynamic processes and, as such, cell type and population at the implant site change during the healing process[2]. The sequence of local events following implantation is generally regarded as the tissue response continuum in which each individual event leads to the subsequent: injury progresses to acute inflammation, which proceeds to chronic inflammation, followed by granulation tissue formation, foreign body reaction and fibrous encapsulation[2, 52]. The presence of eosinophils and polymorphonuclear (PMN) cells typify acute inflammatory responses while macrophages and fibroblasts signify the chronic form[53]. Neutrophils, together with monocytes and macrophages, release cathepsins during the process of degranulation [54, 55]. Cathepsins are proteolytic enzymes responsible for digesting foreign material [48].

Here, we describe the first methods for examining biomaterial biocompatibility *in vivo*, using fluorescence reflectance screening. The novelty of this technique lies in its ability to repeatedly analyze foreign body responses in the same animal. The macrophage recruitment and protease enzyme activity, both of which serve as markers of biocompatibility, were monitored *in vivo*, in real-time. We believe the methods developed here provide the first rapid techniques for parallel determination of biomaterial biocompatibility *in vivo* in a non-invasive manner.

## **2.3. MATERIALS AND METHODS**

### **2.3.1. Molar Absorptivity.**

The absorbance of the two fluorophores, ProSense-680 and F4/80 pan macrophage monoclonal antibody conjugated to Fluorescein isothiocyanate (FITC), were monitored using UV/Vis absorbance spectroscopy over the 200 to 800 nm range. Solutions were diluted in 0.9% w/v NaCl and housed in 1 cm path-length quartz cuvettes. Absorbances were measured on a Cary 100 Bio UV/Vis Spectrophotometer.

### **2.3.2. Ethics Statement.**

The research protocol was approved by the local animal ethics committees at Massachusetts Institute of Technology (Committee on Animal Care) and Children's Hospital Boston (Institutional Animal Care and Use Committee) prior to initiation of the study.

### **2.3.3. Animals.**

8-12 week old male SKH1 mice were obtained from Charles River Laboratories (Wilmington, MA). The mice were maintained at the animal facilities of Massachusetts Institute of Technology, accredited by the American Association of Laboratory Animal care, and were housed under standard conditions with a 12-hour light/dark cycle. Both water and food were provided *ad libitum*.

### **2.3.4. Injections.**

Injections were performed in accordance with ISO 10993-6: 2001. Prior to injection all materials were sterilized. Saline was sterilized via 0.22  $\mu\text{m}$  filtration; alginate was autoclaved for 20 min. at 121°C; and polystyrene particles were washed in 70% ethanol and re-suspended in sterile saline. The mice were anesthetized via isoflurane inhalation at a concentration of 1-4% isoflurane/balance O<sub>2</sub> to minimize movement. Their backs were scrubbed with 70% isopropyl alcohol and the animals were injected with saline, a solution of 2%-w/v alginate (Protanal LF 10/60, FMC BioPolymer, Newark, DE, having high guluronic acid composition (65-75%), mean molecular weight of 180kDa), or 10%-w/v polystyrene beads (3.0  $\mu\text{m}$ , Sigma Aldrich, St. Louis, MO) in an array format on the mouse's back. Eight injections were made in each mouse in a random fashion to establish position-dependent inflammatory responses. Injection volumes ranged from 30 – 100  $\mu\text{l}$ . All experiments were conducted in quadruplicate for each imaging time-point. In addition, a set four mice were imaged at every time-point and sacrificed at the 28 day time-point.

### **2.3.5. Imaging.**

The following two imaging agents were co-injected into the tail vein 24 hours before *in vivo* fluorescence imaging: ProSense-680 (VisEn Medical, Woburn, MA, excitation wavelength 680  $\pm$  10 nm, emission 700  $\pm$  10 nm)[40] for imaging cathepsin activity, 2 nmol in 150  $\mu\text{l}$  sterile Phosphate Buffered Saline (PBS), and FITC-mAb F4/80 (Abcam, Cambridge, MA, excitation wavelength 495 nm, emission 521 nm) for imaging macrophage recruitment, 5  $\mu\text{g}$  in 100  $\mu\text{l}$  sterile PBS.

*In vivo* fluorescence imaging was performed with an IVIS-Spectrum measurement system (Xenogen, Hopkinton, MA). The animals were maintained under inhaled anesthesia using 1-4% isoflurane in 100% oxygen at a flow rate of 2.5 L/min. A binning of 8  $\times$  8 and a field of view of 13.1 cm were used for

imaging. Exposure time and f/stop – the relative size of the opening of the aperture - were optimized for each acquired image. Data were acquired and analyzed using the manufacturer’s proprietary Living Image 3.1 software. All images are presented in fluorescence efficiency which is defined as the ratio of the collected fluorescent intensity to an internal standard of incident intensity at the selected imaging configuration. Regions of interest (ROIs) were determined around the site of injection. ROI signal intensities were calculated in fluorescent efficiency. Images were obtained 1, 3, 7, 14, 21, and 28 days post-injection with four replicates imaged at each time point. A separate set of four replicates were imaged at all six time points.

### **2.3.6. Histology.**

Histology evaluated the severity of inflammation resulting from the injected biomaterials. Mice were euthanized via CO<sub>2</sub> asphyxiation and the injected biomaterial and surrounding tissue were excised. The tissues were then fixed in 10% formalin, embedded in paraffin, cut into 5 μm sections, and stained using hematoxylin and eosin (H&E) for histological analysis by a board certified pathologist. Fibrosis was rated on a scale where a zero involved no fibrosis, a one indicated partial coverage with one to two layers of fibrosis, a two is designated a thicker fibrotic layer that nearly covered the implant, and a three denoted concentric fibrotic coverage of the polymer. Both polymorphonuclear (PMN) cells and macrophages were rated on a scale where no observed cells were indicated with a zero, scattered cells scored a one, numerous cells clustering on the sides of the polymer scored a two, and numerous cells surrounding the material resulted in a three.

### **2.3.7. Statistical Analysis.**

The values of the histologic scores and the ROIs were averaged and expressed as the mean ± standard error of the mean. Comparisons of values were performed by the Student’s unpaired two-tailed *t*-test. *P* values less than 0.05 were considered significant.

## **2.4. RESULTS**

### **2.4.1. Linearity of Fluorescence Response to Dose Concentration.**

Prior to quantifying responses *in vivo*, the linearity of the *in vitro* fluorescence response to concentration of dye was assessed, facilitated by the stationary superficially implanted target Fluorescence intensity  $F$  is proportional to the intensity of the excitation beam that is absorbed by the system. That is,

$$F = K'(I_0 - I) \quad (1)$$

Where  $I_0$  is the intensity of the incident excitation beam and  $I$  is the detected fluorescence intensity after traversing a length  $b$  of the medium - in this case - the tissue of the animal. The constant  $K'$  depends upon the quantum efficiency of the fluorescence process. In order to relate  $F$  to the concentration  $c$  of the fluorescing species, Beer's law can be written in the form:

$$\frac{I}{I_0} = 10^{-\epsilon bc} \quad (2)$$

Where  $\epsilon$  is the molar absorptivity of the fluorescing molecules and  $\epsilon bc$  is the absorbance. Inserting Beer's law into equation 1, we obtain:

$$F = K' I_0 (1 - 10^{-\epsilon bc}) \quad (3)$$

Which can be approximated for absorbances less than 0.05 to:

$$F = 2.3K' \epsilon bc I_0 \quad (4)$$

Assuming that  $I_0$  is constant, the fluorescence intensity is linearly proportional to concentration at low absorbances. The molar absorptivities were determined by UV-visible absorbance to be  $2.90 \pm 0.04 \times 10^6 \text{ M}^{-1} \text{ cm}^{-1}$  and  $2.30 \pm 0.06 \times 10^5 \text{ M}^{-1} \text{ cm}^{-1}$  for ProSense-680 and FITC mAb-F4/80, respectively. With an *in vivo* penetration depth for visible light of  $\sim 5$  mm in reflectance mode,[37] the onset of nonlinear relations between fluorescence and concentration would present at doses 5 and 2.5 times larger than those injected for FITC mAb-F4/80 and ProSense-680, respectively, indicating the ability for relative quantitative analysis.

#### **2.4.2. *In Vivo* Imaging of Cathepsin Activity and Macrophages.**

Mice were injected with alginate, polystyrene, or saline in an array format (Figure 2.1) in volumes of 30, 50, 70, and 100  $\mu\text{l}$ . Alginate is a bio-inert material used in a variety of biomedical applications including encapsulation of insulin producing islets for diabetes therapy [56-59], wound healing[60, 61], implants for cardiac remodeling following infarction[62, 63]. In contrast, Polystyrene exhibits high cellular adhesive properties, induces a strong inflammatory response and was chosen as a positive control. Polystyrene particles below 10  $\mu\text{m}$  activate macrophages and are easily phagocytosed[64], allowing them to serve as positive controls. Saline serves as a negative control to assess the background fluorescence level and aid in determination of the detection limit. After injection, the mice were imaged at prescribed time points for cathepsin activity and macrophages as shown in Figures 2.2A-C and 2.3A-C.

Fluorescent regions of interest (ROIs) were quantified for each image and are presented in Figures 2.2D,E and 2.3D,E for cathepsin activity and macrophages recruitment.

Qualitatively, for saline, the cathepsin activity and macrophage fluorescent signal appear to be very low with the exception of cathepsin activity on day 7. For polystyrene, cathepsin activity follows very similar trends wherein protease activity is detected on day one, peaks at three weeks, and begins to decline at four weeks. Recruitment of immune cells to alginate displays a different trend than polystyrene in which cathepsin activity remains constant from the first day to the fourth week. Macrophage recruitment for polystyrene reached a plateau at day seven. Alginate arrived at this plateau earlier, at the third day.

Quantitative performance criteria of methods are necessary in determining whether this technique is suitable in analyzing inflammatory responses. Detection limits are defined as the blank plus three times the standard deviation of the blank and limit of quantification (LOQ) is ten times the standard deviation of the blank. For macrophage detection, the detection limit is a fluorescence efficiency of  $9.4 \times 10^{-7}$  and the LOQ is a fluorescence efficiency of  $2.3 \times 10^{-6}$ . ProSense-680 has a fluorescence efficiency detection limit of  $1.1 \times 10^{-5}$  and the fluorescence efficiency LOQ is  $1.8 \times 10^{-5}$ . Quantification of fluorescence efficiency of both cathepsin activity and macrophage recruitment is above the LOQ as shown in Figures 2.2 and 2.3. Cathepsin activity on the first day after injection of polystyrene was not above the LOQ and therefore not included in Figure 2.2D. Macrophage recruitment on day one for alginate and polystyrene were also below the LOQ and not included in Figure 2.3D and E.

### 2.4.3. Histology

Validation of the *in vivo* imaging technique for biocompatibility described required histologic analysis subsequent to each imaging time point. Several inflammation markers were quantified: PMNs, macrophages, and fibrosis. PMNs and macrophages were scored on the basis of zero being normal cell populations, one being scattered cells, two being numerous cells mostly populating the sides of the polymer, and three being the most severe where numerous cells surrounded the material. Quantified scores and representative images are shown in Figures 2.4 and 2.5, respectively. Minimal PMNs are seen infiltrating the injection site for saline whereas for alginate neutrophils completely surround the injection site from day one to day 28. For polystyrene, neutrophils are present the first day following injection, reaching a maximum population at day 21 and subsequently decreasing.

Macrophage recruitment for the saline injections is very low (Fig. 2.4B). Slightly elevated levels of macrophages on days three and seven likely result from trauma of the injury, not the biocompatibility of



saline, and agrees with previous results[65]. A more pronounced reaction occurs in response to polystyrene and alginate. The macrophage signal for polystyrene reaches a plateau seven days post-injection, while that for alginate levels out at day three. The size of the polystyrene particles (3.0  $\mu\text{m}$ ) lends to being easily phagocytosed, which can be seen in Figure 2.5.

Fibrosis of the implants was also analyzed histologically in which a score of zero denotes no fibrosis, one signifies partial coverage with one to two layers of fibroblasts, two indicates a thicker layer nearly covering the implant, and three represents concentric fibrotic coverage of the polymer. As seen in Figure 2.4C, fibrosis for alginate and polystyrene gradually increases reaching a maximum at fourteen days. This observation is in line with previous findings[66] in which wound dressings of calcium alginate were grafted in porcine models and found fibrosis to reach a maximum at 14 days. The slight decrease in fibrosis scoring at day 28 might result from myofibroblasts contracting the wound as part of the healing process[67].

## 2.5. DISCUSSION

Chemical signals responsible for invoking a response toward implanted biomaterials may include proteins from invading bacteria, clotting system peptides, complement products, and cytokines that have been released by macrophages located in the tissue near the implantation site[68]. Another group of chemical attractants are chemokines which recruit neutrophils and monocytes from the blood[69]. Macrophages derive from monocytes[70]. Macrophages and monocytes can phagocytose cellular debris and pathogens, and stimulate lymphocytes and other immune cells to respond to the pathogen.

Typically for acute inflammation, neutrophil recruitment peaks 1 – 2 days after implantation and gradually resolves after 7 – 10 days followed by macrophage migration at 1 – 2 days after injury[71]. Fibroblasts typically infiltrate at 2 – 3 days reaching a maximum population at 3 – 4 days[71]. Both macrophages and fibroblasts disperse after 5 – 9 days[71]. Chronic inflammation also begins with recruitment of neutrophils[72]. Additionally, protease levels are reported to be higher in chronic wounds[73]. Fibroblasts and macrophages become numerous one to two weeks after injury and diminish at six weeks[71, 74]. Histologic analysis and *in vivo* fluorescence imaging showed very similar trends in macrophage recruitment and also in comparing cathepsin activity derived from *in vivo* imaging to neutrophils evaluated via histology, suggesting that a significant portion of the protease secreted derives from neutrophils. Cathepsin may also derive from macrophages[75]. Christen *et al*[47] have shown that ~75% of the prosense signal is macrophage derived in transplant rejection. Early markers of

inflammation – macrophages and cathepsin activity – have been chosen to assess biocompatibility of various polymers.

Traditionally, the local pathological effect of a material on living tissue that is placed into an implant site is evaluated at both the gross level and the microscopic level. Various biological parameters such as cellular responses and histopathological changes are evaluated via *ex vivo* histology[52]. The throughput of histology is typically on the order of days to several weeks and involves steps such as fixation, embedding, processing, and staining. *In vivo* fluorescent images can be acquired in minutes and only require anesthetization of the subject, thus greatly reducing the time required to screen libraries of compounds. Recently, Sabaliauskas *et al*[76] have made advances in improving the throughput of histology by automating and digitizing data acquisition. Gersner *et al*[77] have developed laser scanning cytometry methods to quantify histological specimens, increasing the throughput of analysis. Specimen preparation still remains a costly, labor-intensive bottleneck in histology and, thus, in biocompatibility screening.

Aside from quantitative detection limit and LOQ, comparison of the dynamic ranges between histology and *in vivo* imaging is also necessary in determining the abilities of fluorescence imaging in assessing immune responses. In comparing histologic scores of polystyrene with fluorescence imaging for cathepsin activity (neutrophils), scores greater than 0.5 are above the detection limit, meaning that the injection sites are distinguishable from the background autofluorescence of the mouse. Histologic scores above 1 appear to correlate to fluorescence efficiencies above the LOQ for cathepsin activity (neutrophils). Comparing fluorescence imaging to histologic scores for macrophages leads to the conclusion that the detection limit and LOQ obtained for *in vivo* imaging corresponds to a histologic score of 1.5, indicating the possibility for false negatives in detecting macrophage infiltration and the necessity for histologic analysis. However, the use of amplification mechanisms such as use of fluorescent nanoparticles avidly taken up by macrophages[40] will likely enhance sensitivity. Although this technique is semi-quantitative owing to the poor depth penetration of visible light[37], in conjunction with histology it possesses the ability to transform the rapidity with which libraries of novel materials are assessed for biocompatibility.

## 2.6. CONCLUSION

The methods developed here provide for rapid, *in vivo* analysis of several different materials simultaneously, thereby allowing for rapid, kinetic analysis of the foreign body response to a number of biomaterials, as well as eliminating labor intensive tissue processing steps typically necessary for

histology. We anticipate that *in vivo* fluorescence imaging may therefore help address bottlenecks in analyzing biocompatibility of polymers and aid in understanding foreign body responses to biomaterials. *In vivo* fluorescence imaging also holds the advantage of monitoring temporal immune cell changes, thus eliminating mouse-to-mouse variations present when making a static histological assessment.

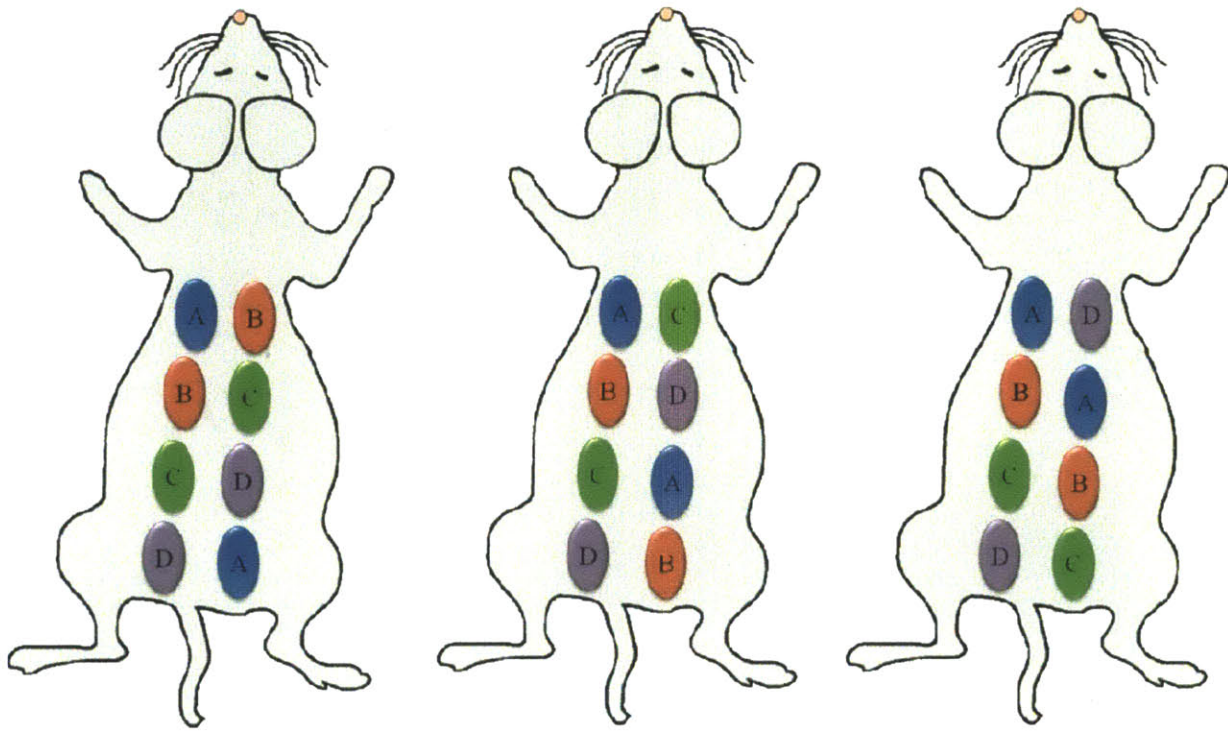


**Figure 2.1: Subcutaneous Injection arrays.**

Three array formats used for injecting saline and polymers subcutaneously in mice where A is 30  $\mu$ l, B is 50  $\mu$ l, C is 70  $\mu$ l, and D is 100  $\mu$ l

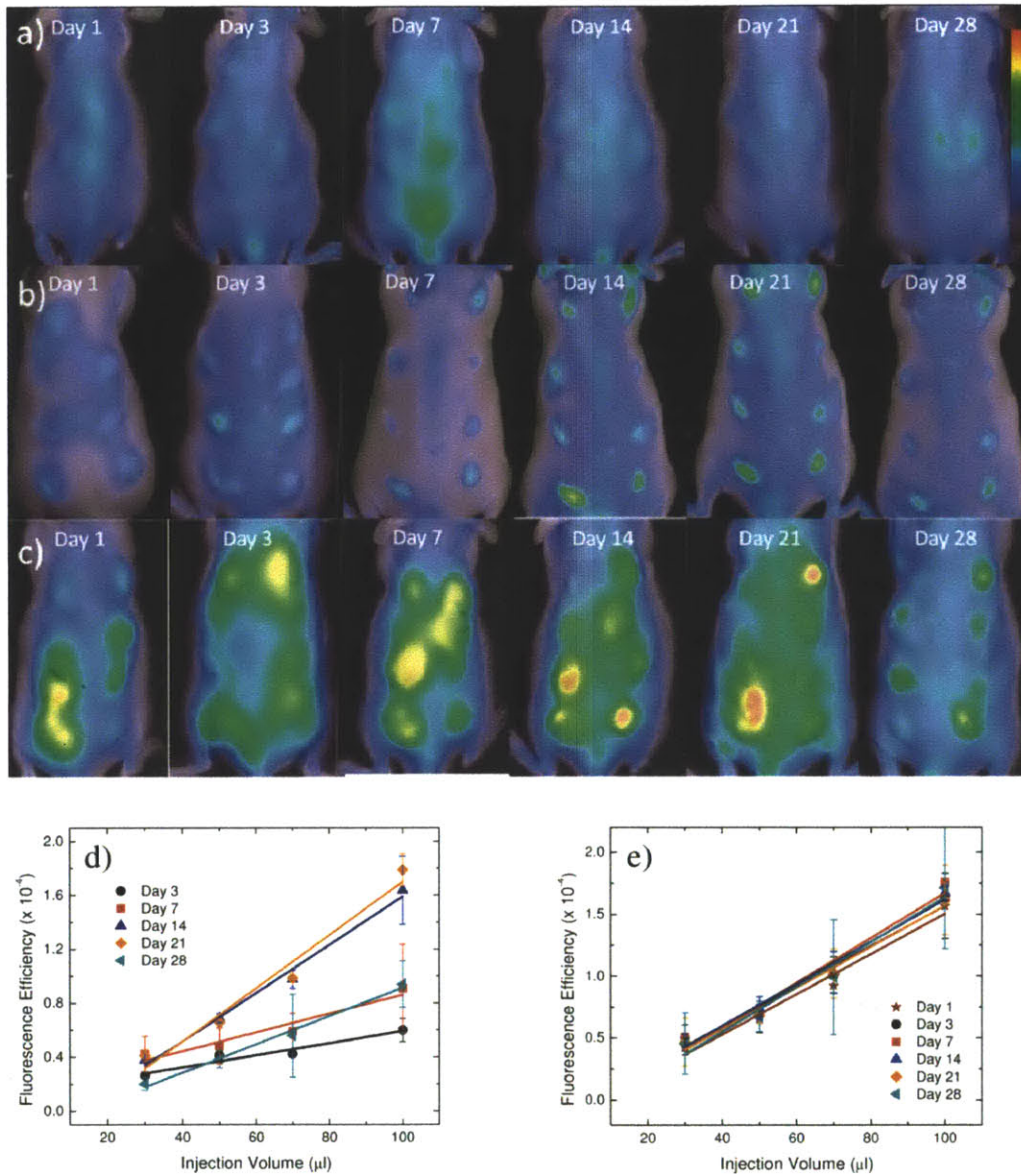


**Figure 2.2: Time evolution of cathepsin activity in response to injected materials fluorescently imaged.** *In vivo* fluorescence imaging using ProSense 680 for cathepsin activity at various time points for **A)** saline, **B)** polystyrene, and **C)** alginate. The scale bar ranges  $0 - 6 \times 10^4$  in fluorescence efficiency. The quantified fluorescence efficiencies of cathepsin activities are shown for **D)** polystyrene and **E)** alginate as the mean with standard deviation. Symbols represent data points and lines represent linear regressions.

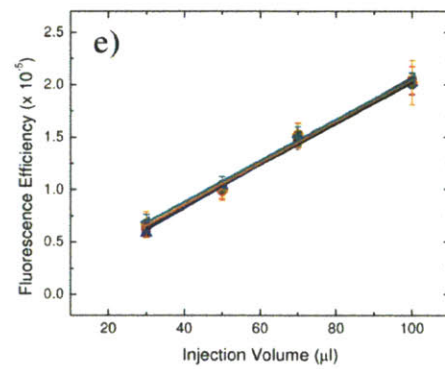
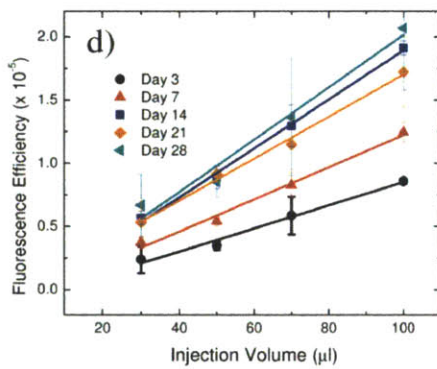
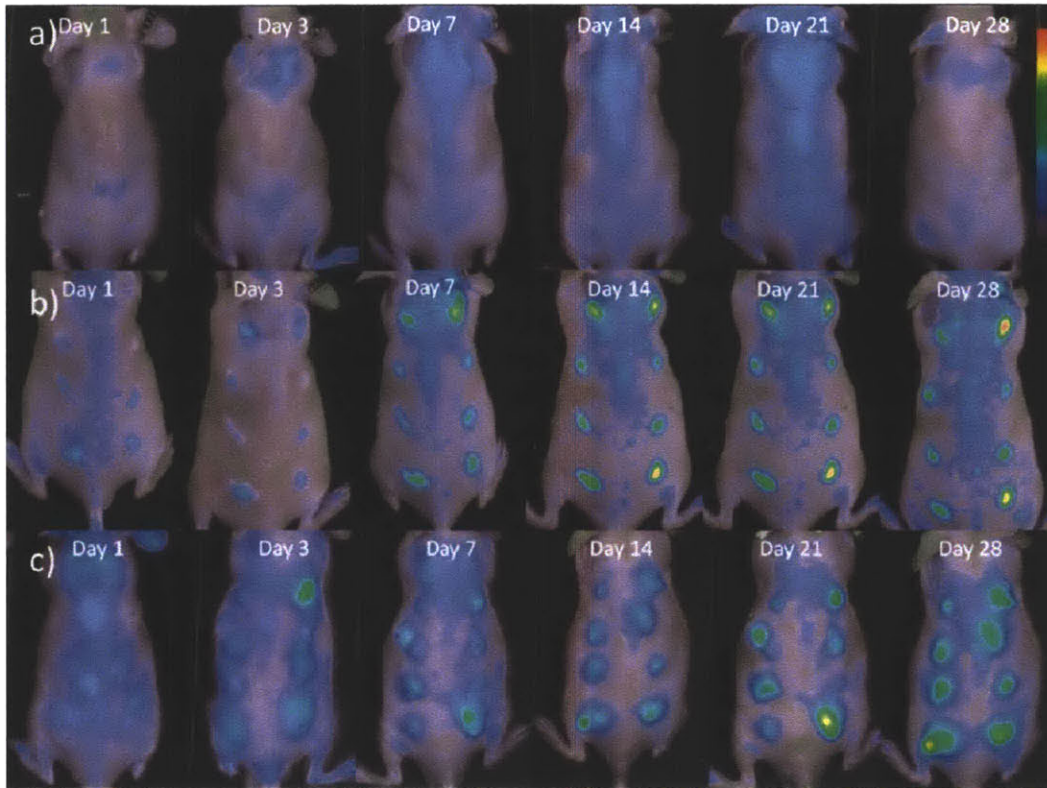


**Figure 2.3: Time evolution of macrophage response to injected materials fluorescently imaged.**

*In vivo* fluorescence imaging of F4/80 pan macrophage antibody at various time points for **A)** saline, **B)** polystyrene, and **C)** alginate. The scale bar ranges 0 –  $1.5 \times 10^{-4}$  in fluorescence efficiency. The quantified fluorescence efficiency of F4/80 pan macrophage responses are shown for **D)** polystyrene and **E)** alginate as the mean with standard deviation. Symbols represent data points and lines represent linear regressions.

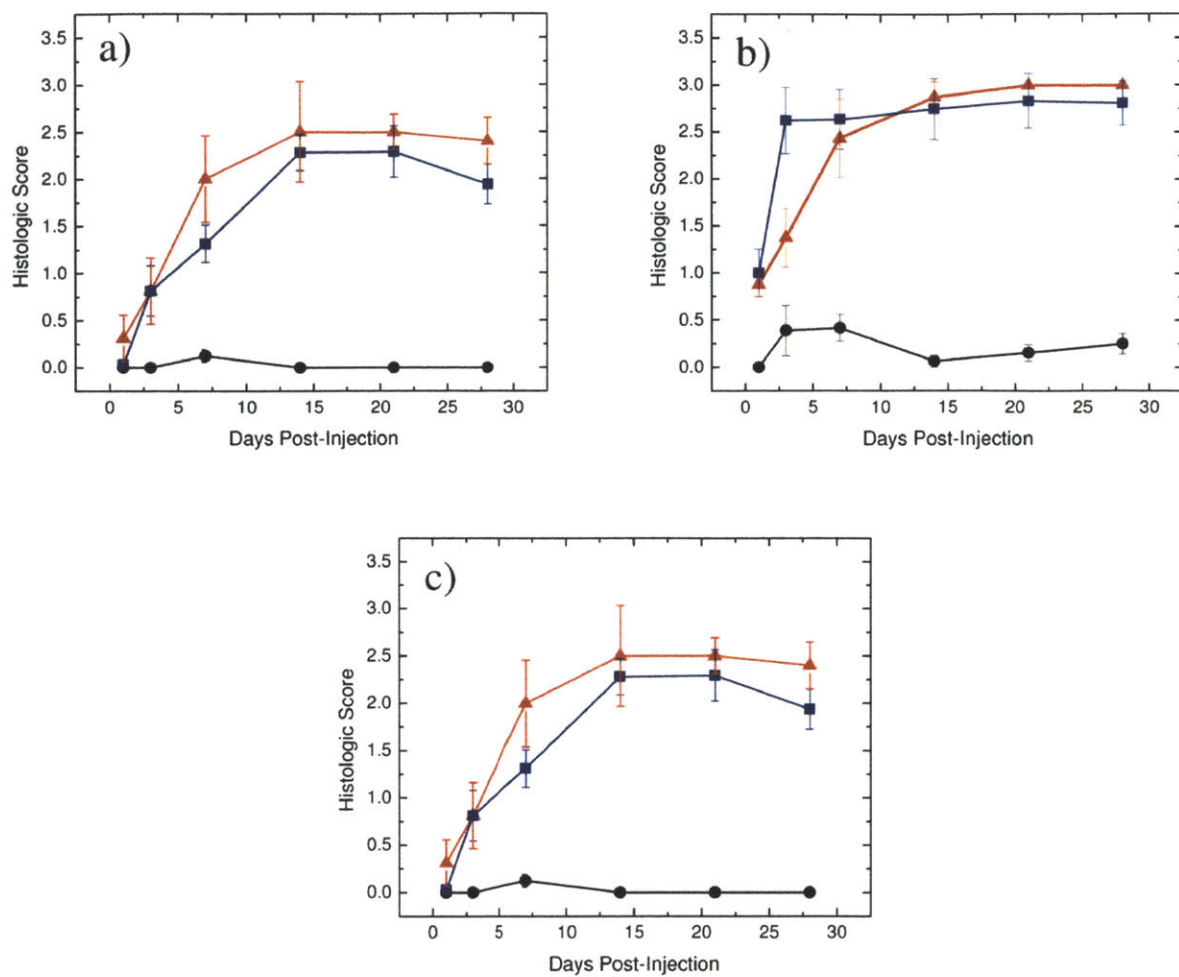


**Figure 2.4: Histological scores of materials subcutaneously injected.**

Histological scores of **A)** neutrophils, **B)** macrophages, and **C)** fibrosis determined for tissue excised at various time points with injections of saline (●), polystyrene (▲), and alginate (■). Values shown are means with standard deviations.

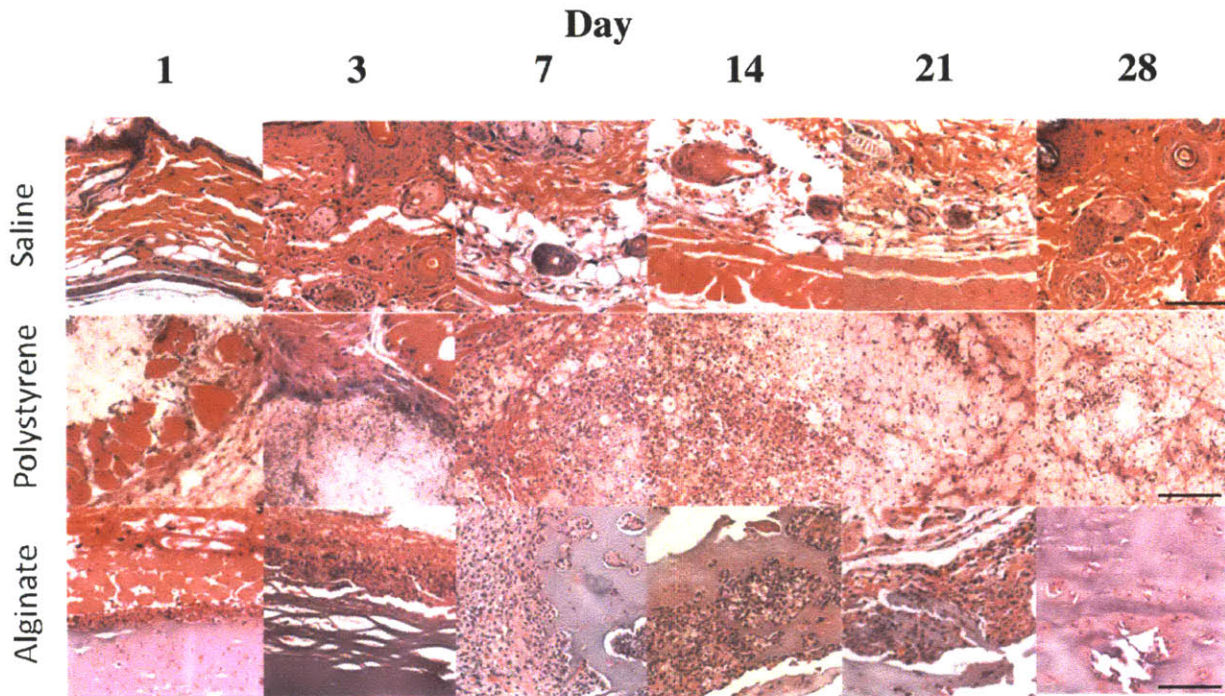


**Figure 2.5: H&E staining of representative sections subcutaneously injected materials.** Representative sections stained with H&E are shown for saline, polystyrene, and alginate at various time points (1, 3, 7, 14, 21, and 28 days post-injection). (Magnification 20 $\times$ , scale bar = 100  $\mu$ m)



## **CHAPTER 3 – IMAGING SPATIO-TEMPORAL EFFECTS OF A CONTROLLED-RELEASE ANTI-INFLAMMATORY DRUG**

The content of this chapter has been published in whole or in part in the following peer-reviewed journal article and incorporated into the following patent applications.

**Dang TT**, Bratlie KM, Bogatyrev SR, Chen XY, Langer R, Anderson DG. "Spatiotemporal effects of a controlled release anti-inflammatory drug on the cellular dynamics of host response". *Biomaterials* 2011;32(19):4464-70

Anderson D.G, Langer R, and **Dang TT**. "Hybrid Microcapsules containing islets and anti-inflammatory drugs for diabetes therapy". U.S.S.N. 61/444206, filed on Feb. 2011.

Anderson D.G, Langer R, and **Dang TT**. "Hydrogel-encapsulated cells and anti-inflammatory drugs". U.S.S.N. 13/400,382 and PCT/US2012/025806, filed on Feb 2012.

### **3.1. ABSTRACT**

In general, biomaterials induce a non-specific host response when implanted in the body. This reaction has the potential to interfere with the function of the implanted materials. One method for controlling the host response is through local, controlled release of anti-inflammatory agents. Herein, we investigate the spatial and temporal effects of an anti-inflammatory drug on the cellular dynamics of the innate immune response to subcutaneously implanted poly(lactic-co-glycolic) (PLGA) microparticles. Noninvasive fluorescence imaging was used to investigate the influence of dexamethasone drug loading and release kinetics on the local and systemic inhibition of inflammatory cellular activities. Temporal monitoring of host response showed that inhibition of inflammatory proteases in the early phase was correlated with decreased cellular infiltration in the later phase of the foreign body response. We believe that using controlled-release anti-inflammatory platforms to modulate early cellular dynamics will be useful in reducing the foreign body response to implanted biomaterials and medical devices.

### **3.2. INTRODUCTION**

One major challenge to clinical application of biomaterials and medical devices is their potential to induce a non-specific host response[10, 15, 49, 78-82]. This reaction involves the recruitment of early innate immune cells such as neutrophils and macrophages, followed by fibroblasts which deposit collagen to form a fibrous capsule surrounding the implanted object [2, 3, 10, 82, 83]. Fibrotic cell layers can hinder electrical[28] or chemical communications and prevent transport of analytes [84-86] and nutrients, thus leading to the eventual failure of many implantable medical devices such as glucose

sensors[15, 49, 87], neural probes[30], immunoisolated pancreatic islets[88-90] and biodegradable polymeric stents[79].

The incorporation of controlled-release delivery systems of anti-inflammatory drugs into medical devices has been proposed to mitigate host response and improve device durability [6, 27, 91-93]. This approach has shown promise in a number of clinical applications. For example, controlled elution of steroids from pace-maker leads has reduced fibrosis formation and enhanced long-term electrical communication between the leads and surrounding cardiac tissue[28]. However, similar attempts to improve the performance of other medical devices such as implanted glucose sensors [29] and immunoisolated islets for diabetes therapy have proven challenging [10]. There remains a substantial need to better understand the immunomodulatory effects of anti-inflammatory drugs on the host-tissue biology at the implant site[27]. Such knowledge can lead to better design of controlled-release drug delivery systems to improve the biocompatibility of implanted medical devices.

Researchers developing controlled-release drug formulations to mitigate host response have largely focused on decreasing the number of inflammatory cells infiltrating the host-device interface. Hickey *et al.* designed a mixed microsphere system containing dexamethasone, a steroidal anti-inflammatory drug, to achieve zero-order *in vitro* release kinetics and to suppress tissue response to thread-induced injuries in rats for up to one month[94, 95]. Recent studies on a hydrogel composite containing dexamethasone-loaded PLGA particles also suggested that sustained release of this drug may minimize the inflammatory reactions at the tissue-material interface [33, 96, 97]. While these studies have provided invaluable information, they only addressed the effects of these drug delivery systems via *ex vivo* analysis of the cell types, quantity and distribution in excised tissues. However, various factors in the design of controlled -release formulations such as drug selection, drug loading, particle sizes and corresponding release kinetics can dynamically affect a range of biological activities in the host response. The presence of anti-inflammatory drugs may alter not only the quantity and variety of immune cells recruited but also the kinetics of cellular activities such as the secretion of inflammatory enzymes or cell signaling pathways[98, 99]. *In vivo* cellular secretory products might affect the degradation rate of the polymeric matrix[11-13] used to encapsulate drugs, and are partly responsible for the discrepancy between *in vitro* and *in vivo* release kinetics[14]. Therefore, we hypothesize that monitoring the spatial and temporal dynamics of enzymatic activity in the host response will offer new insight into the efficacy of controlled-release systems of anti-inflammatory drugs.

In this study, we examined the real-time effects of controlled-release anti-inflammatory therapeutics on the host response to subcutaneously implanted polymeric materials. Poly(lactic-co-

glycolic) (PLGA 50/50) microparticles with and without dexamethasone were subcutaneously injected in a six-spot array on the dorsal side of immunocompetent mice. Monitoring the *in vivo* activity of cathepsins, a class of inflammatory proteases, by *noninvasive* fluorescent imaging revealed that microparticles with low drug loading (1.3wt%) locally inhibited these enzymes, while high drug loading (26wt%) formulation resulted in systemic immunosuppression. The low dexamethasone loading (1.3wt%) was sufficient to attenuate the coverage of the implanted polymer by fibrotic cell layers. Temporal monitoring of the anti-inflammatory effect was carried out by *in vivo* imaging and *ex vivo* histological analysis.

### **3.3. MATERIALS AND METHODS**

#### **3.3.1. Fabrication and characterization of PLGA microparticles**

Microparticles with or without dexamethasone were prepared using a single-emulsion method [100] with biodegradable PLGA 50/50 (inherent viscosity of 0.95-1.20dL/g) from Lactel (Pelham, AL). Typically, a 5mL solution of PLGA and dexamethasone dissolved in dichloromethane, at concentrations of 40mg/ml and 2mg/ml respectively, was quickly added to a 25mL solution of 1% (w/v) polyvinyl alcohol and homogenized for 60s at 5000rpm (Silverson L4R, Silverson Machines Ltd., Cheshire, England). The resulting suspension was quickly decanted into 75mL of deionized water and stirred for 30s prior to rotary evaporation (Buchi Rotavap, Buchi, Switzerland) for 3min. The suspension was washed five times by centrifugation at 3000rpm for 3min. The particles were collected by filtration using 0.2µm filter, flash-frozen in liquid nitrogen, and lyophilized to dryness. Particle size distribution and morphology were examined by Scanning Electron Microscopy (JSM-6060, Jeol Ltd., Peabody, MA, USA). Fluorescence spectra of the PLGA polymer microparticles were collected by a Fluorolog-3 spectrofluorometer (Horiba Yvon Jobin, Edison, NJ, USA). The dexamethasone loading of all microparticles was determined by dissolving 2mg of microspheres in 1mL of acetonitrile and comparing the resulting UV absorbance at 234 nm to a standard curve of known concentrations of dexamethasone in acetonitrile.

#### **3.3.2. *In vitro* drug release kinetics**

The sample preparation and separation methods reported elsewhere were utilized to study the release of drug from microparticles[101]. Briefly, 3.5mg of dexamethasone-loaded PLGA microparticles were suspended in 1mL of 0.9% (w/v) NaCl solution in a 1.5mL centrifuge tube. The centrifuge tube was incubated at 37°C on a tilt-table (Ames Aliquot Mixer, Miles). At predetermined intervals, the tube was

centrifuged at 12krpm for 5min using an Eppendorf 5424 microcentrifuge. The supernatant was collected and replaced with an equal volume of fresh 0.9 % (w/v) aqueous NaCl solution. After a release period of thirty days, the suspension of remaining particles was completely dissolved in acetonitrile overnight. The concentration of dexamethasone in all collected samples was quantified using UV absorbance at 234nm against a standard curve of known drug concentrations. The percentage of drug release at each time point was calculated by normalizing the cumulative amount of drug collected at each point with the total amount of drug initially encapsulated in the particles. The release kinetics reported for each particle formulation was obtained from the average of quadruplicate experiments.

### **3.3.3. Animal care**

The animal protocol was approved by the local animal ethics committees at Massachusetts Institute of Technology (Committee on Animal Care) and Children's Hospital Boston (Institutional Animal Care and Use Committee) prior to initiation of the study. Male SKH-1E mice at the age of 8–12 weeks were obtained from Charles River Laboratories (Wilmington, MA, USA). The mice were housed under standard conditions with a 12-hour light/dark cycle at the animal facilities of Massachusetts Institute of Technology, accredited by the American Association of Laboratory Animal Care. Both water and food were provided *ad libitum*.

### **3.3.4. Subcutaneous injection of polymeric microparticles**

Before subcutaneous injection of microparticles, mice were kept under inhaled anesthesia using 1–4% isoflurane in oxygen at a flow rate of 2.5L/min. Lyophilized microparticles with or without encapsulated drug were suspended in sterile 0.9% (w/v) phosphate buffered saline at a concentration of 50mg/mL. A volume of 100 $\mu$ L of this suspension was injected subcutaneously via a 23G needle at each of the six spots on the back of the mouse.

### **3.3.5. *In vivo* fluorescent imaging of whole animals**

Mice were started on a non-fluorescent alfalfa-free diet (Harlan Teklad, Madison, WI, USA) three days prior to subcutaneous injections of microparticles and maintained on this diet till the desired sacrifice time point for tissue harvesting. The imaging probe ProSense-680 (VisEn Medical, Woburn, MA, USA), at a concentration of 2nmol in 150 $\mu$ l of sterile phosphate buffered saline, was injected into the mice tail vein. After 24 hours, *in vivo* fluorescence imaging was performed with an IVIS-Spectrum measurement system (Xenogen, Hopkinton, MA, USA). The animals were maintained under inhaled anesthesia using 1–4% isoflurane in oxygen at a flow rate of 2.5L/min. For monitoring cathepsin activity,

whole-animal near-infrared fluorescent images were captured at an excitation of 605nm and emission of 720nm and under optimized imaging configurations. A binning of 8×8 and a field of view of 13.1cm were used for imaging. Exposure time and f/stop (the opening size of the aperture) were optimized for each acquired image. Background autofluorescence of PLGA particles was also imaged at an excitation of 465nm and emission of 560nm. Data were analyzed using the manufacturer's Living Image 3.1 software. All images are presented in fluorescence efficiency which is defined as the ratio of the collected fluorescent intensity normalized against an internal reference to account for the variations in the distribution of incident light intensity. Regions of interest (ROIs) were determined around the site of injection. ROI signal intensities were calculated in fluorescent efficiency.

### **3.3.6. Tissue harvest and histology processing**

At the desired time points, mice were euthanized via CO<sub>2</sub> asphyxiation. The injected microparticles and 1cm<sup>2</sup> area of full thickness dermal tissue surrounding the implant were excised, placed in histology cassettes and fixed in 10% formalin overnight. Following fixation, the tissues were dehydrated by transferring the cassettes to 70% ethanol solutions. The polymer particles with surrounding fixed tissues were embedded in paraffin and sectioned into samples of 5µm thickness. These samples were stained with hematoxylin and eosin (H&E) for histological analysis.

### **3.3.7. Histology analysis by laser scanning cytometry**

The extent of cellular infiltration to injected polymer spots was determined by semi-quantitative imaging cytometry using the iCys Research Imaging Cytometer with iNovator software (CompuCyte, Cambridge, MA, USA). A scanning protocol for quantification was configured with excitation by blue 488nm laser and a virtual channel for hematoxylin detection. Low resolution tissue scans with the 20x objective were performed to capture preliminary images of all tissue sections in each slide. High resolution tissue scans were subsequently acquired using the 40x objective and step size of 0.5µm. The threshold in the hematoxylin channel for detection of cell nuclei was optimized to selectively contour individual nuclei. Cross-sectional areas of the polymer spots excluding the dermal and skeletal tissues were defined. The nuclei number and nuclei area measurements were taken from within these regions. The extent of cellular infiltration into each polymer spot was calculated as the ratio of the total nuclei area to total polymer cross-sectional area.

### **3.3.8. Statistical analysis**

The values of the fluorescent signals and the extent of cellular infiltration were averaged and expressed as the mean  $\pm$  standard error of the mean. Comparisons of values were performed by the Student's two-tailed two-sample *t*-test. *P*-values less than 0.05 were considered significant.

## 3.4. RESULTS AND DISCUSSION

### 3.4.1. Spatial effect of a controlled-release anti-inflammatory drug

#### 3.4.1.1. Effect of drug loading on controlled-release properties

We first investigated the inhibitory effect of microparticles with different loadings of an anti-inflammatory drug. Dexamethasone, a synthetic steroid, was selected for incorporation into PLGA microparticles because it is the most potent long-acting glucocorticoid [102] which has been reported to decrease cellular recruitment to implanted biomaterials[30, 31, 95, 97] and to minimize fibrotic deposition on FDA-approved pace-maker leads[28]. PLGA particles with or without different drug loadings were fabricated by a water-in-oil emulsion method. Each formulation of drug-loaded particles was tested via subcutaneous injections at three alternating sites on the dorsal side of each mouse as shown in the injection scheme (Figure 3.1A). Control particles without encapsulated drug were similarly administered at the three remaining sites on the same mouse. Each mouse was imaged 24 hours after intravenous administration of Prosense680, a near-infrared fluorescent probe to detect the activity of cathepsin enzymes which are inflammatory proteases secreted by immune cells[103-105].

Figure 3.1B-C shows the imaging results at day 4 for two representative mice corresponding to two particle formulations with low (1.3wt%) and high (26wt%) drug loadings. For the mouse with low loading particles (Figure 3.1B), cathepsin activity of inflammatory cells was observed at three injection sites with control particles. This near-infrared fluorescent signal was absent for the drug-loaded particles at the remaining sites on the same mouse. The juxtaposition of cathepsin-absent sites next to cathepsin-active sites suggested that the anti-inflammatory effect was spatially localized at the injection sites of dexamethasone-loaded particles. Though the mechanism of action for dexamethasone is not completely understood, it is known to act via a variety of pathways[99] resulting in the attenuation of inflammatory cell cascades when administered systemically[106]. *Ex vivo* histology studies also reported that this drug decreases fibroblastic recruitment and collagen production at implant sites[107]. Our data showed *in vivo* for the first time that controlled-release formulations of dexamethasone (1.3wt% drug loading) exhibited specific and localized inhibition of cathepsin activity in host response to subcutaneously implanted materials.

With the higher drug loading, there appeared to be a systemic immunosuppressant effect causing the disappearance of cathepsin signals from all six injection sites (Figure 3.1C). This might be due to the significant initial burst release from the particles with higher drug loading, as illustrated by the *in vitro* drug release profile (Figure 3.1D). Several mice administered with particles of high drug loading died after 7-10 days. Conversely, mice receiving particles with low drug loading maintained healthy body conditions till sacrifice at 28 days. Understanding the effect of drug loading on the *in vivo* inhibitory properties is important in selecting drug delivery formulations for incorporation into medical devices. Choosing an appropriate anti-inflammatory drug release profile may minimize unwanted side effects of systemic circulation, while ensuring sufficient mitigation of the host response to achieve long-term device performance.

#### *3.4.1.2. Anti-inflammatory drug attenuated coverage of implanted polymer by immune cell layers*

When we imaged the mice with low drug-loading particles at both near-infrared and green wavelength conditions (Figure 3.2), we discovered an interesting phenomenon relating to the optical properties of immune cell layers surrounding the injected polymer particles. Shown here are representative images from one mouse, displaying near-infrared (Figure 3.2B) and green (Figure 3.2C) fluorescent signals overlaid on a gray photograph at day 10 after subcutaneous injection of particles. Figure 3.2D shows the multiplex image combining the two fluorescent signals. Three injection sites with control particles showed fluorescence under near-infrared excitation, but no green signal when imaged at visible wavelengths. Conversely, for the remaining injection sites with drug-loaded particles, green fluorescence was detected but near-infrared signal was absent. This phenomenon was observed consistently in other mice. In addition, the fluorescent excitation-emission spectra of solid PLGA 50/50 particles *in vitro* (Figure 3.2E) revealed that both control and drug-loaded microparticles gave strong autofluorescence in the green visible wavelengths but undetectable signals in the near-infrared region.

We hypothesized that the presence or absence of immune cell layers accounted for the difference in fluorescent signals observed in figures 3.2B and 3.2C. As illustrated in figure 3.2F, inflammatory cells were extensively recruited to the injection sites of control particles, covering them in compact cellular layers and reducing the green polymer auto-fluorescence by tissue scattering and absorption[108]. However, infiltration of immune cells to the drug-loaded particles was inhibited due to the anti-inflammatory effect of dexamethasone. The absence of immune cells enabled the detection of green

autofluorescence from the polymer. No near-infrared autofluorescent signal was detected from the drug-loaded particles because PLGA 50/50 polymer does not autofluoresce in this region.

Our hypothesis was confirmed by *ex vivo* imaging of the excised polymer particles. Figures 3.2G-I show the excised mouse skin with the dermal-subcutaneous surface facing upwards, exposing the polymer microparticles to the imaging camera. A colored photograph of the same tissue (Figure 3.2G) verified that the control polymer spots were compacted in extensive fibrotic tissue while the drug-loaded microparticles remained flattened against the skin, with minimal coverage by immune cell layers. In Figure 3.2H, the near-infrared cathepsin activity of the *ex vivo* tissue was consistent with the *in vivo* data. At the green wavelength condition in Figure 3.2I, *ex vivo* control particles also showed some autofluorescence that was not as intense as that of the drug-loaded particles. This weak autofluorescence of the control particles was not seen during *in vivo* imaging as the polymer spots were underneath the skin layer. Overall, our data suggest that inhibition of cathepsin activity by a controlled-release anti-inflammatory drug correlates with decreased coverage of the implanted particles by immune cell layers. Our observation regarding the optical properties of immune cell layers may be used to noninvasively monitor long term fibrosis in response to subcutaneously implanted materials.

### **3.4.2 Temporal effect of a controlled-release anti-inflammatory drug**

#### *3.4.2.1. Time-evolution of cathepsin activity*

The *in vivo* host response to implanted materials is a dynamic process that involves many different cell types and biological pathways. Neutrophils, monocytes and macrophages release cathepsins during the process of degranulation[54, 109]. To kinetically monitor the effect of controlled-release dexamethasone on the activity of these immune cells, cathepsin activity was imaged in mice administered with dexamethasone-loaded particles (1.3wt% drug loading) following the timeline in Figure 3.3A. The results for one representative animal at four different time points are shown in Figure 3.3B. Cathepsin activity in response to control PLGA 50/50 particles was highest at days 3 and 10, and decreased significantly at later time points. However, for the microparticles containing dexamethasone, such cellular activity was suppressed at earlier time points and remained absent over the entire period of 28 days. Quantification of the time-evolution of this cathepsin activity is presented in Figure 3.3C showing statistically significant differences between the two particle formulations at days 3 and 10. This temporal analysis suggests that monitoring of cathepsin activity is useful in detecting the anti-inflammatory effect of controlled-release therapeutics in the early phase of host response.



### 3.4.2.2. Time-evolution of cellular infiltration

To understand how the temporal dynamics of *in vivo* cathepsin activity was related to time-dependent cellular infiltration between the implanted microparticles, we also performed standard histological analysis of excised tissues. Three mice were sacrificed at days 3, 10, 17 and 28 corresponding to the imaging time points in Figure 3.3. The excised polymer and surrounding tissues were fixed, processed histologically and stained with Hematoxylin and Eosin. Figure 3.4A shows representative tissue sections in which cell nuclei stained dark blue while collagen and cytoplasmic materials stained pink.

Qualitative evaluation of samples collected on days 3 and 10 revealed that the central portions of many polymer sections were detached during histology processing, while samples collected on days 17 and 27 remained intact. The non-homogenous properties of dermal tissue containing polymer particles rendered it fragile during histological processing steps such as microtome sectioning and exposure to various organic solvents such as xylene or alcohol[110]. In the earlier phase of the foreign body response, cellular layers surrounding the implants might have been thinner and weaker; hence samples on days 3 and 10 were more prone to dissociation from the dermal tissue. In the later phase of days 17 and 27, wound healing might have already resolved[3] with the formation of strong fibrotic cell layers holding the particles together; and thus the samples became more resilient during histology processing.

Despite the lower quality of samples collected on days 3 and 10, we observed neutrophils infiltrating the spaces between polymer particles for both control and drug-loaded samples, and minimal collagen deposition. At the later time points of days 17 and 27, extensive macrophage infiltration and collagen deposition were observed throughout the polymer sections of control samples, while drug-loaded samples were free of cellular infiltration.

We used laser scanning cytometry to quantify the amount of inflammatory cells recruited to the polymer injection sites according to established protocols[6-9, 14]. Figure 3.4B shows the extent of cellular infiltration into each polymer spot, calculated as the ratio of total nuclei area to total polymer cross-sectional area. The cellular coverage ratio was not statistically different for days 3 and 10, possibly due to the sample detachment at earlier time points. However, the extent of infiltration of inflammatory cells was significantly lower for drug-encapsulated polymers at later time points (days 17 and 27). Together, the histological data and fluorescent imaging provided complementary information to confirm that incorporation of dexamethasone decreased early protease activity and long-term cellular infiltration in the host response to subcutaneously implanted materials.

### 3.5. CONCLUSION

In this study, we have demonstrated the *in vivo* spatial and temporal host response to a subcutaneously-implanted, controlled-release anti-inflammatory drug formulation. Microparticles with low drug loading (1.3wt%) locally inhibited the activity of cathepsin enzymes from immune cells, while high drug loading formulation (26wt%) resulted in systemic immunosuppression. We also learned that incorporation of dexamethasone at a low loading (1.3wt%) attenuated the coverage of polymeric microparticles by immune cell layers. Temporal monitoring of the drug effect confirmed that incorporation of dexamethasone decreased early enzymatic activity and long-term cellular infiltration to implanted materials. Although only one drug was tested in our study, this strategy may potentially be extrapolated to investigate other existing drugs or to screen for new small molecules to expand the pool of anti-inflammatory drugs. Various parameters influencing drug release kinetics, such as particle size and polymer molecular weight, may also be explored. The ability to control the effects of anti-inflammatory therapeutics on the host response should aid in the design of microsphere systems for implanted biomedical devices including cardiovascular stents and glucose sensors.

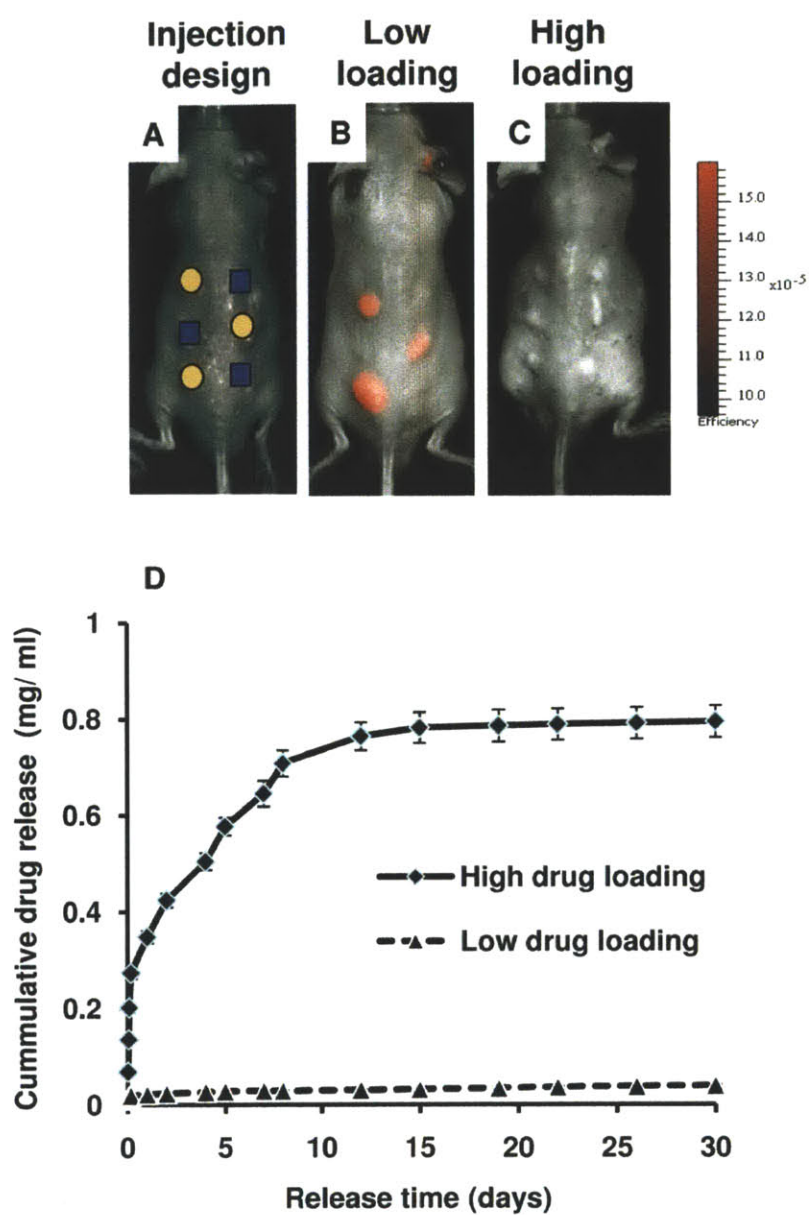


**Figure 3.1: Effect of drug loading on the localization of anti-inflammatory properties.**

**(A)** Injection pattern showing administration sites of PLGA particles without (●) and with (■) dexamethasone. **(B)** Near-infrared fluorescent imaging on day 4 showed a high level of cathepsins at the injection sites of control particles but localized inhibition of these enzymes at the sites of particles with low drug loading. **(C)** Inhibition of cathepsin activity at all injection sites was observed on day 4 when particles with high drug loading were investigated. **(D)** *In vitro* release profiles of dexamethasone showed a more pronounced initial burst release from microparticles with high drug loading.

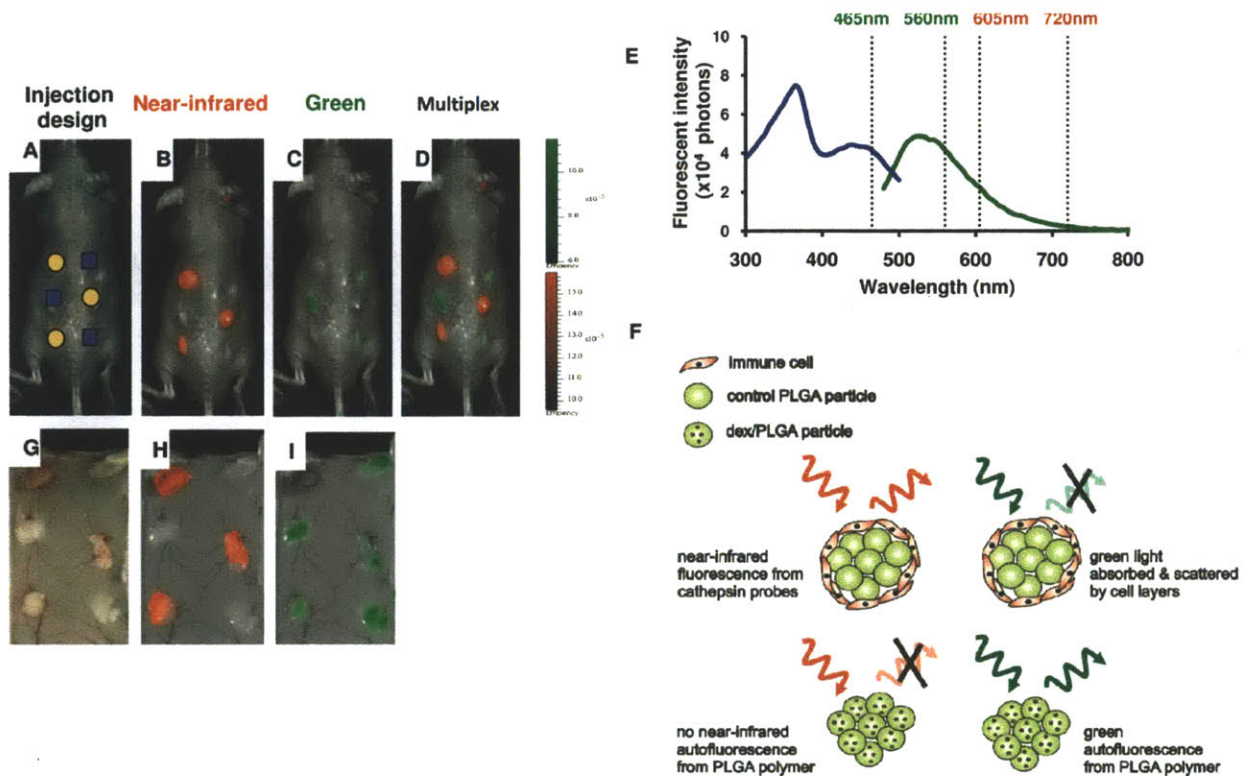


**Figure 3.2: Anti-inflammatory drug attenuated coverage of implanted polymer by immune cell layers.** (A) Injection pattern showing administration sites of PLGA particles without (●) and with (■) dexamethasone. (B-C) Fluorescent imaging of the same mouse at different wavelengths showed near-infrared signal of cathepsin activity (B) only at the sites of control particles and green polymer autofluorescence (C) only at the sites of drug-loaded particles (D) Multiplex image combining *in vivo* fluorescent signals at both wavelengths. (E) Fluorescent excitation-emission spectra of PLGA (50/50) microparticles in solid state showed significant green autofluorescence but no near-infrared autofluorescence. (F) Schematic illustration of the optical effect of immune cell layers. (G) Colored photograph of the excised skin tissue showed that control polymer particles were compacted in extensive fibrous tissue which reduced polymer auto-fluorescence at green wavelengths. The drug-loaded microparticles remained flattened against the skin with minimal cellular coverage thus retaining their auto-fluorescence. (H-I) Fluorescent imaging of *ex vivo* tissue at different wavelengths showed near-infrared cathepsin activity (H) consistent with *in vivo* data. At the green wavelength condition (I), *ex vivo* control particles also showed some auto-fluorescence of lower intensity than that of drug-loaded particles.

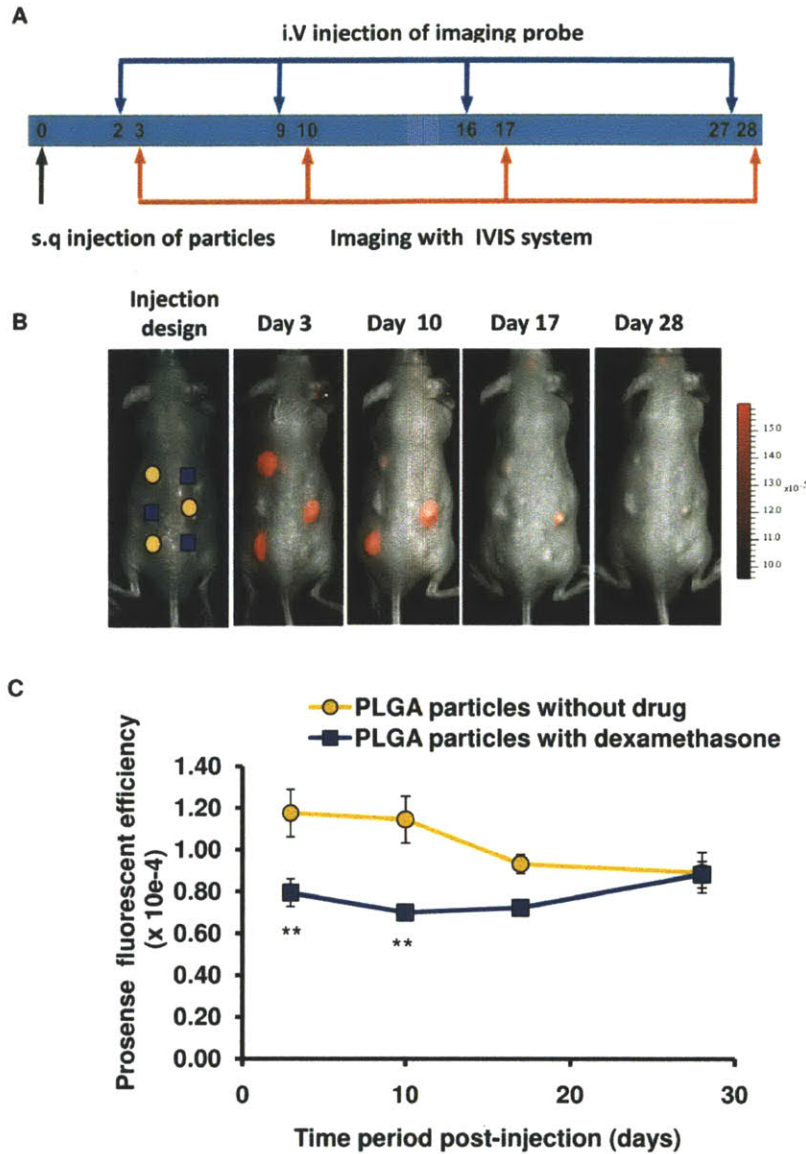


**Figure 3.3: Quantitative temporal monitoring of cathepsin activity.**

(A) Timeline of probe administration and imaging. (B) Near-infrared fluorescent images of one representative mouse over a period of 28 days demonstrated the inhibitory effect of dexamethasone at the earlier time points. All figures are of the same color scale. (C) Quantification of near-infrared fluorescent signals from four replicates showed that cathepsin activity at the sites of control microparticles was higher than drug-loaded microparticles at days 3 and 10. (\*\*) indicates  $P < 0.05$  by the Student's two-sample two-tailed t-test.

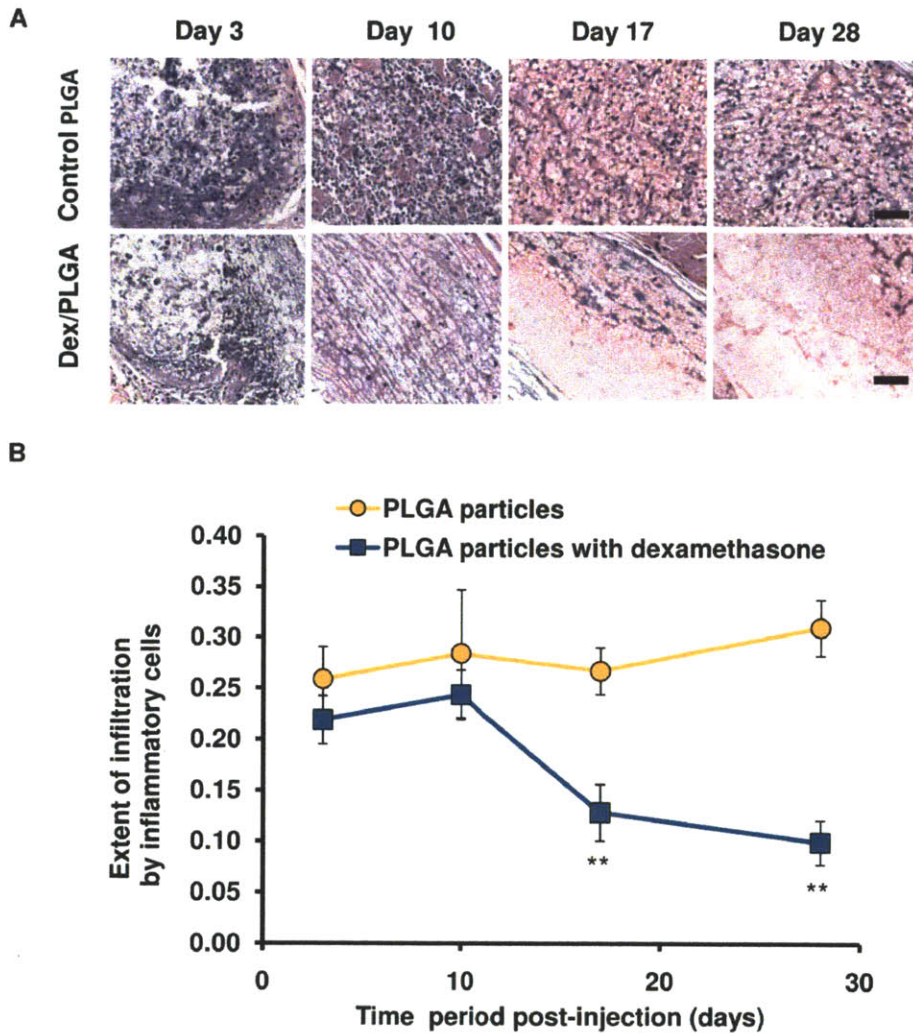


**Figure 3.4: Quantitative monitoring of cellular infiltration to the inter-particle spaces.**

(A) Representative histology sections of excised tissues containing PLGA particles with and without dexamethasone from different mice sacrificed at various time points. Scale bar represents 50um for all pictures. (B) Quantitative analysis of cellular infiltration by laser scanning cytometry showed the inhibitory effect of dexamethasone at later time points: days 17 and day 28. Extent of infiltration by inflammatory cells was defined as the ratio of total nuclei area to total polymer cross-sectional area. (\*\*) indicates  $P < 0.05$  by the Student's two-sample two-tailed t-test.

### 3.6. SUPPLEMENTAL INFORMATION

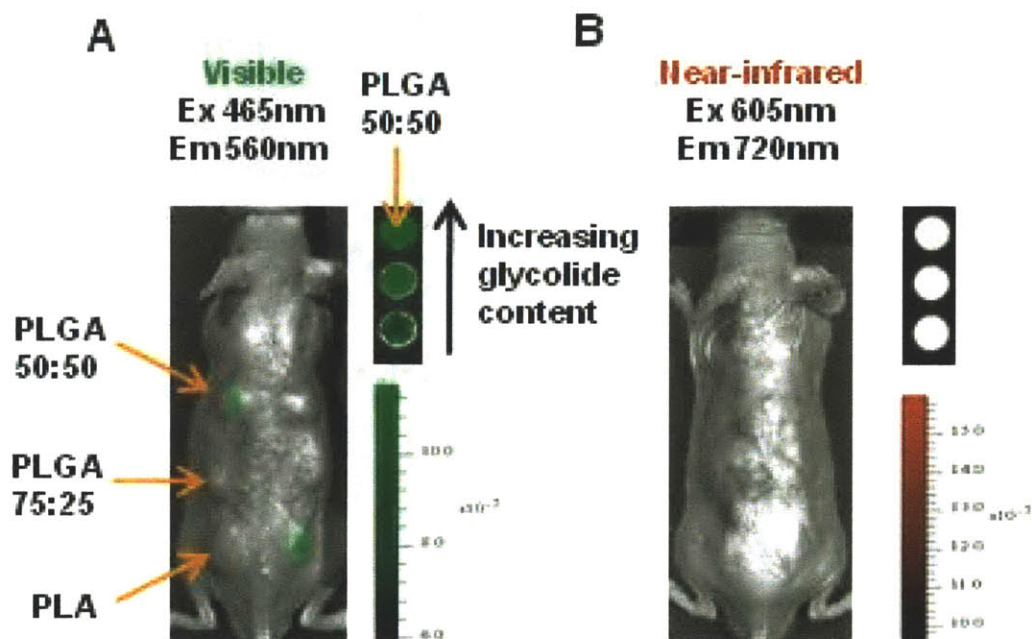


**Figure 3.5: *In vitro* and *in vivo* fluorescent images of PLGA microparticles with different glycolide monomer contents.**

When imaged at the green wavelength configuration (excitation at 465nm, emission at 560nm), microparticles fabricated from PLGA 50/50 show the strongest autofluorescent intensity, both *in vitro* and *in vivo*. No significant signal was detected at the near-infrared imaging configuration used to detect cathepsin activity (excitation at 605nm, emission at 720nm).

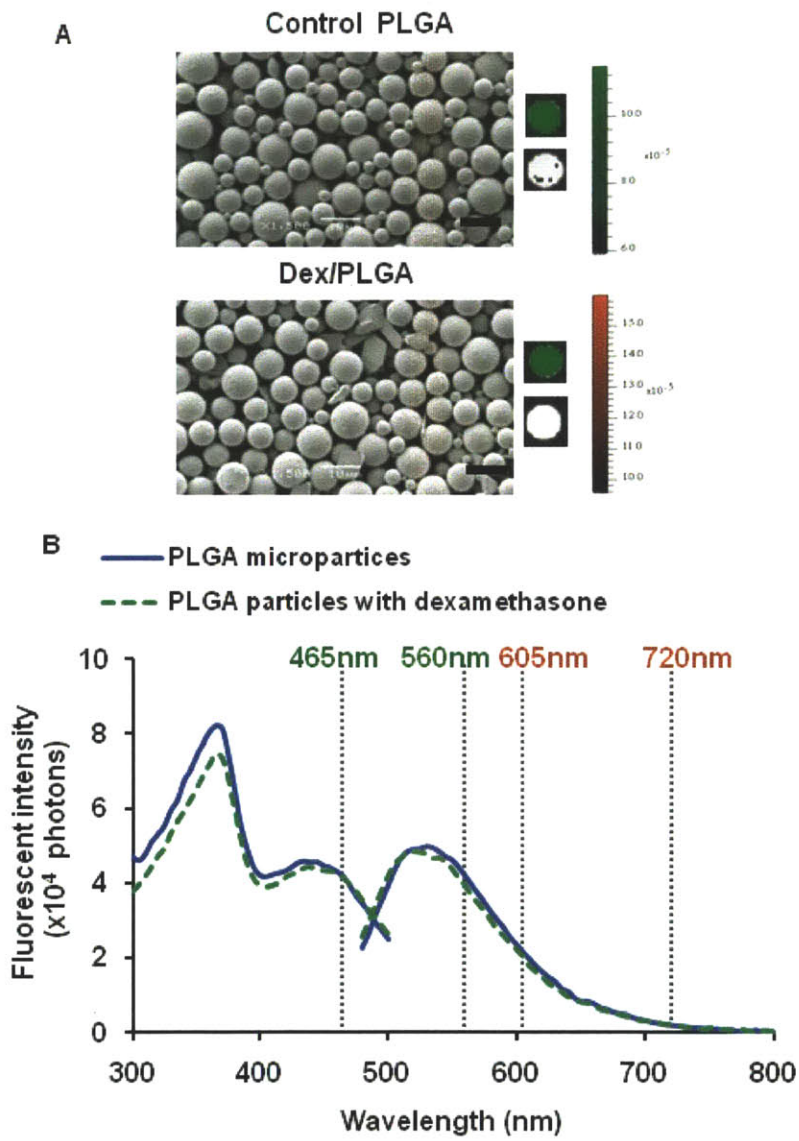


**Figure 3.6: Incorporation of dexamethasone did not alter the physical properties of the microparticles.** A) SEM images showed similar particle sizes and spherical morphology of control PLGA particles and those encapsulating dexamethasone. All scale bars represent 10  $\mu\text{m}$ . Adjacent fluorescent images showed strong auto-fluorescence at visible wavelength and no detectable signal at near-infrared imaging condition for both particle formulations. B) Similar fluorescent excitation and emission spectra of PLGA microparticles with and without dexamethasone.



## **CHAPTER 4 – ANTI-INFLAMMATORY DRUGS FOR IMPROVED EFFICACY OF ENCAPSULATED ISLETS**

The content of this chapter constitutes a manuscript to be submitted for peer-reviewed journal publication and has also been incorporated in whole or in part in the following patent applications.

Anderson D.G, Langer R, and Dang TT. “Hybrid Microcapsules containing islets and anti-inflammatory drugs for diabetes therapy”. U.S.S.N. 61/444206, filed on Feb. 2011.

Anderson D.G, Langer R, and Dang TT. “Hydrogel-encapsulated cells and anti-inflammatory drugs”. U.S.S.N. 13/400,382 and PCT/US2012/025806, filed on Feb 2012.

### **4.1. ABSTRACT**

Host response to implanted biomaterials leads to the formation of fibrotic cell layers which can impair essential functions of implantable medical devices. Anti-inflammatory drugs have the potential to overcome this challenge and improve device durability. Herein, we performed *in vivo* subcutaneous screening of several classes of small molecule anti-inflammatory drugs encapsulated in PLGA microparticles in immunocompetent hairless SKH-1E mice. Using parallel non-invasive fluorescent and bioluminescent imaging during the acute inflammation phase, we demonstrated that a glucocorticoid, dexamethasone, most effectively inhibited the activities of inflammatory proteases while curcumin, a polyphenol drug, decreased the presence of reactive oxygen species secreted by early immune cells. These drugs also decreased subsequent cellular infiltration and fibrosis formation surrounding the subcutaneously injected polymeric microparticles. Next, we designed hybrid alginate hydrogel microcapsules co-encapsulating pancreatic rat islets and drug candidates identified from the subcutaneous screening. The results demonstrated that curcumin effectively reduced fibrotic response against encapsulated islets and improved glycemic control in a C57B6/J mouse model of chemically-induced type I diabetes. Overall, our approach represents a promising strategy to identify effective anti-inflammatory drugs for potential applications in a broad range of implantable medical devices and encapsulated therapeutic cells.

### **4.2. INTRODUCTION**

Implantable biomedical devices such as biosensors, stents, and encapsulated therapeutic cells offer exciting potential to advance human health. However, during the implantation of a biomedical device, tissue injury activates the inflammation cascade which leads to migration of inflammatory cells to the surgery sites, release of cytokines and growth factors that promote cellular proliferation and protein

synthesis as well as complement activation, blood clotting and fibrinolytic cascades [1]. If left uncontrolled, this sequence of events can trigger the proliferation of fibroblasts which synthesize and deposit extracellular matrix to form granulation scar tissues resulting in limited *in vivo* functionality and longevity of implanted devices[5].

Immuno-isolated therapeutic cells is an example of technologies hindered by the host response despite its potential to address many critical medical challenges such as neurodegenerative diseases and hormone or enzyme deficiencies [111]. Non-autologous cells are encapsulated in a semi-permeable hydrogel membrane which prevents direct contact between transplanted donor cells and host immune cells while allowing exchange of nutrients, oxygen and secreted therapeutic molecules [112]. For instance, microencapsulated pancreatic islets can produce insulin to restore normoglycemia in diabetic animal recipients without the need for exogenous insulin administration[16, 113-116]. However, despite encouraging results in various animal models, translation of preclinical results to clinical outcome for diabetes management has remained elusive [17-19].

One factor implicated in the limited success of encapsulated islets is the host immune response responsible for the functional impairment and limited survival of the transplanted islet grafts. Though direct cell-to-cell contact is mitigated by the presence of the isolating hydrogel membrane, the host immunological systems might still be able to attack the encapsulated islets via the secretion of soluble inflammatory mediators [26, 117-119] and the development of long-term pericapsular overgrowth[88]. Early immune cells recruited to the injury sites after surgical implantation secrete soluble molecules such as nitric oxide, free radicals or cytokines which have the potential to induce islet toxicity and early islet mass loss [25, 26, 120, 121]. These inflammatory mediators can diffuse through the semi-permeable hydrogel membrane and cause islet dysfunction or morphological disintegration in a dose-dependent manner [26, 122-124]. Furthermore, subsequent recruitment of fibroblasts can also result in formation of fibrotic cell layers and collagen deposition on the surface of transplanted microcapsules [90, 125]. Such pericapsular overgrowth reduces oxygen and nutrient transport which in turn lead to necrosis of the islet cores and eventual failure of the transplanted grafts [90, 126].

Administration of anti-inflammatory drugs has been proposed as a strategy to mitigate host response and improve the stability of implantable biomedical devices [6, 27, 91, 93, 127]. Incorporation of controlled-release formulations of potent glucocorticoids or anti-proliferative drugs have reduced fibroblast proliferation and collagen deposition resulting in clinical applications of drug-eluting pacemaker leads and stents as well as preclinical development of biosensors in animal models [28, 31, 128-131]. However, similar attempts to utilize anti-inflammatory drugs in cell-based therapeutics have

remained largely unsuccessful. Short-term systemic delivery of steroids and antifibrotic drugs can transiently inhibit recruitment of inflammatory cells, reduce fibrosis formation or improve the protein secretion function of the immuno-isolated cellular grafts [132-134]. Nonetheless, such systemic administration of immunosuppressants also resulted in deleterious side effects such as increased insulin resistance, opportunistic infection, and nephrotoxicity [135, 136]. Recent studies suggested that temporary localized delivery of immunomodulating agents within the immediate vicinity of the encapsulated cells can reduce the tissue response caused by the limited biocompatibility of the encapsulating hydrogel membrane. Bunger *et al* reported that temporary release of encapsulated steroid from empty alginate-poly-L-lysine microcapsules reduced fibroblast proliferation 4 weeks after intraperitoneal transplantation in rats[21]. Others also claimed that biodegradable microparticles containing an NSAID may be used to reduce pericapsular overgrowth on Alginate-Poly-L-Ornithine-Alginate microcapsules[137, 138]. However, despite providing useful information, all existing studies have been limited to the use of only a few anti-inflammatory drugs to address the fibrotic response resulting solely from the limited biocompatibility of the hydrogel materials itself. They were also short-term studies and involved only nonfunctional empty capsules in non-diabetic animals. Thus, it is of great interest to explore the larger reservoir of existing anti-inflammatory molecules and identify promising drug candidates which can better support islet functionality and survival. It is also important to evaluate the efficacy of such combination drug-islet systems in relevant animal models of diabetes.

In this study, we employed non-invasive imaging techniques to perform systematic *in vivo* screening of several classes of small molecule anti-inflammatory drugs in immunocompetent SKH1E mice. We successfully identified drug candidates which suppressed early inflammation markers such as reactive oxygen species and inflammatory proteases in the acute phase of the host response to subcutaneously injected biomaterial. Hybrid hydrogel microcapsules were subsequently designed to co-encapsulate selected drugs and xenogeneic pancreatic islets for efficacy evaluation in a mouse model of chemically-induced type I diabetes. We found that hybrid drug-islet capsules containing curcumin, a naturally occurring polyphenol, were able to reduce pericapsular overgrowth and improve graft function.

## **4.3. MATERIALS AND METHODS**

### **4.3.1. Animal care and use**

The animal protocol was approved by the local animal ethics committees at Massachusetts Institute of Technology (Committee on Animal Care) prior to initiation of the study. Male SKH-1E hairless

immunocompetent mice, aged 8–12 weeks, were obtained from Charles River Laboratories (Wilmington, MA, USA). Male Sprague–Dawley rats, 200–250 g, also obtained from Charles River Laboratories, were used as islet donors. Diabetic male C57B6/J mice (Jackson Laboratory, Maine, USA) were the recipients of encapsulated islets. Diabetes was induced in C57B6/J mice via a research contract with Jackson Laboratory, Maine, USA. Briefly, male C57B6/J mice, aged 6–8 weeks, were subjected to multiple low-dose intraperitoneal injections of streptozotocin (STZ) (Sigma Aldrich) at a daily dose of 50 mg/kg. 200  $\mu$ l of STZ freshly dissolved in saline at a concentration of 5 mg/ml was administered to each mouse daily for a period of 5 consecutive days. Induction of diabetes was confirmed 10–14 days post STZ-administration by the presence of hyperglycemia when fed blood glucose levels of these mice rose above 300 mg/dL for two consecutive daily readings. Most animals reached this criterion by day 10 after STZ administration, and only those with stable hyperglycemia were used for subsequent transplantation. The mice received from Jackson laboratory were housed under standard conditions with a 12-hour light/dark cycle at the animal facilities of Massachusetts Institute of Technology, accredited by the American Association of Laboratory Animal Care. Both water and food were provided *ad libitum* except for the night before Intraperitoneal Glucose Tolerance Test (IPGTT).

#### **4.3.2. Fabrication and characterization of PLGA microparticles**

Microparticles with or without a drug were prepared using a single-emulsion method with biodegradable PLGA 50/50 (inherent viscosity of 0.95–1.20 dl/g) from Lactel (Pelham, AL). Typically, a 5 mL solution of PLGA dissolved in dichloromethane at concentrations of 40 mg/ml and a predetermined concentration of the desired drug, was quickly added to a 25 mL solution of 1% (w/v) polyvinyl alcohol and homogenized for 60 s at 5000 rpm (Silverson L4R, Silverson Machines Ltd., Cheshire, England). The resulting suspension was quickly decanted into 75 mL of deionized water and stirred for 30 s prior to rotary evaporation (Buchi Rotavap, Buchi, Switzerland) for 3 min. The suspension was washed five times by centrifugation at 3000 rpm for 3 min. The particles were collected by filtration using 0.2  $\mu$ m filter, flash-frozen in liquid nitrogen, and lyophilized to dryness.

#### **4.3.3. Subcutaneous injection of PLGA microparticles**

Before subcutaneous injection of the PLGA microparticles, hairless immunocompetent SKH-1E mice were kept under inhaled anesthesia using 1–4% isoflurane in oxygen at a flow rate of 2.5 L/min. Lyophilized microparticles with or without encapsulated drug were suspended in sterile 0.9% (w/v) phosphate buffered saline at a concentration of 50 mg/mL. A volume of 100  $\mu$ L of this suspension was

injected subcutaneously via a 23G needle at each of the six spots on the back of each hairless immunocompetent SKH-1E mouse.

#### **4.3.4. Non-invasive fluorescent and bioluminescent imaging of SKH-1E mice**

SKH-1E mice were started on a non-fluorescent alfalfa-free diet (Harlan Teklad, Madison, WI, USA) three days prior to subcutaneous injections of microparticles and maintained on this diet till the desired sacrifice time point for tissue harvesting. To monitor cathepsin activity, the imaging probe ProSense-680 (VisEn Medical, Woburn, MA, USA), at a concentration of 2 nmol in 150 ml of sterile phosphate buffered saline, was injected into the mice tail vein. After 24 h, *in vivo* fluorescence imaging was performed with an IVIS-Spectrum measurement system (Xenogen, Hopkinton, MA, USA). The animals were maintained under inhaled anesthesia using 1-4% isoflurane in oxygen at a flow rate of 2.5 L/min. Whole-animal near-infrared fluorescent images were captured at an excitation of 605 nm and emission of 720 nm and under optimized imaging configurations. To monitor reactive oxygen species, a volume of 200ul of Sodium Luminol (Sigma Aldrich) dissolved in PBS buffer at a concentration of 50mg/ml was injected intraperitoneally to each mouse prior to imaging (dose of 500mg/kg). Ten minute after this injection, the mouse was imaged under bioluminescent setting in the IVIS system. Data were analyzed using the manufacturer's Living Image 3.1 software. Fluorescent images are presented in fluorescence efficiency which is defined as the ratio of the collected fluorescent intensity normalized against an internal reference to account for the variations in the distribution of incident light intensity. Regions of interest (ROIs) were determined around the site of injection. ROI signal intensities were calculated in total fluorescent efficiency for fluorescence images and in photons per second for bioluminescent images.

#### **4.3.5. Tissue retrieval and histology processing of subcutaneously injected PLGA microparticles**

At the desired time points, mice were euthanized via CO<sub>2</sub> asphyxiation. The injected polymer and one square centimeter area of full thickness dermal tissue surrounding the implant were excised, placed in histology cassettes and fixed in 10% formalin overnight. Following fixation, the tissues were dehydrated by transferring the cassettes to 70% ethanol solutions. The polymer particles with the surrounding fixed tissues were embedded in paraffin and sectioned into samples of 5 μm thickness. These samples were stained with hematoxylin and eosin (H&E) for histological analysis.

#### **4.3.6. Isolation of rat pancreatic islets**

Male, Sprague-Dawley (SD) rats weighed 200-250g were intraperitoneally anesthetized with 400ul mixture of Ketamine (60-80 mg/kg) and Xylazine (5-10 mg/kg). A laparotomy was then performed and the pancreas was exposed. The common bile duct was ligated at its entrance into the duodenum, cannulated proximally with siliconized tubing (0.023" ID, 0.038" OD, Intramedic) and injected with 8ml of M199 medium (Invitrogen) containing 0.152mg/ml rodent collagenase Liberase TL (Roche). The animal was then sacrificed, and the pancreas was carefully dissected from the surrounding tissue and incubated in a 37°C water bath for 17-23 minutes. Enzymatic digestion was stopped by adding 15ml of cold M199 medium supplemented with 10% fetal bovine calf serum (Invitrogen). The tissue was subsequently washed three times and filtered through a 400um sieve. A density gradient utilizing Histopaque 1077 (Sigma Aldrich) was used to separate the islets from exocrine tissue, and was followed by gravity sedimentation in M199 medium with 10% fetal bovine serum. Isolated islets were then hand-picked under a stereomicroscope, collected into a Petri dish and cultured overnight at 37°C, 5% CO<sub>2</sub>, at a density of 2500 islets/10ml in 35ml of RPMI-1640 medium supplemented with 10% fetal bovine serum (FBS), 100 units/ml penicillin and 100 µg/ml streptomycin (Invitrogen).

#### **4.3.7. Fabrication of hybrid alginate microcapsules co-encapsulating drug and islets**

Alginate with high glucuronic acid content SLG20 (Novamatrix, FMC Polymer, Drammen, Norway) was dissolved in sterile 0.9% (w/v) NaCl to give a solution of 1.5% (w/v). To prepare hybrid drug-islet capsule, 1.5%(w/v) alginate was mixed with curcumin (Sigma Aldrich) at 1.0mg/ml or with dexamethasone (Sigma Aldrich) at 2mg/ml and stirred for 4 days to ensure that the drug is homogeneously dispersed. During this mixing period, the curcumin-alginate mixture was wrapped in aluminium foil to avoid light exposure which might oxidize this drug. One day after islet isolation, islets were washed twice with Ca-free KREBS buffer (135mM NaCl, 4.7mM KCl, 25mM HEPES, 1.2mM KH<sub>2</sub>PO<sub>4</sub>, 1.2mM MgSO<sub>4</sub>) and mixed with the alginate suspension with or without dispersed drug. Microcapsules encapsulating islets with or without drugs were produced using an electrostatic droplet generator by extrusion of the islet–alginate suspension through a 22G needle at a volume flow rate of 0.155ml/min and a voltage of 6kV into a cross-linking bath of 20 mM BaCl<sub>2</sub> solution. Encapsulated islets were then left to cross-link in this solution for 5 minutes before being collected into a 50ml Falcon tube. The capsules were subsequently washed four times with HEPES buffer (132mM NaCl, 4.7mM KCl, 25mM HEPES, 1.2mM MgCl<sub>2</sub>) and two times with RPMI-1640 medium supplemented with 10% Fetal Bovine Serum and 100units/ml penicillin and 100 µg/ml streptomycin (Invitrogen). The final microcapsule diameter was in the range of 500-600 µm.

#### **4.3.8. Transplantation of encapsulated islets into STZ-induced diabetic C57B6/J mice**

Xenogeneic transplants of encapsulated rat islets into diabetic C57B6/J mice recipients were performed to examine the reversibility of diabetes. One day after isolation from Sprague–Dawley rats, islets were encapsulated with or without an anti-inflammatory drug (curcumin or dexamethasone). Shortly thereafter, islet-containing capsules were sampled in quadruplicates; and the total islet number was counted. Each aliquot of the capsules suspended in culture media were prepared to contain 250IE. Capsule aliquots were kept on ice and washed twice in sterile 0.9wt% sodium chloride solution before the surgery. They were then transplanted intraperitoneally via a laprotomy procedure with a 5–10 mm abdominal incision into diabetic C57B6/J mice kept under 1-4% isoflurane-in-oxygen anaesthesia. Typically, each mouse received 250IE (post-encapsulation islet count) in a total capsule volume of 500ul.

#### **4.3.9. Blood glucose monitoring and Intraperitoneal Glucose Tolerance Test**

##### *4.3.9.1. Daily blood glucose monitoring :*

Animal blood glucose was determined between 9-11am using a portable glucometer (Clarity Plus). Blood was taken from a tail vein with the total volume drawn per collection not exceeding 5ul.

##### *4.3.9.2. Intraperitoneal glucose tolerance test (IPGTT):*

C57B6/J mice were fasted overnight (6pm-9am) the night before IPGTT. On the day of the glucose challenge, each animal was injected intraperitoneally with 400ul of 10%(w/v) of glucose in sterile 0.9% NaCl, and its blood glucose was taken at 15, 30, 60,75, 90,105 and 120 minutes post-injection. Diabetic and non-diabetic C57B6/J mice were also included as control animals.

#### **4.3.10. Retrieval of transplanted capsules from the intraperitoneal cavity**

Sixty days after transplantation of islet-containing capsules, the mice were sacrificed by carbon dioxide asphyxiation. A laprotomy was performed to expose the abdominal cavity and capsules were retrieved by an abdominal lavage with HEPES buffer. The abdominal cavity was examined closely to identify remaining capsules, which if found were gently removed using a pair of atraumatic tweezers. The retrieved capsules were subsequently washed several times in HEPES buffer and imaged at 2x magnification using an EVOS microscope (AMG). The internal organs of each mouse were examined carefully to ensure that all capsules were retrieved. Finally, capsules were transferred into a 1.5ml Eppendorf tube, and frozen at -20°C for future analysis.

#### **4.3.11. Quantification of fibrosis by DNA fluorescent staining**

50ul of the retrieved capsules were transferred to each well of a 24well Millicell® cell culture insert (Millipore) using wide-orifice pipette tips (Fisher Scientific, Pittsburgh, PA, USA). The capsules were incubated at 37°C for 45minutes in 800ul of 0.001mg/ml Hoersch 33342 dye (Invitrogen) prepared from dye stock solution by dilution with HEPES buffer. Afterwards, these capsules were washed four times with HEPES buffer. The capsules were contained in the upper Millicell® insert which had a porous bottom membrane separating the capsules from the lower container well. The use of a porous insert helped to avoid the loss of capsules during washing steps as washing buffer could be removed by aspiration from the lower well or draining away from the upper insert by placing a Kimwipe below the porous membrane. All capsules were subsequently transferred in 300µl of HEPES buffer into a black 96 well plate (Greiner BioOne). Finally, fluorescent signals from the stained capsules were obtained using a Tecan UV-VIS absorbance plate reader at with the excitation and emission wavelengths of 350nm and 460nm respectively.

#### **4.3.12. Statistical analysis**

All values were averaged and expressed as the mean  $\pm$  standard error of the mean. Fluorescent or bioluminescent signals from injection sites of drug-loaded microparticles and control microparticles were compared using the Student's two-tailed two-sample *t*-test. Comparison of the blood glucose levels and quantified DNA fluorescence signals were performed using one-way ANOVA with Fisher's LSD post-hoc test. *P*-values less than 0.05 were considered significant.

### **4.4. RESULTS**

#### **4.4.1. *In vivo* subcutaneous screening of small molecule anti-inflammatory drugs**

We first sought to evaluate the effects of anti-inflammatory agents on the early cellular dynamics of host response to implanted biomaterials by *in vivo* subcutaneous screening of 16 small molecule drugs (Table 4.1). These agents belong to several different classes of drugs whose efficacies in inhibiting inflammation have been reported such as steroidal [99, 102, 139, 140] and non-steroidal immunosuppressants [141], non-steroidal anti-inflammatory drugs (NSAIDs) [98, 102, 142], and naturally occurring polyphenols [143]. Each drug was encapsulated in poly-lactic-co-glycolic microparticles at three different theoretical loadings (5,10,15wt%) by a water-in-oil emulsion method[100]. The subcutaneous space was selected for initial screening of the drugs as it is the implant site that induces aggressive host response, hence providing a stringent threshold to identify effective



drug candidates [144]. The subcutaneous site also facilitates microparticles injection and monitoring of the host response by non-invasive imaging techniques [104, 145-147]. In the subcutaneous screening, we employed a platform of non-invasive *in vivo* imaging which allows analysis of multiple particle formulations injected into the same mouse[145]. Each formulation of drug-loaded microparticles was injected in triplicate on the dorsal side of each mouse. Control particles without encapsulated drug were similarly administered at the three remaining sites on the same mouse. Two markers of inflammation secreted by early immune cells, namely cathepsin enzymes and reactive oxygen species (ROS), were monitored using a combination of non-invasive fluorescent and bioluminescent imaging techniques following procedures previously reported by our laboratory [104, 145-147]. Cathepsin enzymes, a class of inflammatory proteases, were detected by a fluorescent-activated probe whose signal correlates with the presence of neutrophils in the acute inflammatory response [104, 147]. Luminol was oxidized by ROS emitting bioluminescent signal which can be used to assess host response to implanted biomaterials [147]. Relative fluorescent or bioluminescent signal was calculated as a ratio of the signal from the drug-loaded microparticles to that from the control particles in the same mice (n=6 replicate injections in 2 mice for each drug-loaded particle formulation). A lower relative signal indicates a lower activity of each inflammation marker and a value below 1.00 corresponds to a decreased activity compared to the control formulation.

Figure 4.1 summarizes the imaging data from the *in vivo* screening of all drug formulations on day 3 after the microparticles were subcutaneously injected. Analysis of the results revealed several trends regarding the effects of the drugs on the activities of cathepsin enzymes and reactive oxygen species. Fluorescent imaging data (Figure 4.1A) showed that several steroidal agents such as dexamethasone, hydrocortisone, flurocortisones and prednisolone suppressed the activity of cathepsin enzymes while NSAIDs and other non-steroidal immunosuppressants generally did not. Curcumin caused a slight decrease in cathepsin activity while resveratrol did not, though both drugs belong to the same class of polyphenol compounds. In contrast, bioluminescent data (Figure 4.1B) illustrated that most drugs did not cause any reduction in ROS activity, with the exception of curcumin, sunlindac, rapamycin and flurocortisone. When arranged in descending order of relative imaging signal (Supplementary Figure 4.6), dexamethasone and curcumin formulations were identified as most effective in suppressing cathepsin and ROS activities respectively.

#### **4.4.2. Effect of selected drugs on the subcutaneous cellular dynamics and fibrosis formation**

To further examine the effects of promising drug candidates, temporal monitoring of the activities of early immune cells was performed for three selected drug formulations over an extended time period. A higher number of injection replicates (n=15 injections i.e 3 injections of each drug formulation in 5 different mice) was carried out for better statistical significance. Dexamethasone 5wt% and Curcumin 15wt% were chosen to represent the drug formulations most effective in decreasing cathepsin activities and reactive oxygen species respectively. Ketoprofen 15wt% was selected to represent the drug formulation with no effect on both types of inflammation markers. After subcutaneous injection of the microparticles in to SKH1E mice, the animals were imaged daily for reactive oxygen species during first 7 days and for cathepsin activities on days 3, 9, 15, 21 and 28. Quantification of the imaging signals (Supplementary Figure 4.7) showed that, for the polymer particles without drugs, ROS activity was the highest during the first 3 days while cathepsin activity was the highest at days 3 and 9. Both signals decreased significantly at later time points.

Figure 4.2A shows the injection pattern of the PLGA microparticles with and without drugs. Figure 4.2B-D shows bioluminescent images of representative mice at the peak of ROS activity on day 2. Quantification of the peak ROS signals (Figure 4.2E) confirmed the observation from the subcutaneous screening that curcumin significantly reduced ROS activity at the implant sites ( $p < 0.01$ ) by approximately three fold. Dexamethasone also caused a slight decrease ( $p < 0.05$ ) while ketoprofen did not affect ROS production in the host response to PLGA particles. Representative fluorescent images at the peak of cathepsin activity on day 9 are shown in Figure 4.2F-H. Quantification of these fluorescent signals on day 9 (Figure 4.2I) showed that dexamethasone reduced this protease activity significantly ( $p < 0.0001$ ) by approximately two-fold. Curcumin caused a less significant decrease ( $p < 0.01$ ) while ketoprofen did not affect cathepsin activity. The differences that exist in the fluorescent and bioluminescent signals, can be attributed to the different cellular products measured[147]. This may be resultant of the different effects the drugs exert on the different cell-type populations present at the implant sites as well as their activities in response to the drug-PLGA formulation.

To monitor the cellular infiltration into the inter-particle spaces of the injected microparticles, we performed histology analysis of excised tissues from mice sacrificed at different time points up to 28 days. Figure 4.3 shows representative Hematoxylin and Eosin sections of tissues with control particles and particles containing dexamethasone, curcumin and ketoprofen. For the control samples (Figure 4.3A-E), cellular infiltration and collagen deposition followed the typical time-course of the host response as reported in previous studies [2, 3]. In the early phase, neutrophils occupied the spaces between the microparticles while at the later time points, extensive macrophage infiltration and

collagen deposition were observed throughout the polymer sections of the control samples. In contrast, the samples containing dexamethasone-loaded particles (Figure 4.3F-J) were almost free of immune cells and collagen for at least four weeks, except for a few cells present at the edges of the samples. Curcumin also minimized the host response; samples containing this drug remained free of cellular infiltration for up to 2 weeks (Figure 4.3K-M). After this time point, gradual infiltration of macrophages to curcumin-loaded particles was observed from partial cellular coverage at day 15 to complete coverage on day 28 (Figure 3N-O). However, ketoprofen did not inhibit the host response; all samples containing this drug showed similar pattern of cellular and collagen infiltration compared to the control samples (Figure 4.3P-T)

#### **4.4.3. Improved glycemic control by alginate microcapsules co-encapsulating drug and islets in diabetic mice**

We hypothesized that delivery of a suitable anti-inflammatory drug directly from the microcapsules containing donor islets can mitigate the harmful impact of early inflammatory cells and reduce long-term fibrosis to achieve better islet functionality and survival. Based on the results from subcutaneous *in vivo* screening, we examined the potential of top performing drugs in reducing the host response to encapsulated pancreatic islets and improving their efficacy in diabetes therapy. Hybrid drug-islet microcapsules co-encapsulating curcumin or dexamethasone with pancreatic islets isolated from Sprague-Dawley rats were fabricated using an electrostatic droplet generator. Drug molecules were homogeneously dispersed in 1.5wt% SLG20 alginate at a concentration of 1mg/ml or 2mg/ml for curcumin or dexamethasone respectively. These drug concentrations were determined as optimal from preliminary experiments with different drug loadings ranging from 0.3 to 3.0mg/ml. Due to each drug's hydrophobic nature, higher drug concentrations were avoided as these conditions often resulted in a large fraction of defective capsules with non-uniform sizes, non-spherical shape and undesirable irregularities which can potentially lead to increased attachment of immune cells [88, 90, 148, 149]. Figure 4.A-C shows the hybrid drug-islet capsules with uniform spherical shape and diameters of 500-600um. Dexamethasone-loaded capsules appeared white while curcumin capsules appeared yellow due to the intrinsic color of each drug.

To evaluate the *in vivo* efficacy of the hybrid drug-islet capsules, we utilized a xenogeneic mouse model of chemically-induced type I diabetes with marginal islet mass transplantation [150, 151]. Our objective is to determine whether the hybrid drug-islet capsules improve graft survival and function with a minimal amount of transplanted islets. Male C57B6/J mice were intraperitoneally administered with

streptozotocin (STZ) to destroy the native beta cells of their pancreas and induce a state of insulin-dependent hyperglycemia[152]. The amount of encapsulated Sprague–Dawley rat islet tissue that would marginally cure these STZ-diabetic C57B6/J mouse recipients was determined in preliminary transplant experiments with different islet doses (Supplementary Figure 4.9). All mice transplanted with 75 and 150 islet equivalents (IE, an islet with a diameter of 150um containing approximately 1500-2000 cells[153, 154]) did not reverse diabetes but animals with 300IE were able to reverse diabetes for more than 2 weeks. A marginal islet mass of 250 IE was chosen for evaluation of the hybrid drug-islet capsules. Two types of hybrid capsules, each containing curcumin or dexamethasone, and control capsules which contain only the islets were transplanted into STZ-induced diabetic mice for comparison (n=6-7). All transplants achieved normo-glycemia within the first 11 days. Over the two months post-transplantation, capsules with curcumin achieved better glycemic control compared to control capsules and capsules with dexamethasone as shown in Figure 4.4D. During the time period of day 29 to day 60, the blood glucose level of mice with curcumin capsules were statistically lower than that of the control mice. However, the difference between blood glucose levels of the animals transplanted with dexamethasone-loaded capsules and control capsules was not significant. The average blood glucose level of the curcumin-loaded capsules only rose above 200mg/dl after day 30 while the failure of the islet grafts in the control and dexamethasone-containing capsules occurred earlier, at approximately days 15 and 21 respectively.

In addition, intraperitoneal glucose tolerance tests (IPGTT) showed that the islets co-encapsulated with curcumin remained responsive to glucose after 2 months (Figure 4.4E). After overnight fasting (at time point of 0 min), mice with curcumin-loaded capsules had lower fasting blood glucose levels which are similar to the values for non-diabetic mice ( $p>0.438$ ) while animals with the control islet capsules ( $p<0.001$ ) and dexamethasone-loaded capsules ( $p<0.05$ ) had significantly higher fasting blood glucose compared to the non-diabetic mice. During the two-hour IPGTT, the blood glucose levels of all diabetic mice transplanted with control or hybrid capsules reached a peak at 30 minute which is a slight delay compared with a peak at 15 minute in non-diabetic mice. At each time point, significantly lower blood glucose levels were observed in the mice that received curcumin-loaded capsules compared to the animal group with control islet microcapsules ( $p<0.01$  at all time points till 105 min and  $p<0.05$  at 120 min). The IPGTT data indicated that islets co-encapsulated with curcumin were able clear glucose more effectively than the control islet capsules. Dexamethasone-loaded capsules did not significantly improve the glucose clearance compared to the control capsule.

#### **4.4.4. Reduced fibrotic overgrowth on explanted hybrid drug-islet capsules**

We also evaluated the effect of the anti-inflammatory drugs in reducing the fibrotic overgrowth on microcapsules encapsulating islets. Previous studies have attempted to quantify the extent of pericapsular overgrowth on explanted encapsulated islets. Each sample of explanted capsules was observed by an investigator, and assigned a numerical score depending on the estimated percentage of capsules with pericapsular overgrowth [118, 126, 155-157]. However, these traditional approaches remained semi-quantitative, time-consuming and potentially subjective, depending on the individual performing the assessment and the quality of the images captured for the samples [26]. To overcome these limitations, we developed a new method for rigorous quantification of fibrotic overgrowth on explanted capsules. The capsules were stained with Hoestch 33342 dye whose fluorescence was enhanced when bound to the DNA of the immune cells covering the capsule surface. Measurement of this fluorescence signal provided a quantitative assessment of the number of cells attached to the capsules (Supplementary Figure 4.10).

The new DNA-staining method was used to assess fibrotic overgrowth on encapsulated islets which were retrieved from diabetic mice by peritoneal lavage on day 60 after transplantation (Figure 4.5). These animals were the same mice that received control and hybrid drug-islet capsules whose effects on glycemic control were previously shown in Figure 4.4. Figures 4.5A-C show the fluorescent images of three types of explanted capsules after DNA staining while figures 4.5D-F are the phase contrast images of the same capsules. Fibrotic capsules appeared darker in the phase contrast images and showed enhanced blue emission in the fluorescent images due to the binding of Hoestch 33342 dye to the DNA of fibrotic cell layers covering the surface of the capsules. In contrast, capsules without pericapsular overgrowth appeared transparent in the phase contrast images and gave no fluorescent signal. Figure 4.5J shows the quantified fluorescence signals from hybrid drug-islet capsules containing curcumin or dexamethasone in comparison with control capsules without any drug. Curcumin significantly reduced fibrosis compared to the control capsules while dexamethasone did not.

Figure 4.5G-I showed representative histological cross-sections of explanted capsules embedded in agar hydrogel and stained with Hematoxylin and Eosin. The histology data confirmed the presence of immune cellular layers on the surface of retrieved control and dexamethasone-loaded capsules. Some dark purple circular cross-sections of the alginate capsules have been lost during histological processing but the pericapsular overgrowth on fibrotic capsules remained as exterior rings comprising of a single or several cell layers.

## 4.5. DISCUSSION

Our *in vivo* subcutaneous screening demonstrated that several but not all steroidal glucocorticoids were able to suppress cathepsin activities in the early host response to implanted PLGA microparticles. Steroidal glucocorticoids act through numerous genomic and non-genomic pathways to block the synthesis of metabolites which are important mediators for cytokine production, leukocyte recruitment and activation in early inflammation [99, 102, 139, 140]. Though these drugs have been assumed to act through similar general mechanisms, the detailed pathways of their action are still not comprehensively understood [99]. In addition, the ability of each drug to suppress immune cells and hence their secretion of inflammatory proteases might also vary depending on its individual pharmacodynamic properties, glucocorticoidal potency or other factors such as drug loading and hydrophobicity which can influence its controlled release kinetics. Among these glucocorticoids, the most effective drugs in suppressing cathepsin activity such as dexamethasone, flucortisones, and prednisolone appear to correlate with the highest glucocorticoidal potency [102].

ROS are oxygen-derived free radicals produced by several types of immune cells such as neutrophils and macrophages. They are activators of transcription factors  $\text{N}\kappa\text{-B}$  mediating cell and tissue injury during inflammation [158-161] and also play a role in degradation of aliphatic polyesters [162]. Any inhibitory effect of steroidal glucocorticoids on ROS activity is not apparent from the bioluminescent screening data, except for dexamethasone, the most potent steroid, which has previously been reported to be ROS-inhibiting by Selvam *et al* [163]

Polyphenols are a large family of naturally occurring plant products that are widely distributed in fruits, vegetables, nuts, seeds, flowers and bark [164]. These compounds are reported to be responsible for the blockage of the transcription factor  $\text{N}\kappa\text{-B}$  which is required for transcription of genes involved in the inflammatory responses [143, 165]. In our study, curcumin significantly inhibited ROS activity and cathepsin enzymes, albeit to a lesser extent. Histology analysis of curcumin-loaded PLGA microparticles excised from SKH1E mice during the first two weeks indicated that the recruitment of early inflammatory cells to these samples was effectively inhibited. Therefore, we could confirm that the reduced bioluminescent signal for curcumin-loaded microparticles resulted from the ability of this drug to inhibit cellular migration in the subcutaneous host response. Surprisingly, resveratrol did not reduce ROS or cathepsin expression though these two drugs belong to the same class of compounds and have been assumed to have similar mechanism of action [166-168].

Non-steroidal anti-inflammatory drugs (NSAIDs) bind to the hydrophobic active sites of cyclooxygenase (COX) enzymes to inhibit the COX-mediated generation of proinflammatory molecules

and hence limit the extent of inflammation, fever and pain [98, 102, 142]. Our study demonstrated that locally released NSAIDs, especially ketoprofen, were not effective in suppressing both cathepsin and ROS in the subcutaneous host response to implanted PLGA microparticles. This finding was surprising given numerous existing studies reporting the effectiveness of NSAIDs in alleviating inflammation when administered systemically [98, 102, 142] and a limited number of studies claiming the efficacy of their locally administered formulations in reducing fibrosis formation [6, 137]. However, Schneider *et. al.* has also demonstrated that when systemically administered, dexamethasone but not diclofenac, an NSAID, can modulate the host response to improve the survival of encapsulated myoblasts [132]. These discrepancies can potentially be explained by the difference in dosages or the pharmacodynamic properties of controlled-release NSAID formulations versus systemic administration of the same compounds.

In addition, other non-steroidal immunosuppressant drugs such as tacrolimus and cyclosporine whose potent properties result primarily from inhibition of T and B lymphocyte activation [141] did not effectively inhibit ROS or cathepsin enzymes. This finding is not surprising because the cell populations impacted by these drugs belong to the adaptive immune systems while the subcutaneous host response mainly involved innate immune cells such as neutrophils, macrophages and fibroblasts [2, 3, 169]. Furthermore, T and B lymphocytes are not known to produce ROS or cathepsin and hence the effects of these drugs on these adaptive immune cells, even if present, were not likely to be captured by our *in vivo* imaging assays.

Dexamethasone and curcumin, the most effective anti-inflammatory agents identified from the subcutaneous screening, were incorporated in hybrid drug-islet alginate capsules to mitigate fibrotic response against the transplanted capsules containing pancreatic rat islets. Fibrosis or pericapsular overgrowth has been implicated in the limited long-term survival of encapsulated islets in various animal models [24, 26, 126, 156, 170]. Cellular and collagen deposition on the surface of transplanted microcapsules has been reported to result in delayed insulin secretion in response to plasma glucose fluctuations, reduced nutrient transport and subsequent decrease in graft viability and function [24, 171, 172]. In our current capsule design, curcumin reduced fibrotic overgrowth, improved graft survival and function while dexamethasone did not. However, in the subcutaneous screening with PLGA microparticles, dexamethasone was able to inhibit cellular infiltration for a longer time period than curcumin. The effects of these two drugs on the encapsulated islet system did not correlate directly with their impact on the subcutaneously injected PLGA microparticles. Several major differences in these

two systems might be accountable for this discrepancy such as the encapsulating polymers, the administration sites, and the effects of the drugs on the encapsulated therapeutic cells.

Alginate is a non-degradable hydrophilic hydrogel [173, 174] while PLGA is a biodegradable hydrophobic polymer [2, 175-177]. The mechanism of drug release from the PLGA particles involves both passive drug diffusion out of the polymer pores and drug release due to the degradation of the polymer matrix [178, 179]. In contrast, only the diffusional mechanism influences the drug release kinetics from the non-degradable alginate capsules. In the intraperitoneal space, the close proximity between the drug-loaded alginate microcapsules and the intestinal vasculature could facilitate faster clearance of the drug and their metabolites resulting in more rapid drug diffusion outside of the alginate capsules. The less hydrophobic dexamethasone could have diffused into the intraperitoneal space faster than curcumin and thus the reservoir of encapsulated dexamethasone was exhausted more rapidly resulting in a loss of its inhibitory effect on the attacking immune cells. Residual curcumin remained in the alginate hydrogel capsules for a longer period of time (Supplementary Figure 4.11) and thus prolonged its effectiveness in mitigating the fibrotic response, possibly due to its lower aqueous solubility (0.6 $\mu$ g/ml at room temperature) [180] compared to that of dexamethasone (1mg/ml at 37°C) [181]. In the subcutaneous space, the diffusion and absorption of a drug and its metabolites into the surrounding vasculature is less effective than into the intraperitoneal space [182, 183]. There is potentially less significant difference between the release kinetics of dexamethasone and curcumin, so the potency in inhibiting cellular filtration is more dominant factor compared to drug solubility or hydrophobicity resulting in dexamethasone being more efficacious subcutaneously.

In addition, the incorporated drugs also have varying effects on the encapsulated islets. Dexamethasone and other potent synthetic steroids have been reported to have diabetogenic effect and inhibit insulin secretion from islets [34]. Even though potent glucocorticoids might be effective in mitigating the host response, they might not be efficacious for incorporation in cell-based therapeutics as it might adversely affects cell viability and function [35, 36]. In contrast, several studies have reported that due to its anti-oxidant capacity, curcumin can protect islets against pro-inflammatory cytokines *in vitro*, prevent the progression of diabetes *in vivo* and is effective in islet cryopreservation [184, 185]. These protective effects of curcumin on islets could be accountable for its ability to maintain better glycemic control and graft survival compared to dexamethasone in the hybrid drug-islet alginate microcapsules. Our findings suggested that the subcutaneous screening approach is valuable in narrowing the choices of promising anti-inflammatory drugs; however, the efficacy of each drug



candidate for a desired application still needs to be further evaluated in medically relevant context to take into account other application-specific factors.

Several strategies could potentially be explored in future studies to improve the efficacy of the drug-islet hybrid capsules. Firstly, improved release kinetics of less hydrophobic anti-inflammatory agents such as dexamethasone can potentially be achieved by covalently attachment of the drug to the alginate hydrogel via a degradable linking moiety such as an ester group or a hydrazide group. Hydrolysis of the linking ester groups *in vivo* can release dexamethasone at a slower rate over an extended period of time to match the cellular recruitment timeline of the host response. Secondly, a combination of both dexamethasone and curcumin or other combinations of anti-inflammatory agents might have the potential to act synergistically in suppress immune responses against non-self materials. However, in this case, the effects of potential overdose, systemic toxicity or drug interference must be carefully considered. Thirdly, a next generation of hybrid drug-islet capsules can be designed to have a core-shell structure in which the cells are encapsulated in the inner core and the anti-inflammatory drugs are encapsulated within an external shell. In this future design, the drug and the therapeutic cells will be compartmentalized in two different layers within the hydrogel capsules. Confining the drug to the surface of the hydrogel capsules facilitates outward drug diffusion, maximizes drug interaction with immune cells, and minimizes its interference with the therapeutic cells inside.

## 4.6. CONCLUSION

In this study, we performed comparative characterization of a variety of small molecule anti-inflammatory drugs utilizing both non-invasive *in vivo* imaging and end-point histology. Dexamethasone and curcumin were most effective in inhibiting the activities of early inflammatory proteases and reactive oxygen species as well as minimizing cellular infiltration and collagen formation in the subcutaneous host response to implanted PLGA microparticles. Application of this finding to immunolated islets for the treatment of type I diabetes showed that curcumin was able to improve glycemic control and mitigate the formation of pericapsular overgrowth on alginate microcapsules transplanted into chemically-induced diabetic mice. Therefore, *in vivo* screening of the anti-inflammatory agents in the subcutaneous space is a useful strategy for rapid identification of promising small molecule drugs which can minimize host response to implanted biomaterials. We believe that our findings have potential applications in a broad range of implantable medical devices and cell transplantation therapies for the treatment of neurodegenerative diseases and hormone deficiencies.

**Table 4.1: Small molecule anti-inflammatory drugs investigated in the *in vivo* subcutaneous screening.** Different classes of compounds including naturally-derived polyphenols, NSAIDs, non-steroidal immunosuppressants and steroidal glucocorticoids were screened in hairless immunocompetent SKH-1E mice. For most compounds, several formulations with different percentages of drug loading were tested.

Compound name	Theoretical drug loading (wt%)	Drug classification
Curcumin	15, 10, 5	Polyphenol
Resveratrol	15	Polyphenol
Ketoprofen	15	NSAIDs (COX-1 inhibitor)
Diclofenac	15	NSAIDs (COX-1 inhibitor)
Sunlindac	15	NSAIDs (COX-1 inhibitor)
Piroxicam	15	NSAIDs (COX-1 inhibitor)
Celecoxib	15, 10, 5	NSAIDs (COX-2 inhibitor)
Rapamycin	15, 10, 5	Non-steroid immunosuppressant
Tacrolimus	15, 10, 5	Non-steroid immunosuppressant
Cyclosporin	15, 10, 5	Non-steroid immunosuppressant
Dexamethasone	10, 5, 2	Steroidal glucocorticoid
Fludrocortisone	15, 10, 5	Steroidal glucocorticoid
Methylprednisolone	15, 10, 5	Steroidal glucocorticoid
Prednisolone	10, 5	Steroidal glucocorticoid
Prednisone	15, 10, 5	Steroidal glucocorticoid
Hydrocortisone	15, 10, 5	Steroidal glucocorticoid

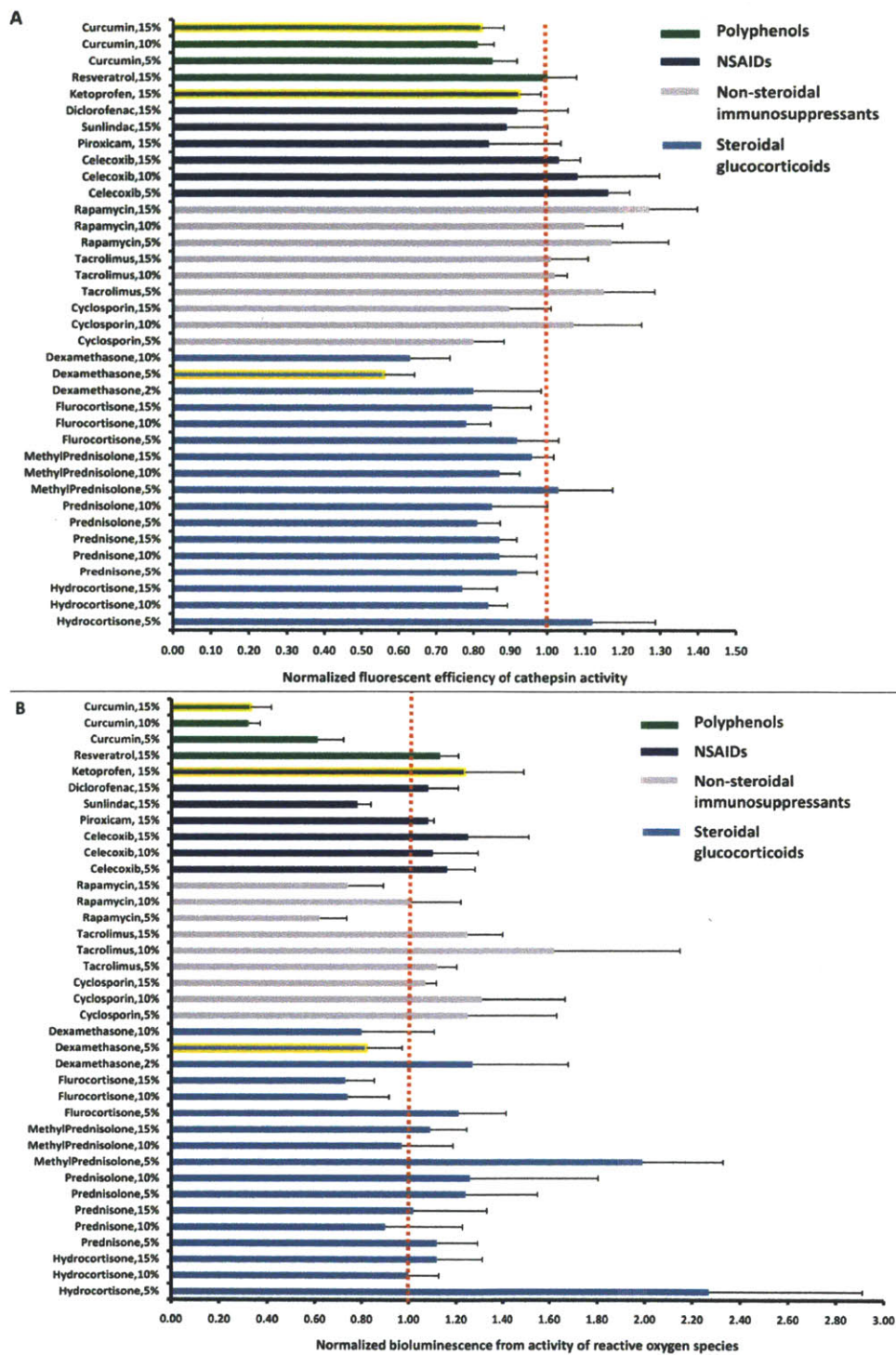


**Figure 4.1: *In vivo* subcutaneous screening of anti-inflammatory drugs encapsulated in PLGA microparticles.**

**A)** Activity of cathepsin enzymes was quantified using Prosense 680, a fluorescence-activated imaging probe. **B)** Presence of reactive oxygen species was quantified using luminol which emits bioluminescence when oxidized by ROS. Relative fluorescent or bioluminescent signal was calculated as a ratio of the signal from the drug-loaded microparticles to that from the control particles in the same mice. Each data point represents the average signal  $\pm$  s.e.m (n=6 replicate injections).

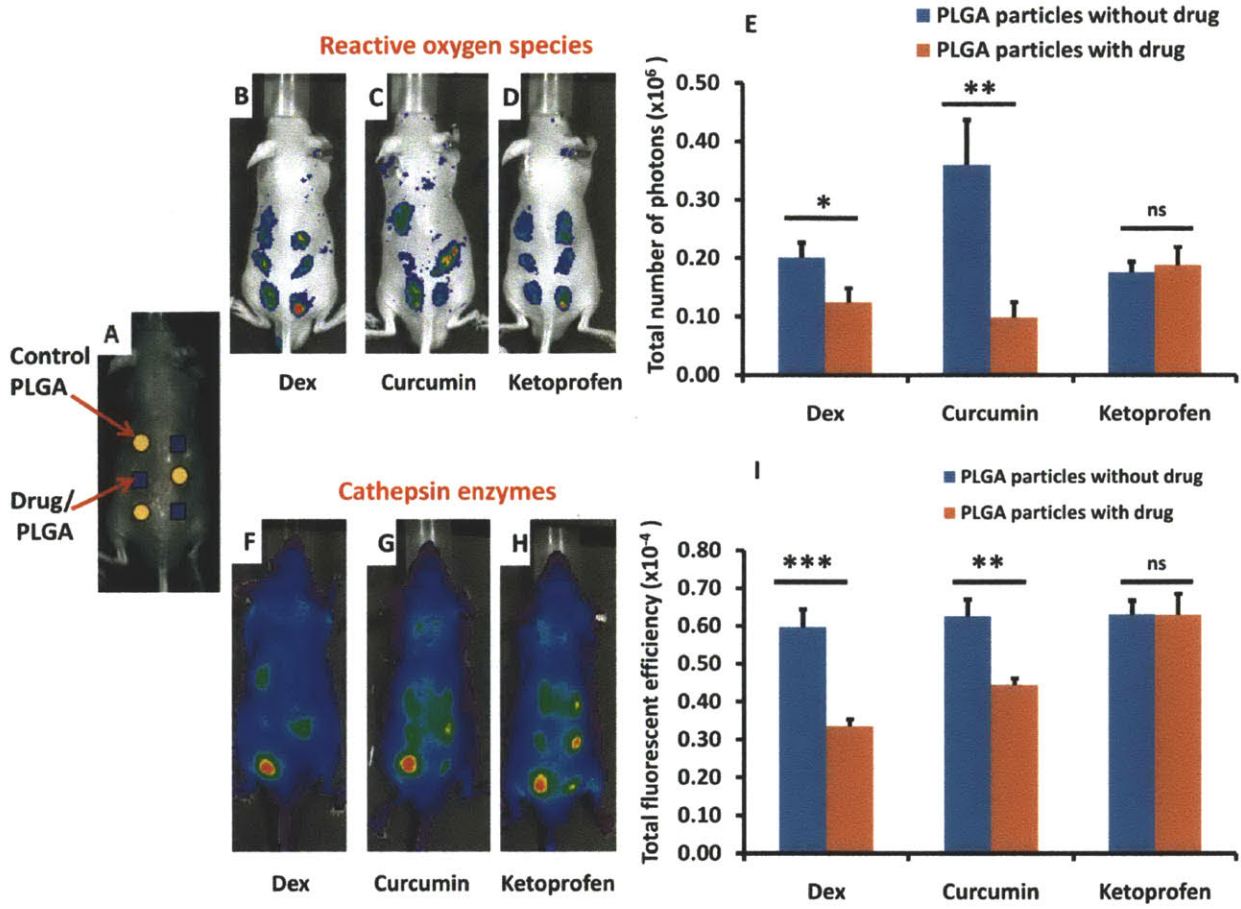


**Figure 4.2: Effects of selected drugs on the peak activities of cathepsin enzymes and ROS in the subcutaneous host response to PLGA microparticles.**

**A)** Injection pattern of the PLGA microparticles without (●) and with drugs (■). **B-D)** Bioluminescent images of representative mice on day 2 at the peak of ROS activity. **E)** Quantification of the bioluminescent signals on day 2 (n=15 replicate injections) showed that curcumin significantly reduced ROS activity at the implant sites. Dexamethasone also caused a slight decrease while ketoprofen did not affect ROS production. **F-H)** Fluorescent images of representative mice on day 9 at the peak of cathepsin activity. **I)** Quantification of the fluorescent signal on day 9 (n=15 replicate injections) showed that dexamethasone reduced this protease activity significantly. Curcumin caused a less significant decrease while ketoprofen did not affect cathepsin activity. Each data point represents the average signal ± s.e.m. (\*, \*\*, \*\*\* denotes p<0.05, 0.01, 0.0001 respectively).

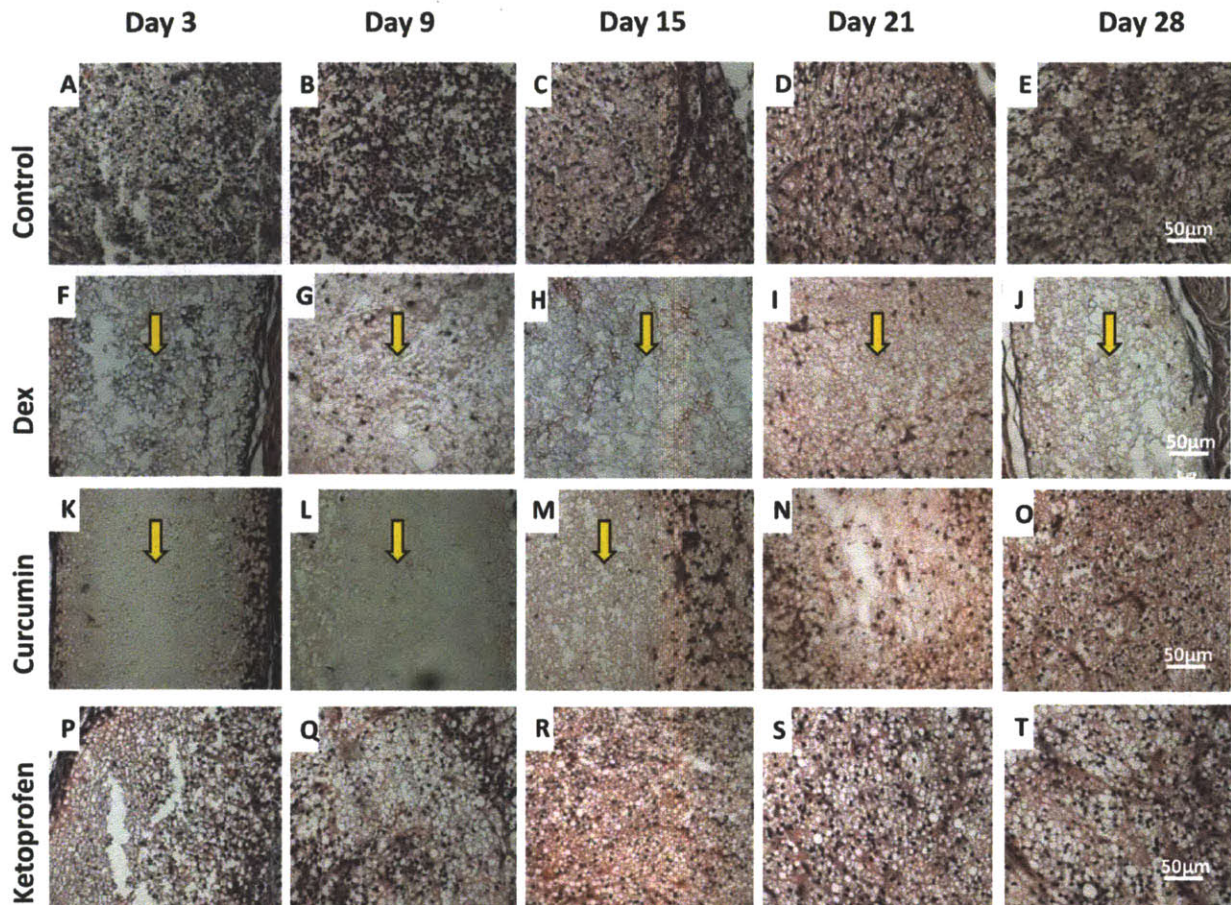


**Figure 4.3: Histology analysis of subcutaneously injected PLGA microparticles with and without drugs excised from SKH-1E mice at different time points over a period of 28 days.**

Scale bar represents 50µm for all images. Yellow arrows indicate areas with minimal infiltration of immune cells. **A-E)** Samples with the control microparticles showed the typical time-course of the subcutaneous host response with neutrophil infiltration at the earlier time points (A-B) and macrophage recruitment as well as collagen deposition at the later time points (C-D). **F-J)** Samples containing dexamethasone showed minimal infiltration of immune cells or formation of collagen matrix throughout the 28 day duration. **K-O)** Samples containing curcumin remained free of immune cells and collagen matrix during the first two weeks (K-M) but gradual macrophages and collagen were present at later time points (N-O). **P-T)** Samples containing ketoprofen showed the similar pattern of cellular and collagen infiltration as the control particles.

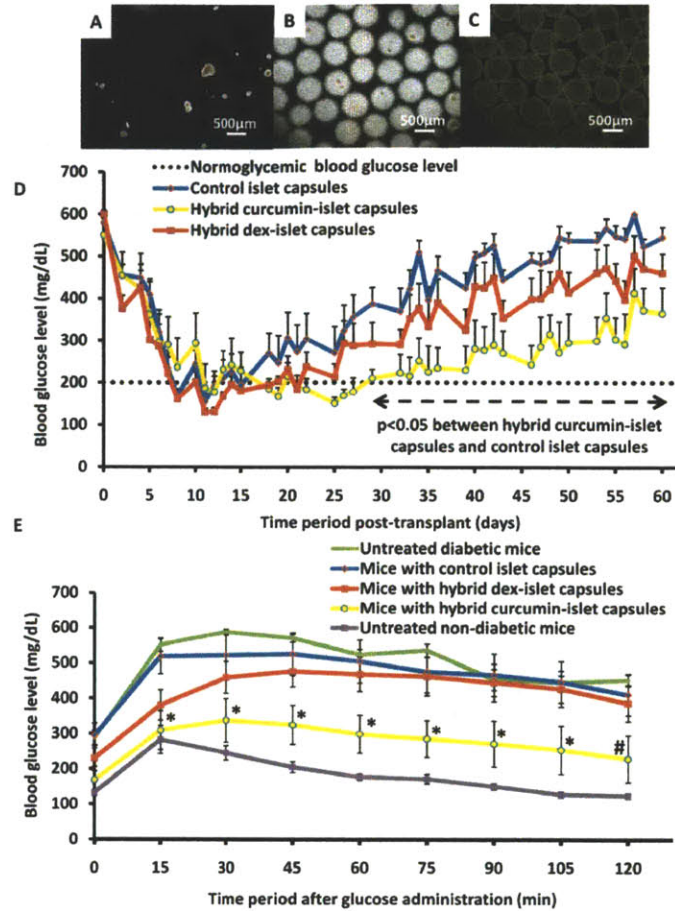


**Figure 4.4: Effects of hybrid drug-islet capsules on glycemic control of STZ-induced diabetic mice transplanted with a marginal islet mass of 250 IE.**

**A-C)** Phase contrast images of alginate microcapsules without any drug (A), with dexamethasone (E) and curcumin (F). **D)** Daily non-fasting blood glucose level of STZ-induced diabetic C57B6/J mice transplanted with control islet capsules (n=7), capsules containing dexamethasone (n=7) and curcumin (n=6) co-encapsulated with islets isolated from Sprague-Dawley rats. Improved glycemic control and prolonged graft function by islets co-encapsulated with curcumin. **E)** Fasting blood glucose level of the same groups of mice during the IPGTT on day 60. Mice transplanted with islets co-encapsulated with curcumin were able clear glucose most effectively compared to the other two microcapsule formulations. (\*) and (#) represent p<0.01 and p<0.05 respectively, indicating a statistically difference between the blood glucose levels of mice with curcumin-loaded capsules and control capsules.

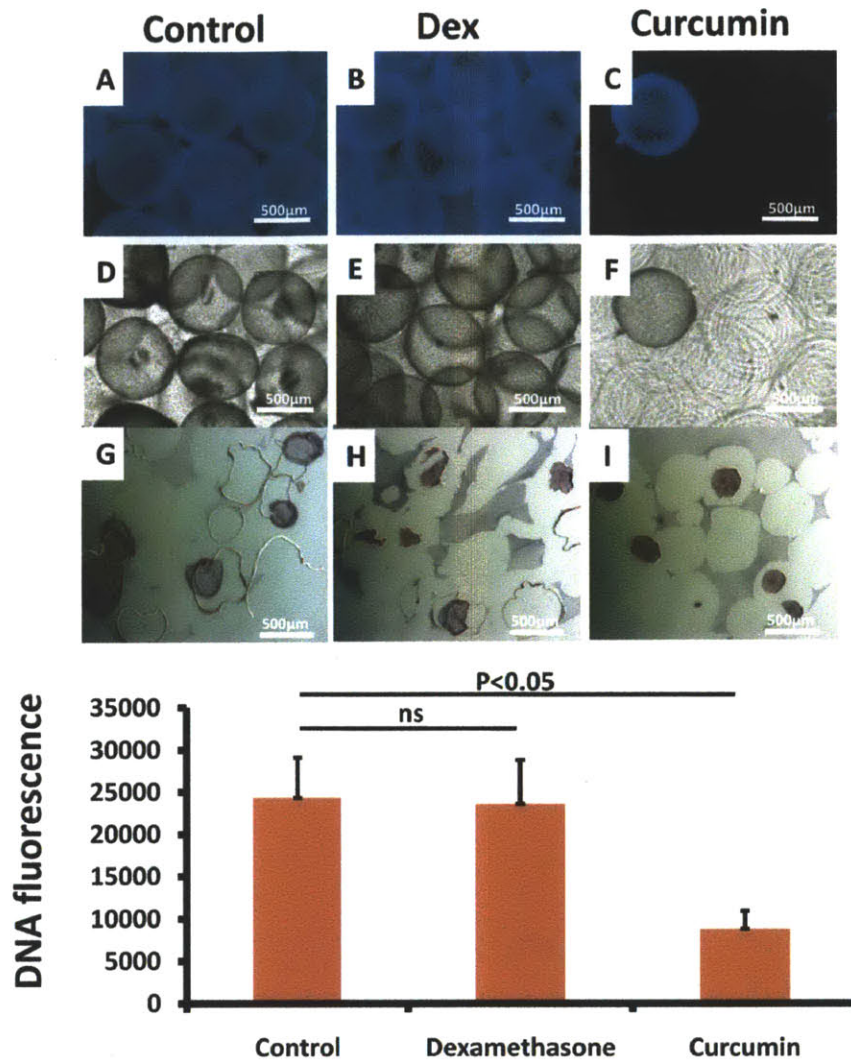


**Figure 4.5: Characterization of fibrotic pericapsular overgrowth on microcapsules retrieved 60 days after transplantation into STZ-induced C57B6J diabetic mice.**

**A-C)** Fluorescent images of retrieved control microcapsules (A) and microcapsules with dexamethasone (B) or curcumin (C) after DNA staining with Hoestch 33342 dye. **D-F)** Phase contrast images of the same control microcapsules (D) and microcapsules with dexamethasone (E) or curcumin (F). **G-I)** Histology H&E sections of retrieved control microcapsules (G) and microcapsules with dexamethasone (H) or curcumin (I). **J)** Quantification of fluorescent signals from the three types of retrieved microcapsules. Each data point represent the average signal  $\pm$  s.e.m (n=6 or 7)

## 4.7. SUPPLEMENTARY INFORMATION

### 4.7.1. Supplementary results

#### 4.7.1.1. Subcutaneous screening of different formulations of anti-inflammatory drugs

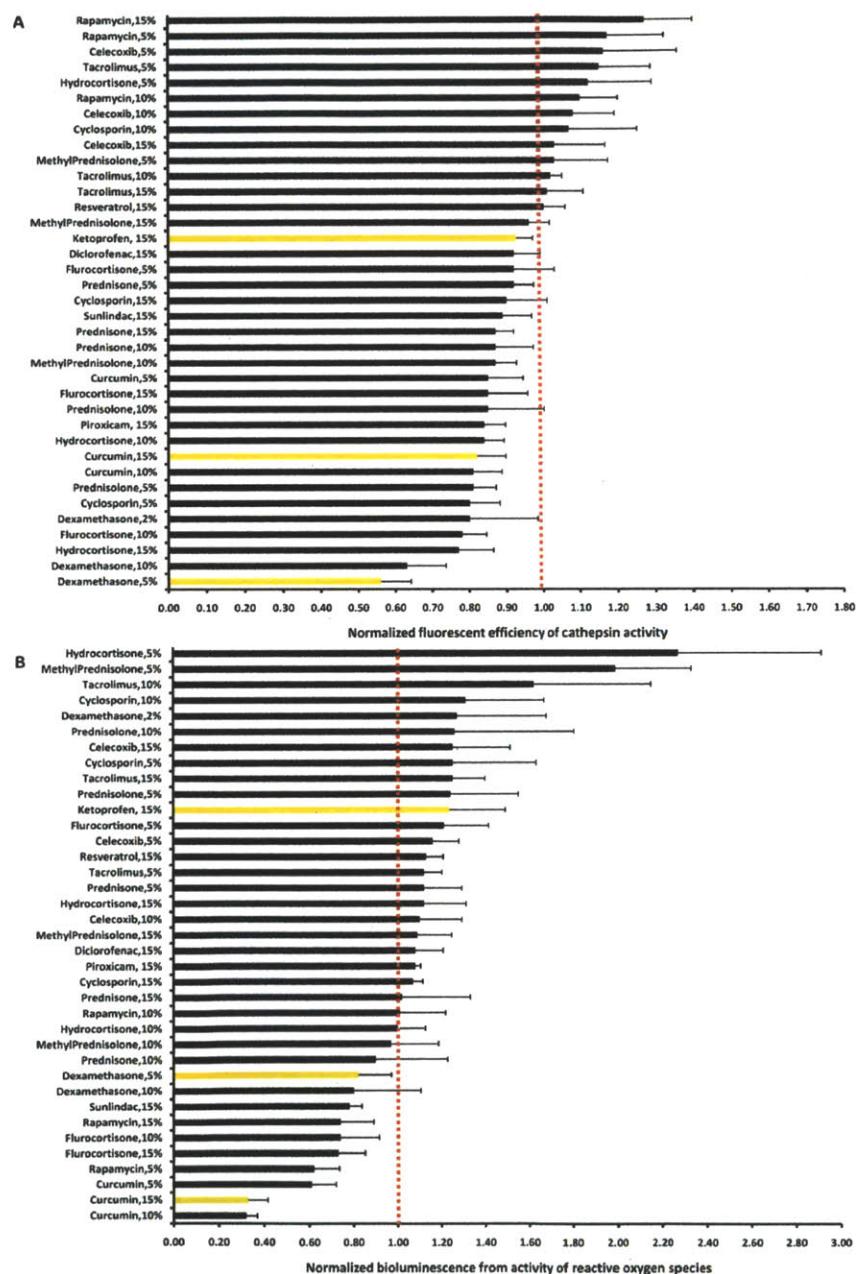


**Figure 4.6:** *In vivo* subcutaneous screening of anti-inflammatory drugs encapsulated in PLGA microparticles.

Data arranged in order of decreasing relative fluorescent or bioluminescent signals. **A)** Activity of cathepsin enzymes was quantified using Prosense 680, a fluorescence-activated imaging probe. **B)** Presence of reactive oxygen species was quantified using luminol which emits bioluminescence when



oxidized by ROS. Relative fluorescent or bioluminescent signal was calculated as a ratio of the signal from the drug-loaded microparticles to that from the control particles in the same mice. Each data point represents the average signal  $\pm$  s.e.m (n=6 replicate injections).

#### 4.7.1.2. Temporal evolution of inflammation markers in the host response

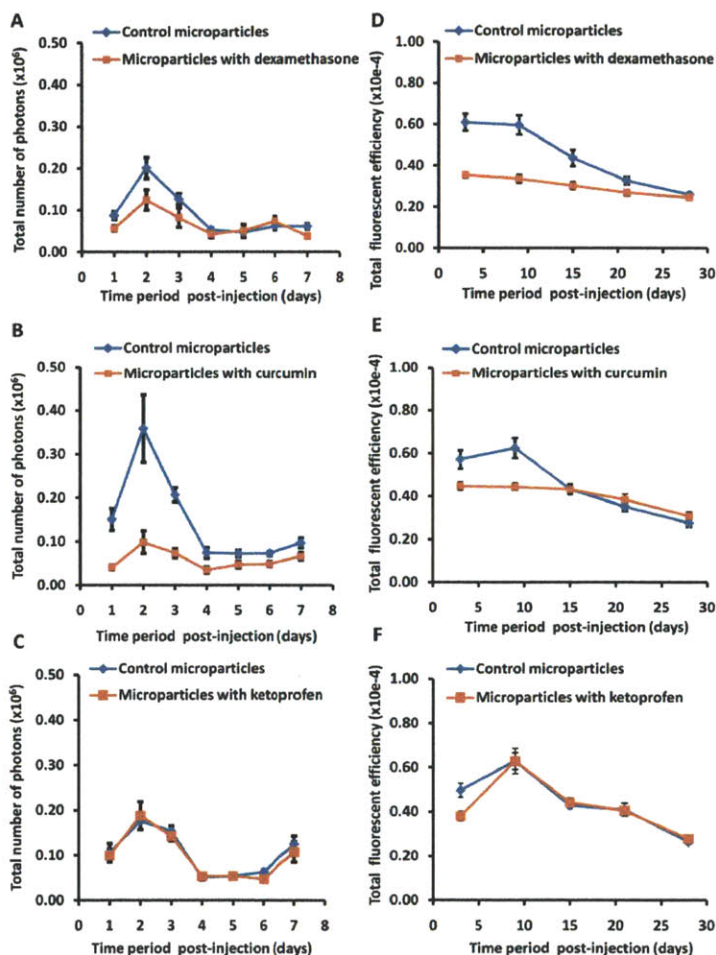


**Figure 4.7: Temporal evolution of cathepsin enzymes and ROS in the host response to PLGA microparticles with and without drugs.**

**A-C)** Quantified time-lapse bioluminescent signals from PLGA microparticles with dexamethasone (A), curcumin (B) and ketoprofen (C) in comparison with control PLGA microparticles in the first seven days after subcutaneous injection. ROS activity was the highest in the first three days for the control particles. During these three days, curcumin-loaded microparticles also showed the most significant suppression of bioluminescent signals. **(D-F)** Quantified time-lapse fluorescent signals from PLGA microparticles with dexamethasone (D), curcumin (E) and ketoprofen (F) in comparison with control PLGA microparticles during the 28 days after subcutaneous injection. Cathepsin activity was the highest in the first 15 days for the control particles. During these 15 days, dexamethasone-loaded microparticles also showed the most significant suppression of fluorescent signals. Each data point represents the average signal  $\pm$  s.e.m (n=15 replicate injections).

#### 4.7.1.3. Analysis of excised PLGA microparticles to determine the presence of residual drugs

To determine whether the drugs were still present in the PLGA microparticles in the subcutaneous space of SKH-1E mice, the microparticles were retrieved from mice sacrificed on day 28. Figure 4.8A-C showed the excised polymer spots for the three different drugs; the presence of curcumin is evident by its intrinsic yellow color in Figure 4.8B. Since ketoprofen and dexamethasone could not be visually detected by their white color, the excised samples corresponding to these two drugs were liberated from surrounding fibrotic tissue by collagenase digestion and analyzed by HPLC to determine the presence of any remaining drug. HPLC analysis of these two samples (Figures 4.8D-E) confirmed that ketoprofen and dexamethasone were present in the samples excised on day 28. Our *ex vivo* analysis proved that the absence of inhibitory effects by ketoprofen (for the entire four week duration of the experiment) and curcumin (after the first two weeks) was not due to the exhaustion of the encapsulated drugs. The data confirmed that, despite their presence till day 28, ketoprofen and curcumin were not effective in suppressing the infiltration of host immune cells in the subcutaneous space at these time points.

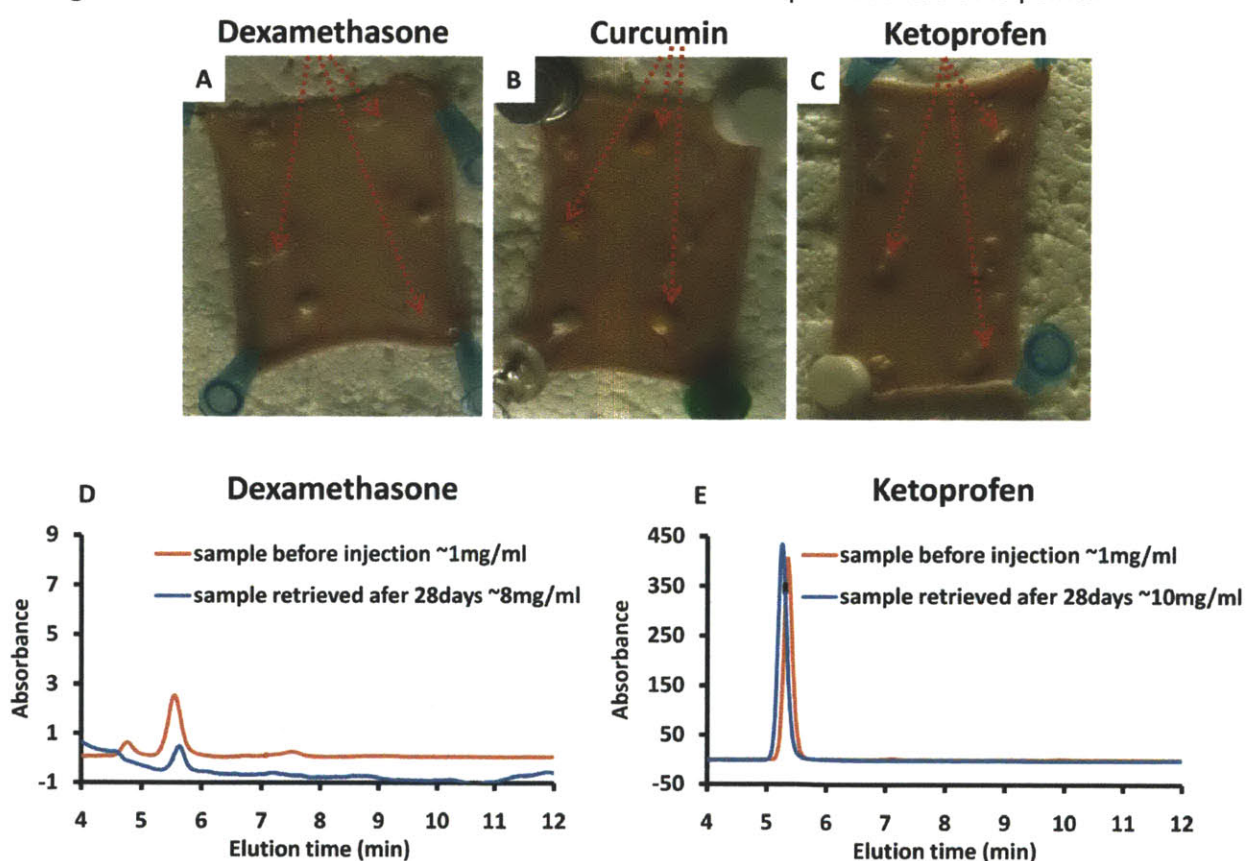


**Figure 4.8: Ex-vivo analysis of PLGA microparticles excised from SKH1E mice at day 28.**

**A-C)** Colored pictures of excised skin tissues containing PLGA microparticles with dexamethasone (A), curcumin (B) and ketoprofen (C). The microparticles in (B) remained yellow indicating the presence of curcumin. **D-E)** HPLC analysis of excised PLGA microparticles from (A) and (C) showed absorbance peaks in (D) and (E) corresponding to dexamethasone and ketoprofen respectively. This data confirmed the presence of these two drugs in the microparticles at day 28.

#### 4.7.1.4. Determination of marginal islet mass for transplantation in diabetic mice

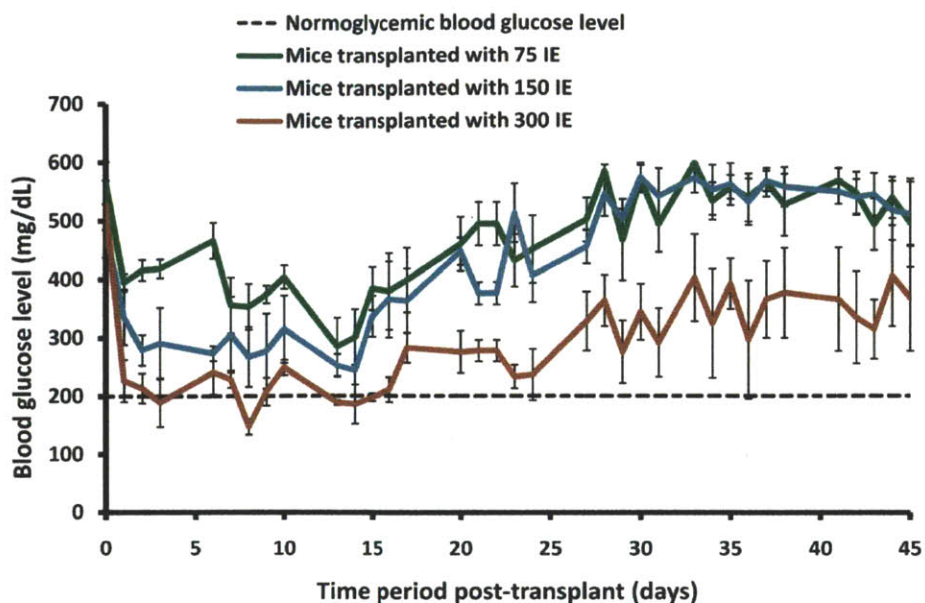


**Figure 4.9: Blood glucose concentrations in STZ-induced diabetic C57B6/J mice depended on the transplanted mass of encapsulated Sprague–Dawley rat islets.**

In the range of 75-300IE, a higher islet mass resulted in lower average blood glucose level (n=3, error bar represents s.e.m). With an islet mass of 300IE, the average blood glucose level remains close to normoglycemic level (~200mg/dl) for about 2 weeks. An islet mass of 250IE was chosen as a marginal mass for evaluation of hybrid drug/islet capsules.

#### 4.7.1.5. Establishing DNA fluorescent staining as a quantitative method for fibrosis assessment

To validate that DNA fluorescent staining with Hoestch 33342 dye can be used as a method to quantify fibrosis formation on retrieved capsules, we stained 20 samples of capsules retrieved on day 60 after intraperitoneal transplantation into STZ-induced diabetic mice. Each sample was visually observed under a light microscope by five different blinded investigators who gave semi-quantitative scores for the percentage of fibrotic capsules. The quantified fluorescent signal from each sample was plotted against the average score from the visual observation (Figure 4.5C) confirming a good linear correlation between the two methods ( $R^2 = 0.883$ ).

In addition, we also stained control samples of the same volumes of empty alginate capsules and encapsulated islets. Both of these samples were freshly prepared and have not been exposed to *in vivo* environment. The samples of freshly encapsulated islets contained islets at a pre-encapsulation density of 1000IE/ml of alginate. Assuming each islet equivalent was a sphere of 150 $\mu$ m diameter, the volume occupied by the islet tissue was approximately 0.18% the total volume of alginate. At this low islet density, the amount of islet DNA was so minimal that the fluorescent signal from the freshly encapsulated islets was the same as that from the empty alginate capsules (Figure 3.5D). The data in Figure 4.5D also confirmed that these two control samples did not emit significant fluorescent signals compared to the transplanted capsules retrieved from diabetic mice. Therefore, we could confirm that the measured fluorescent signals from the retrieved capsules primarily came from the DNA of fibrotic cell layers and not from DNA of the encapsulated islets.

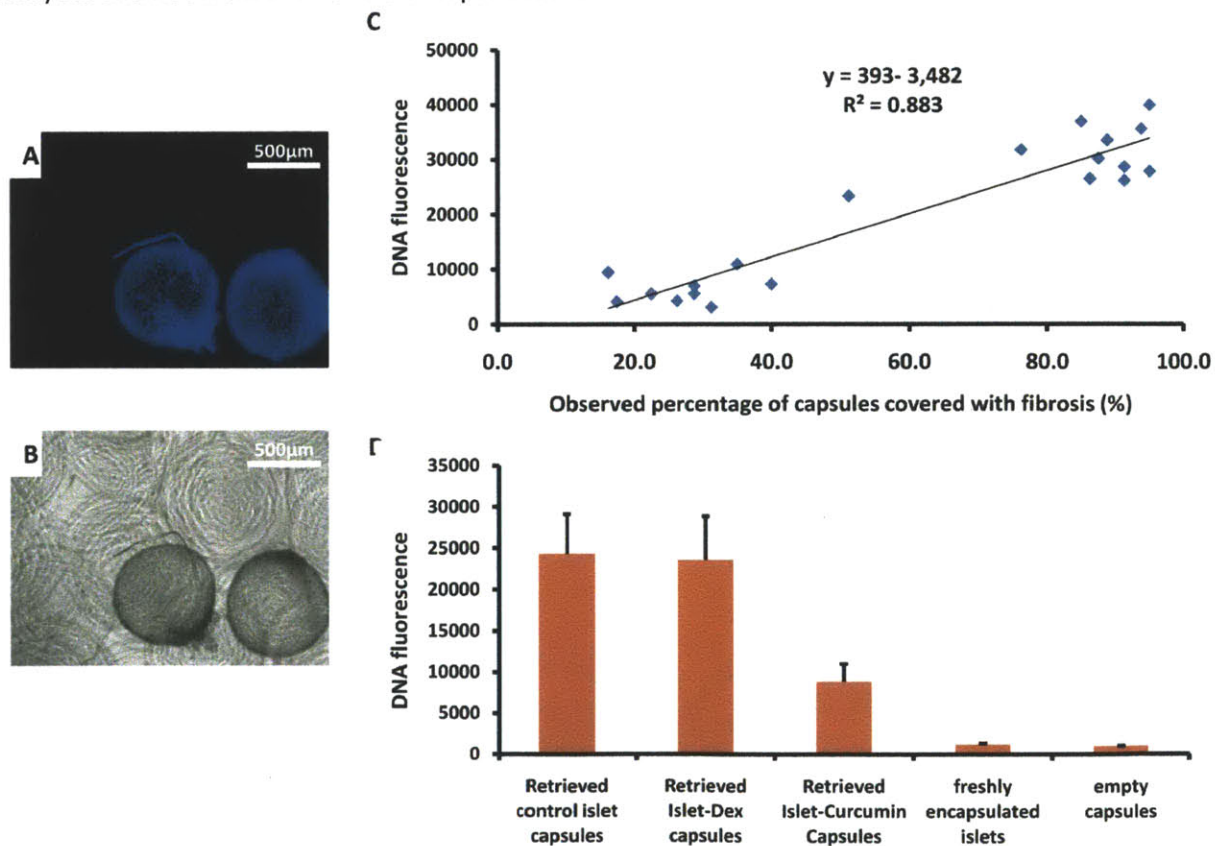
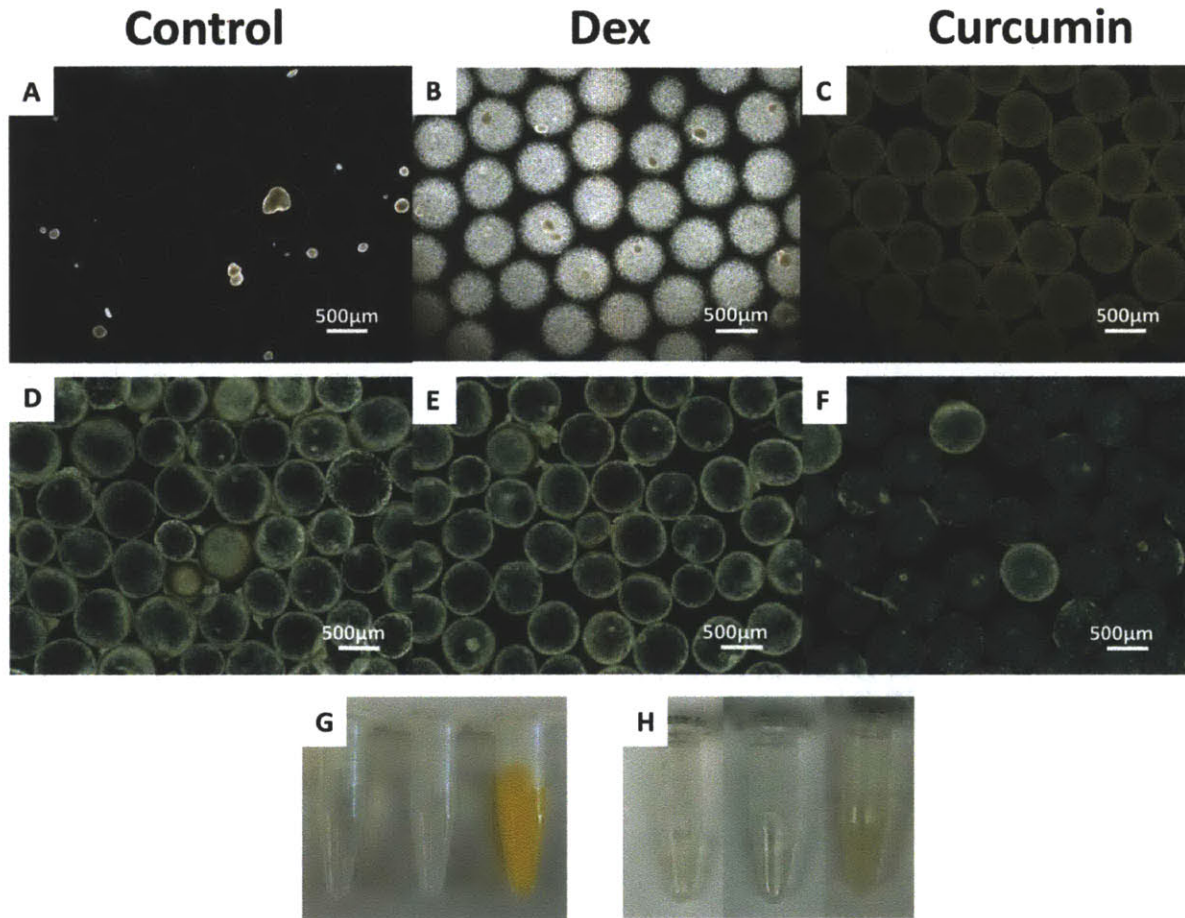


Figure 4.10: DNA fluorescent staining correlated with fibrosis scoring by observation.

**A)** Fluorescent image of retrieved capsules showing blue fluorescent signal for fibrotic capsule and no fluorescence from clean capsules. **B)** Phase contrast image of the same capsules showing fibrotic capsules covered with darker cell layers and transparent clean capsules. **C)** Linear correlation with an R-square value of 0.883 between quantified DNA fluorescent signals and average percentage of fibrotic capsules as visually scored by 5 blinded investigators. **D)** No significant fluorescent signal was detected for the same volume of freshly prepared empty alginate capsules or capsules containing islets at a density of 1000 IE/ml.

*4.7.1.6. Residual drugs from hybrid islet-drug capsules explanted after two months*



**Figure 4.11: Comparison of alginate capsules containing islets before transplantation and after retrieval from C57B6/J diabetic mice on day 60.**

**A-C)** Freshly prepared capsules containing rat islets with or without drug . Control capsules without drug (A) were transparent while capsules with dexamethasone (B) appeared cloudy white and capsules with curcumin (C) appeared yellow due to the intrinsic color of the drugs. **D-F)** Capsules explanted on day 60 after transplantation into STZ-induced diabetic C57B6/J mice. Control capsules (D) and capsules with dexamethasone (E) were covered with fibrotic cell layers while capsules with curcumin (F) remained mostly free of overgrowth. **G)** Colored photographs of eppendorf tubes containing the same freshly-prepared capsules as shown in A-C. From left to right are control capsules, capsules with dexamethasone and with curcumin respectively. **H)** Colored photographs of eppendorf tubes containing

the same explanted capsules as shown in D-F. From left to right are explanted control capsules, capsules with dexamethasone and with curcumin respectively. The yellowish color of the retrieved curcumin-containing capsules indicated the presence of residual curcumin.

#### **4.7.2. Supplementary materials and methods**

##### *4.7.2.1. Detection of residual drug in ex-vivo tissue by HPLC analysis*

PLGA microparticles with encapsulated drugs and surrounding tissue were retrieved 28 days after subcutaneous injection. The microparticles and their surrounding fibrotic cellular layers were gently detached from the skin tissue and placed in an Eppendorf tube containing 1.5ml of 0.2% (w/v) solution of collagenase enzyme type IV (Invitrogen) in  $\text{Ca}^{2+}/\text{Mg}^{2+}$  free HBSS buffer. The tube was placed on a rotational shaker (LabQuake) and incubated at 37°C for 45min with vortexing at every 15 minute interval till all the collagen surrounding the microparticles were digested and the microparticles were released from the fibrotic cell layers. The particles were then washed in deionized water three times to remove the collagenase, flash-frozen with liquid nitrogen and lyophilized till dryness. These lyophilized particles were dissolved in acetonitrile at a concentration of 8-10mg/ml and analyzed with a HPLC (Agilent Technology) following protocols previously reported. The analysis was performed using an Atlantis dC-18 5 $\mu\text{m}$  4.6x250mm reverse phase column (Waters) and a mobile phase of 35:65 (v/v) phosphate buffer to acetonitrile at a constant flow rate of 1ml/min. Sample detection by UV absorbance was recorded at 246 nm and 256nm for dexamethasone and ketoprofen respectively. Drug-loaded microparticles, which have not been injected into SKH1E mice, were also analyzed using the same HPLC methods but at a concentration of 1mg/ml in acetonitrile.

## **CHAPTER 5 – MICROFABRICATION OF CELL-LADEN, ASYMMETRIC HYDROGEL MICROCAPSULES**

The content of this chapter has been published in whole or in part in the following peer-reviewed journal article:

**Dang TT**, Xu Q, Bratlie KM, O’Sullivan ES, Chen XY, Langer R, Anderson DG. “Microfabrication of Homogeneous, Asymmetric Cell-laden Hydrogel Capsules.” **Biomaterials** 2009; 30(36): 6896-6902

### **5.1. ABSTRACT**

Cell encapsulation has been broadly investigated as a technology to provide immunoprotection for transplanted endocrine cells. Here we develop new fabrication methods that allow for rapid, homogenous microencapsulation of insulin-secreting cells with varying microscale geometries and asymmetrically modified surfaces. Micromolding systems were developed using polypropylene mesh, and the material/surface properties associated with efficient encapsulation were identified. Cells encapsulated using these methods maintain desirable viability and preserve their ability to proliferate and secrete insulin in a glucose-responsive manner. This new cell encapsulation approach enables a practical route to an inexpensive and convenient process for the generation of cell-laden microcapsules without requiring any specialized equipment or microfabrication process.

### **5.2. INTRODUCTION**

Cell encapsulation is a strategy to allow for the transplantation of non-autologous cells without the use of immunosuppressive drugs, which have potentially severe side-effects [20, 186-188]. Transplanted living cells are protected from the host immune system because they are encapsulated in a semi-permeable hydrogel membrane which allows the diffusion of nutrients and cellular metabolic products while excluding antibodies and immune cells [189]. This technique has potential applications as therapies for many diseases such as diabetes, hormone deficiencies or hepatic failure [188].

Encapsulated islets have been explored as a method to allow transplantation of allogenic or xenogeneic insulin-secreting cells into diabetic hosts [190-195]. Electrostatic droplet generation is the most widely used method in the production of microcapsules containing islets or other insulin-secreting cells [196]. Typically, a laminar liquid jet is broken into droplets by a harmonically vibrating nozzle combined with an electrostatic dispersion mechanism which prevents droplet aggregation [197]. Currently, droplet generator encapsulation systems are commercially available from several manufacturers such as Inotech Biosystem (Rockville, MD) and Nisco Engineering AG (Zürich,

Switzerland). The electrostatic droplet generator system is appropriate for the continuous production of hydrogel microcapsules (200-600  $\mu\text{m}$  in diameter) from a polymer/cell mixture of an unchanged composition [197]. However, this apparatus, which requires sterilization of the bioreactor chamber after each use, is not convenient for studies which involve screening a large number of different material formulations [198]. Furthermore, this approach does not allow for generation of non-spherical capsules. Therefore, it is desirable to develop new and convenient methods for fast generation of geometrically controlled, cell-laden microcapsules.

Soft-lithography with PDMS molds has been used to fabricate alginate hydrogel microcapsules in 2D arrays as well as discrete single modules [199-202]. Many living cells, including bacteria and mammalian cells, have been encapsulated in hydrogels with this approach [199-202]. However, a potential challenge for this technique is the difficulty of releasing the microcapsules from the PDMS mold without damaging the cells. Even though methods such as mechanical stretching of the mold, swelling the hydrogel capsules in organic solvent [199] or microtransfer molding [201, 203] have been applied to facilitate capsule release, these processes decrease cell viability and capsule yield [201, 202]. Whitesides *et al.* recently demonstrated the production of cell-laden microcapsules using a PDMS membrane with fully penetrating pores to improve the ease of capsule retrieval [204]. However, this method is still limited by the necessity of a microfabrication process to generate the PDMS membranes and the difficulty of obtaining membranes of large area.

Here, we describe an inexpensive and convenient approach utilizing a commercially available polypropylene mesh for the fabrication of cell-laden hydrogel microcapsules without using any specialized equipment or microfabrication processes. The *in vitro* viability, proliferation and insulin secreting function of the encapsulated cells were characterized. We also demonstrated the fabrication of capsules with different geometries and selective modification of the microcapsule surface using this mesh-based fabrication approach.

## **5.3. MATERIALS AND METHODS**

### **5.3.1. Fabrication of alginate hydrogel capsules**

Thermo-molded plastic meshes were purchased from McMaster-Carr and Industrial Netting. The plastic meshes were cut into pieces of 4x3  $\text{cm}^2$  and placed in a Chex-all® II instant sealing pouch. These meshes were autoclaved at 121 °C and kept sterile until use. Sodium alginate (FMC BioPolymer, LF 10/60 LS), with or without materials to be encapsulated, was dissolved in 0.9% NaCl solution at a concentration



of 1.5wt%. When encapsulation of microspheres or cells was desired, 1wt% solid solution of 1 $\mu$ m red fluorescent microspheres (Invitrogen, Eugene, OR) were diluted 500-fold with this 1.5wt% alginate solution while INS-1 cells were suspended in alginate at a density of 1.5x10<sup>6</sup>cells/mL. The resulting mixture was vortexed to obtain a homogeneous mixture which was then centrifuged at 200xg for three minutes. The air bubbles at the top of the mixture were removed by aspiration before this suspension was poured into a sterile Petri dish. A piece of sterile mesh was lightly dipped onto the cell/alginate mixture with the less reflective surface of the mesh in contact with the suspension. Excess alginate was removed by gently wiping the mesh against the edge of a sterile Petri dish. The mesh was immediately immersed in a solution of 100 mM CaCl<sub>2</sub> and subsequently transferred to HEPES buffer (132mM NaCl, 4.7mM KCl, 25mM HEPES, 1.2mM MgCl<sub>2</sub>) for mild washing. The hydrogel capsules were finally released by holding the mesh with a pair of tweezers and gently agitating it in a collecting solution.

### **5.3.2. Asymmetric surface modification of hydrogel capsules**

Before the capsules were released from the mesh template into the collecting solution, one side of the mesh containing cross-linked hydrogels were gently placed on the liquid surface of a 4mg/mL solution of 40-70kDa FITC-labeled poly-L-lysine (Sigma Aldrich, St Louis, MO) for 3 minutes. The mesh was then gently washed in HEPES buffer before the capsules were released into a collection medium.

### **5.3.3. Cell culture**

The rat insulinoma cell line (INS-1) was a gift from the Joslin Diabetes Center (Boston, MA). INS-1 cells at passages of 7-20 were cultured according to a protocol previously described [205]. The cells were cultured in complete medium composed of RPM1 1640 supplemented with 10 mM HEPES, 10% heat-inactivated fetal calf serum (FCS), 2 mM L-glutamine, 100 U/ml penicillin, 100  $\mu$ g/ml streptomycin, 1 mM sodium pyruvate, and 50  $\mu$ M 2-mercaptoethanol. Cultures were incubated at 37 °C in a humidified 95% air-5% CO<sub>2</sub> atmosphere and manipulated under sterile tissue culture hoods. Confluent dish of INS-1 cells was passaged every week at a subculture ratio of 1:3 and fed every 2-3 days. For trypsinization, the adherent cells were exposed to 0.025% trypsin-EDTA solution to yield a cell suspension which was centrifuged at 150xg at 4 °C for 3 min. For preparation of frozen cell stock, freshly trypsinized cells were suspended in complete medium containing 10% of dimethyl sulfoxide and kept at -80°C overnight in a Nalgene® Cryo Freezing container before being transferred to liquid nitrogen for long-term storage.

### **5.3.4. Viability analysis of encapsulated cells**

The viability of INS-1 cells in alginate microcapsules was characterized using the Live/Dead® Viability/Cytotoxicity Assay Kit (Molecular Probe, Carlsbad, CA). Microcapsules were incubated in HEPES buffer containing fluorescent dyes at the concentrations of 2  $\mu$ M Calcein-AM and 12  $\mu$ M ethidium homodimer-1 for 45 minutes. The capsules were washed with HEPES buffer and visualized under a Nikon TE 300 inverted microscope under either phase contrast or fluorescent microscopy settings. Green fluorescence was viewed under a FITC filter and red fluorescence under a TRITC filter. Images were photographed using a CCD camera and Metamorph imaging software (Molecular Devices, Sunnyvale, CA). Confocal images were taken using a Zeiss LSM 510 confocal microscope with an argon excitation source. For live cell imaging, excitation wavelength of 488 nm and a filter set of 505-537 nm were used. Dead cells were imaged using an excitation wavelength of 543 nm and an emission filter set of 559-623 nm.

### **5.3.5. Static glucose-stimulated insulin secretion**

Five 500  $\mu$ l aliquots of microcapsules containing INS-1 cells were cultured over a period of 10 days. At the desired time points, the capsules were subjected to a static glucose stimulation study following a procedure slightly modified from a protocol elsewhere [206]. Briefly, the capsule samples were pre-incubated for one hour in Krebs Ringer buffer Hepes (KRBH) (137 mM NaCl, 4.8 mM KCl, 1.2 mM  $\text{KH}_2\text{PO}_4$ , 1.2 mM  $\text{MgSO}_4 \cdot 7\text{H}_2\text{O}$ , 2.5 mM  $\text{CaCl}_2 \cdot 2\text{H}_2\text{O}$ , 5 mM  $\text{NaHCO}_3$ , 16 mM HEPES, 0.1% (w/v) BSA, pH 7.4) containing 2.8 mM glucose. The *in vitro* insulin secretion was then assessed by consecutive incubations of the capsules in 4 mL of KRBH containing 2.8 mM glucose or 16.8 mM glucose for one hour. The samples were kept at 37 °C in humidified air and 5%  $\text{CO}_2$  for the duration of the pre-incubation and stimulation. The capsules were washed with HEPES buffer in between two incubations to remove residual insulin. At the end of each incubation, 1000  $\mu$ l of the KRBH was removed and frozen at -20 °C for storage before insulin assay. Insulin concentrations were determined using Ultrasensitive EIA assay kits (ALPCO Diagnostics, Salem, NH).

## **5.4. RESULTS AND DISCUSSION**

### **5.4.1. Properties of template meshes for successful capsule fabrication**

We fabricated the alginate hydrogel microcapsules using a process illustrated in Figure 5.1. Briefly, the sterile polymer mesh with an array of uniform pores is brought in gentle contact with the alginate solution (1.5% w/v aqueous solution) with or without materials to be encapsulated. After capillary force completely fills the pores with the alginate solution, the mesh is held vertically so that most of the

excess alginate is removed by gravity. The mesh surface was subsequently wiped against the flat edge of a sterile petri dish to further remove any excess alginate. This polymer mesh containing uniform pores filled with alginate was immediately dipped into an aqueous solution of calcium chloride which cross-links the alginate polymer chains into a hydrogel. After mild washing in HEPES buffer, the hydrogel microcapsules are released by holding the mesh with a pair of tweezers and gently agitating it in a collection solution of culture medium. Figure 5.2A shows large sheets of thermo-molded polypropylene mesh and Figure 5.2B is a mesh template with an array of uniform pores typically used in this fabrication process. Figures 5.2C and 5.2D shows the different pore shapes of the polypropylene meshes from McMaster-Carr and Industrial Netting respectively.

After testing several types of commercial polymer meshes from different suppliers, we determined that the surface properties of the polymer mesh are critical for successful fabrication of individual alginate capsules. Table 5.1 shows the feasibility of capsule formation and retrieval for a variety of thermoplastic meshes manufactured from nylon, polypropylene and Teflon. Filling of mesh pores by alginate solution was classified as easy (+) for instant pore wetting and liquid retention or as difficult (-) if the alginate failed to remain in the pores. Capsule retrieval was considered easy (+) if more than 80% of the freestanding microcapsules are released from the mesh pores instantly during the agitation step. If the capsules formed are connected by a thin film of residual alginate, the retrieval process is considered difficult (-). We observed that meshes made from Teflon are too hydrophobic and the alginate solution is unable to fill the pores. This is similar to observations of trapped air bubbles in PDMS molds[199] and membranes [204] due to the hydrophobic nature of PDMS before surface treatment by oxygen plasma. On the other hand, nylon meshes are too hydrophilic and the alginate solution forms interconnected capsules easily, even after the excess alginate is removed by wiping against the edge of the petri dish. Only polypropylene mesh appears to possess appropriate surface property which enables fabrication of individual free-standing capsules. Furthermore, polypropylene has a high heat-resistant ability which makes it desirable for cell encapsulation applications. Its softening and melting temperatures of 152 °C and 161 °C respectively ensure that the mesh property is unaffected during autoclave sterilization at 121 °C.

#### **5.4.2. Fabrication of hydrogel capsules with different shapes and asymmetrically modified surfaces**

Various microcapsule shapes can potentially be useful as building blocks for engineering of 3D tissue constructs or investigating the effect of hydrogel geometries on the viability, proliferation and

functions of encapsulated cells [207, 208]. Figure 5.3A and 5.3B shows microscopy images of alginate hydrogel capsules fabricated from different mesh templates to produce capsules with rectangular cuboidal and cylindrical shapes. The non-spherical geometries achieved with this mesh template technique complement the spherical capsules produced by conventional droplet generator systems. We are also able to modify a selected surface of the microcapsules by dipping one side of the mesh containing cross-linked hydrogels onto a desired coating material. Figure 5.3C and 5.3D show a bead-encapsulating capsule with FITC-labeled poly-L-lysine modifying a selected surface. Figure 5.3C is the confocal image with only red fluorescence displayed, showing red 1  $\mu\text{m}$  beads encapsulated in a rectangular cuboidal capsule. In Figure 5.3D, the same capsule is visualized with both red and green fluorescence channels, indicating that a green layer of positively-charged FITC-Poly-L-Lysine was selectively coated on one side of the negatively charged alginate capsule. Such asymmetrically modified capsules with two surfaces of opposite charges might have applications in the directed assembly of cell-laden hydrogel capsules for fabrication of 3D tissue constructs [207].

### **5.4.3. Fabrication of hydrogel capsules containing insulin-secreting cells**

To illustrate the applicability of this technique in the encapsulation of insulin-secreting cells, we chose a cell line (INS-1) derived from x-ray-induced insulinoma in rats[205] to fabricate cell-laden hydrogel microcapsules. Alginate microcapsules containing these cells were fabricated following the procedure shown in Figure 5.1 using a suspension of INS-1 cells in 1.5% alginate. Since the presence of cells has an important effect on the rheological properties of alginate, a series of experiments were performed to identify optimal maximum cell-packing density (data not shown). Figures 5.4A and 5.4B shows cell-laden microcapsules fabricated using polypropylene meshes from McMaster (Item #9265T41) and Industrial Netting (Item # XN6080) respectively. The initial cell densities in these microcapsules are in the optimal range of  $1.5 - 2.0 \times 10^6$  cells/cm<sup>3</sup>. This range of maximum initial cell density is comparable to that achieved with the conventional droplet generation method [197].

### **5.4.4. Assessment of viability, proliferation and function of encapsulated cells**

#### *5.4.3.1. Fabrication of hydrogel capsules containing insulin-secreting cells*

We studied the viability and proliferation behavior of the encapsulated cells cultured *in vitro* for a period of ten days. Figures 5.4C and 5.4E show the phase contrast and fluorescent images of the three-day microcapsules fabricated from mesh XN6080 with live/dead staining. This viability assay differentiates live and dead cells on the basis of intracellular esterase activity and plasma membrane

integrity. In this assay, live cells fluoresce green due to the presence of intracellular esterase which converts the nonfluorescent cell-permeable calcein-AM to an intensely green fluorescent product. On the other hand, ethidium homodimer-1 permeates compromised cell membranes and result in the red appearance of dead cells when this dye undergoes enhanced fluorescence upon binding to cellular nucleic acids. After three days in culture, more than 80-90% of the cells were still alive. These viable single cells appeared as individual green dots in Figure 5.4E while some dead cells stained red were also observed. This small fraction of dead cells possibly arose from the original cell stocks or from minimal cell injury during the encapsulation process. After ten days in culture, the encapsulated cells have also proliferated and formed larger clusters as observed in Figure 5.4D and 5.4F. The ten-day hydrogel capsules contained mostly viable cells as shown in Figure 5.4F. Confocal microscopy was also used to examine the 3D distribution of cells throughout the entire microcapsule. Figure 5.5A shows a single capsule at high magnification. Figure 5.5B is the combined projection of multiple images taken at different depths of the same capsule (each optical slice is of 2.5  $\mu\text{m}$  for a total thickness of 200  $\mu\text{m}$ ). Figure 5.5C shows a projected image of the capsule along its diagonal confirming that most cell clusters are alive. These cell clusters are about 20-50  $\mu\text{m}$  in diameter. They are also uniformly viable and homogeneously distributed in all spatial dimensions of the capsules. These results indicate nutrient transport throughout this capsule geometry is sufficient to maintain cell viability and proliferation.

#### 5.4.3.2. *Static glucose-stimulated insulin secretion*

We also performed a static glucose challenge to assess the ability of the encapsulated INS-1 cells to maintain their desired glucose-responsive functions. Figure 5.6 shows the insulin secretion from the cell-laden capsules cultured over a period of ten days in response to two different glucose concentrations. Glucose levels of 2.8 mM and 16.5 mM were used to simulate the physiological basal and hyperglycemic conditions of diabetic patients respectively. At all time points investigated (3 days, 6 days and 10 days) the encapsulated cells were able to maintain the desired glucose-responsive behavior. These cells secreted a higher insulin concentration (1.5 to 3-fold) when subjected to the higher glucose level. The absolute amount of insulin secreted also increases over time confirming that the cells are proliferating in the capsules.

## 5.5. CONCLUSION

Here we have developed an approach for the fabrication of alginate microcapsules containing functional insulin-secreting cells. This technique can be utilized to fabricate non-spherical capsules of

different geometries and unlike conventional droplet methods, allows for asymmetric modification of the surfaces of the microcapsules. The surfaces of such capsules can be asymmetrically tailored with functional coatings of different charges or polarities to introduce directionality to the capsules. This strategy potentially allows for the directed assembly of cell-laden hydrogel capsules by controlling their alignments and orientation for the generation of biomimetic tissue constructs with desired microscale architecture and complexity. In addition, the polymer mesh is mechanically and thermally robust. Thus it can be easily handled and sterilized by autoclaving. The entire encapsulation process using the polypropylene mesh can be conveniently carried out inside a sterile tissue culture hood. This mesh-based method offers a complementary approach to the existing droplet generator system for the fabrication of cell-laden hydrogel capsules. We believe that utilizing an inexpensive and commercially available mesh offers straightforward access to tissue engineers and biologists as this avoids any specialized equipment, making this approach more convenient for widespread use in biological laboratories.

**Table 5.1: Relationship between the feasibility of microcapsule formation and the properties of a variety of thermoplastic meshes.**

Pore filling and capsule release are classified as easy (+) or difficult (-). Assessment of capsule release is not applicable (n/a) if pore filling is unsuccessful. All other meshes were purchased from IndustrialNetting, except mesh 9265T41(\*) from McMaster-Carr.

Sample ID	Mesh Material	Pore shape	Estimated pore dimension (um)	Estimated mesh thickness (um)	Pore filling with alginate	Capsule release
NN-1400	Nylon-6	square	890x890	380	(+)	(-)
NN-1500	Nylon-6	square	710x710	380	(+)	(-)
NN-1800	Nylon-6	square	380x380	510	(+)	(-)
NN-1700	Nylon-6	square	250x250	510	(+)	(-)
9265T41 (*)	Polypropylene	rectangular	530x690	300	(+)	(+)
XN-6080	Polypropylene	rectangular	530x690	360	(+)	(+)
XN-6070	Polypropylene	rectangular	630x760	360	(+)	(+)
XN-7110	Polypropylene	circular	650 (diameter)	360	(+)	(+)
ET-8300	PTFE	diamond	1140x630	460	(-)	(n/a)
ET-8120	PTFE	diamond	630x130	200	(-)	(n/a)

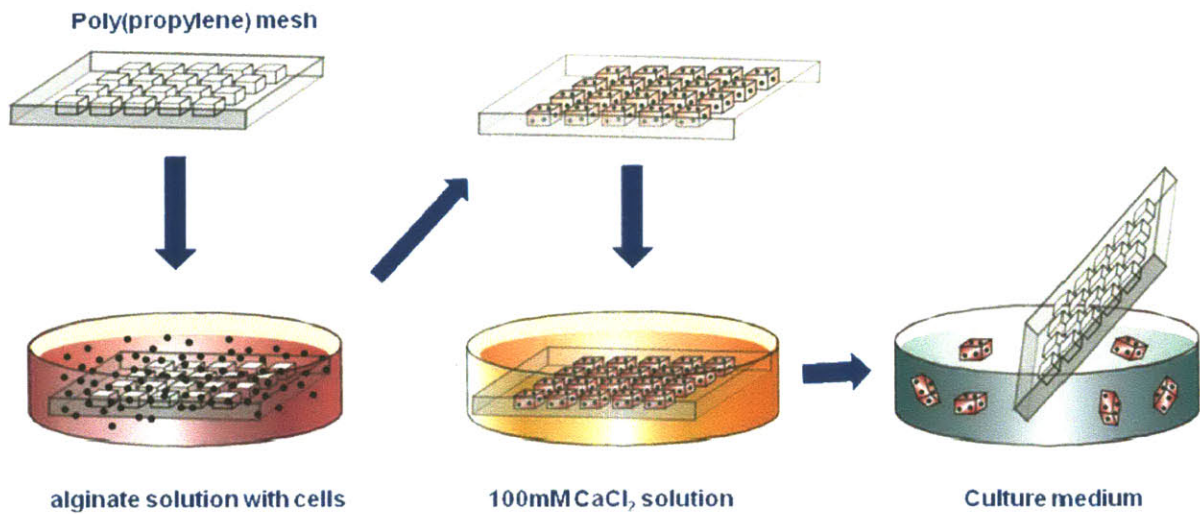


**Figure 5.1: Schematic illustration of the procedure to fabricate alginate microcapsules**

The mesh template is dipped into an alginate solution with or without cells and transferred to a 100mM CaCl<sub>2</sub> solution for cross-linking. Hydrogel microcapsules are released by gently agitating the mesh in cell culture medium.



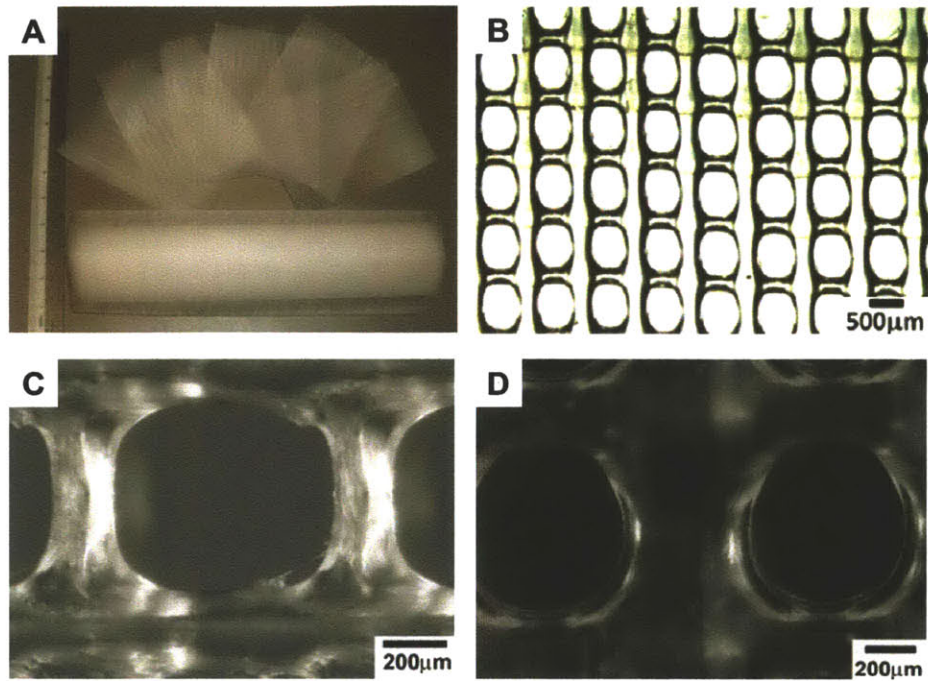


**Figure 5.2: Images of polypropylene meshes used for microcapsule fabrication.**

(A) Photograph of large sheets of thermo-molded polypropylene mesh utilized in microcapsule fabrication. (B) Light microscopy images of mesh templates with an array of uniform pores. Polypropylene meshes with rectangular (C) and circular pores (D).

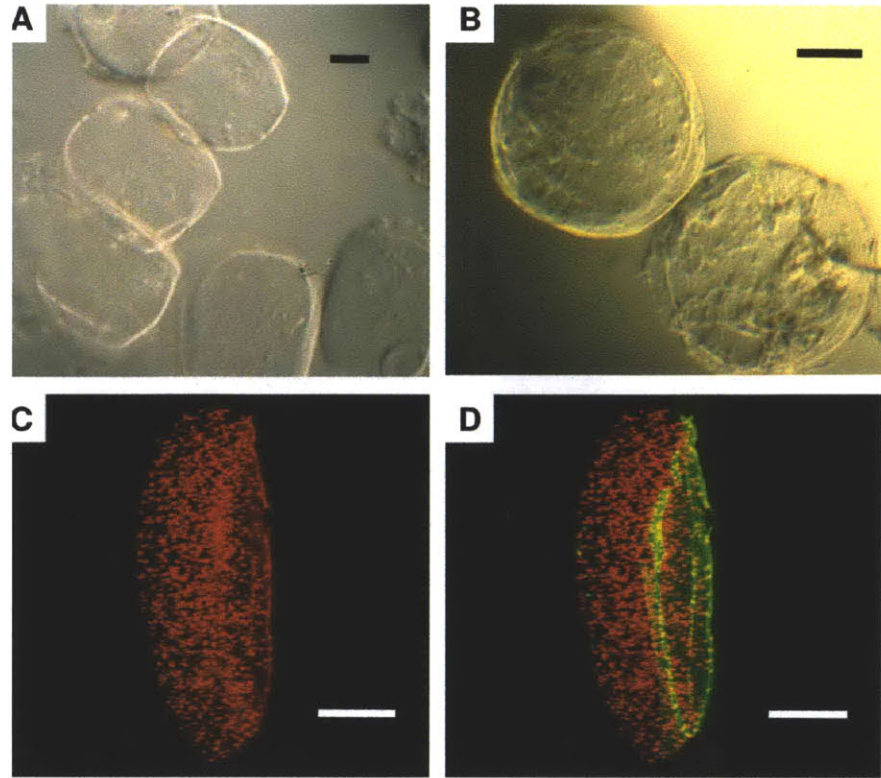


**Figure 5.3: Microcapsules with different geometries and asymmetric modification.**

Light microscopy image of rectangular cuboidal (A) and cylindrical (B) hydrogel capsules. Confocal microscopy images of a rectangular cuboidal capsule encapsulating red fluorescent microbeads with only red fluorescence displayed (C) and the same capsule with both red and green fluorescences displayed (D). A green layer of FITC-Poly-L-Lysine was coated on one side of the capsule. All scale bars represent 200 $\mu$ m

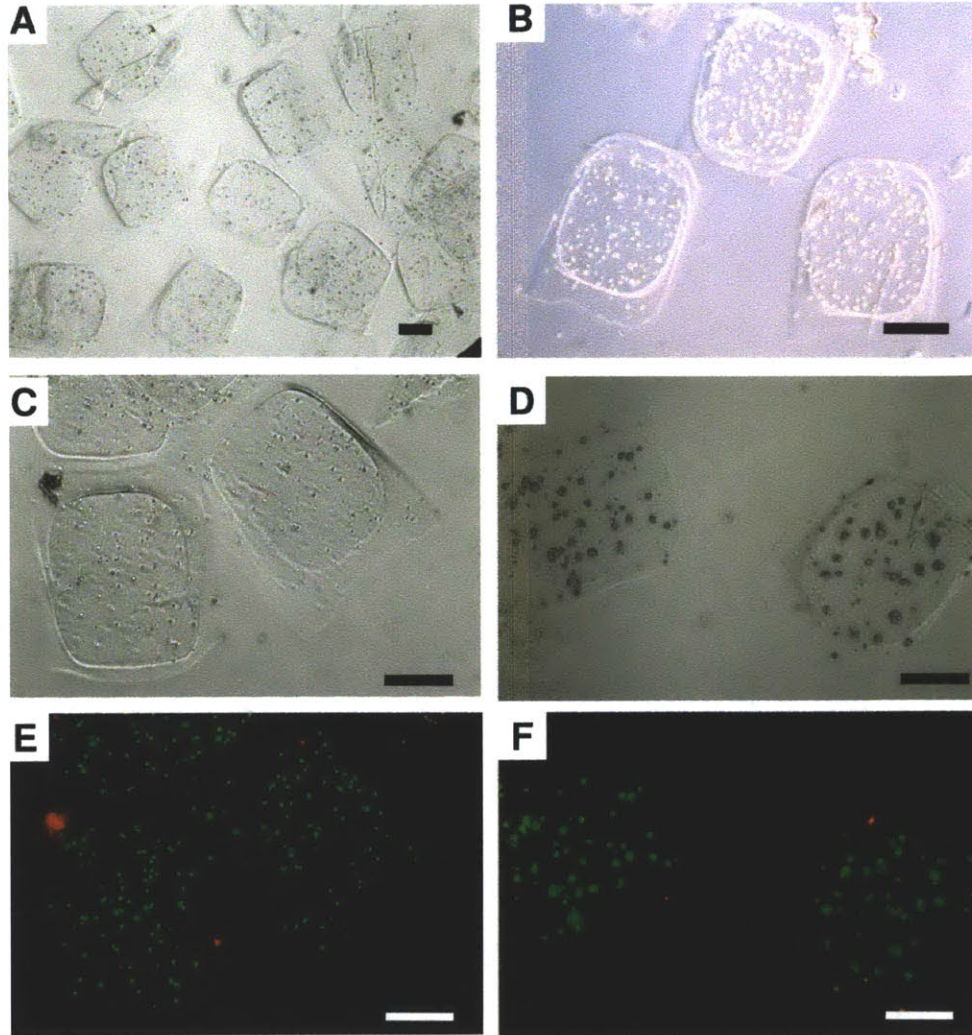


**Figure 5.4: Light and fluorescent microscopy images of alginate microcapsules containing INS-1 cells.** Microcapsules fabricated using (A) mesh 9265T41 and (B) mesh XN-6080 at cell densities of  $1.5 \times 10^6$  cells/mL and  $2.0 \times 10^6$  cells/mL, respectively. Three-day capsules (C) contain single cells which proliferate into larger clusters after ten days (D). Staining of the same capsules with viability markers shows that three-day single cells (E) and ten-day cell clusters (F) maintain good viability. All scale bars represent  $300\mu\text{m}$ .

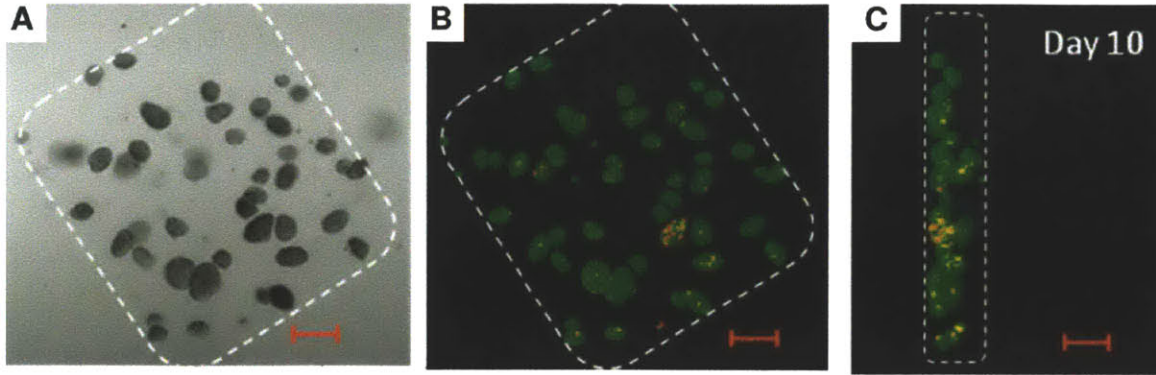


**Figure 5.5: Viability and homogeneous distribution of cell clusters in a single microcapsule.**

(A) Differential Interference Contrast image of a single microcapsule containing INS-1 cell clusters after ten days in culture. Confocal microscopy of the top view (B) and side view (C) along the diagonal of the same capsule shows homogeneous cell distribution and viability. Dashed line indicates the edge of the microcapsule. All scale bars represent 100µm.

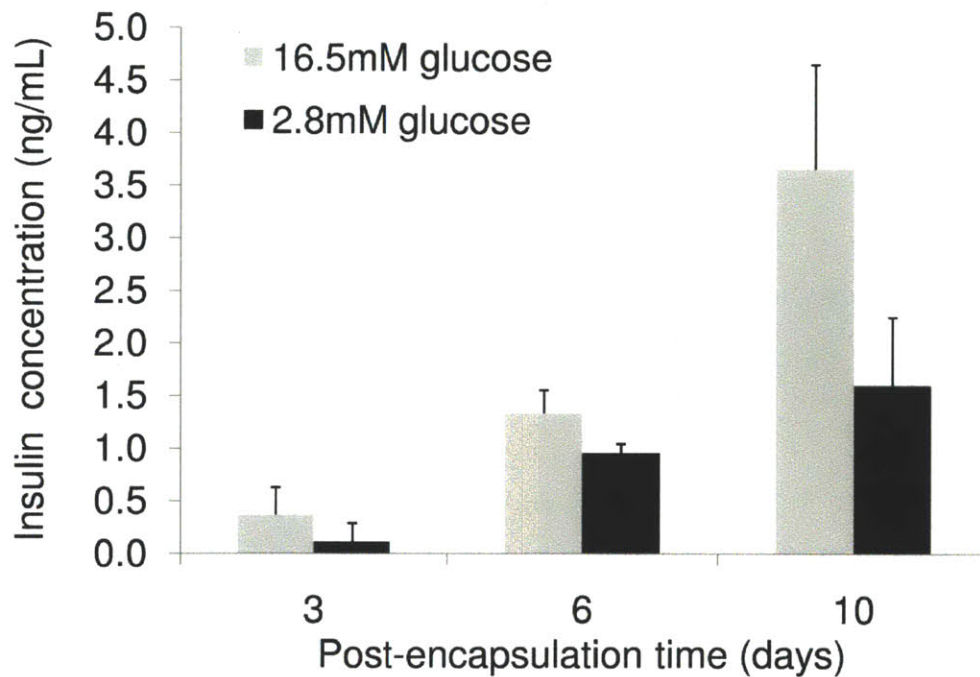


**Figure 5.6: Insulin secretion of encapsulated INS-1 cells over a period of ten days.**

Values are the mean ( $\pm$  S.D) from five independent experiments. Cells maintain glucose-responsive function; and insulin secretion also increased over time confirming cell proliferation.

## **CHAPTER 6 – CONCLUSION AND RECOMMENDATION FOR FUTURE WORK**

### **6.1. CONCLUSION**

In this thesis research, new non-invasive imaging techniques have been developed for parallel *in vivo* biocompatibility analysis of multiple materials and drug formulations using time-lapse fluorescent and bioluminescent imaging. Systematic subcutaneous *in vivo* screening of several classes of small molecule anti-inflammatory drugs was performed using the new imaging techniques to understand their effects on the biomaterial-induced generation of reactive oxygen species and inflammatory proteases. Dexamethasone and curcumin were selected from the screening study for incorporation into hybrid hydrogel microcapsules co-encapsulating donor pancreatic islets for evaluation in a mouse model of chemically induced diabetes. The results demonstrated that the hybrid capsules containing curcumin led to reduced fibrotic response to encapsulated islets and improved their efficacy in glycemic control.

### **6.2. RECOMMENDATION FOR FUTURE WORK**

Firstly, improved release kinetics of the anti-inflammatory agents can potentially be achieved by covalently attachment of the drug, such as dexamethasone, to the hydrogel polymer forming the capsule via a degradable linking moiety such as an ester group or a hydrazide group. Hydrolysis of linking ester groups *in vivo* can release dexamethasone at a slower rate over an extended period of time. Alternatively, anti-inflammatory drugs can also be encapsulated in drug-loaded biodegradable polymeric particles for controlled release. However, the choice of the polymer for the fabrication of these particles must be selective to avoid degradation products that might stimulate an unfavorable immune response or become toxic to the encapsulated cells.

Secondly, a combination of several anti-inflammatory agents might have the potential to act synergistically to suppress immune responses against non-self materials. However, the effects of potential overdose, systemic toxicity or drug interference must be carefully considered.

Thirdly, the drug or drug-loaded polymer particles and the therapeutic cells may be compartmentalized within the hydrogel capsules. Compartmentalizing the drug to the surface of the hydrogel capsules facilitates outward drug diffusion, maximizes drug interaction with immune cells, and minimizes its interference with the mammalian cells inside. A next generation of hybrid drug-islet capsules can be designed to have a core-shell structure in which the cells are encapsulated in the inner core and the anti-inflammatory drugs or drug-loaded polymeric particles are encapsulated within an external shell. The core and shell can be separated by a polycation membrane. Alternatively, core-shell

capsules might be fabricated without a membrane layer using a microfluidic or needle system to form microcapsules with two integrated layers. For example, two con-current liquid streams may be used to form two-layer droplets with the external stream containing the desired drug composition.

Lastly, a planar macro-device encapsulating therapeutics cells can be designed to have one device surface coated with a biocompatible adhesive containing the anti-inflammatory drug or drug-loaded particles. The device can be glued against peritoneal or subcutaneous tissue surface. The anti-inflammatory drug released from the device can help to modulate the host response to the device and improve the efficacy of the encapsulated cells.

## REFERENCES

1. Silver, F.H. and D.L. Christiansen, *Biomaterials Science and Biocompatibility*. 1999, New York: Springer-Verlag.
2. Anderson, J.M. and M.S. Shive, *Biodegradation and biocompatibility of PLA and PLGA microspheres*. *Advanced drug delivery reviews*, 1997. **28**(1): p. 5-24.
3. Anderson, J.M., A. Rodriguez, and D.T. Chang, *Foreign body reaction to biomaterials*. *Seminars in immunology*, 2008. **20**: p. 86-100.
4. Rihova, B., *Immunocompatibility and biocompatibility of cell delivery systems*. *Advanced drug delivery reviews*, 2000. **42**(1-2): p. 65-80.
5. Kumar, V., et al., eds. *Robbins and Cotran Pathologic Basis of Diseases*. 8th ed. 2010, Saunders Elsevier: Philadelphia.
6. Hunt, J.A. and D.F. Williams, *Modification of the soft tissue response to implanted materials through the use of an anti-inflammatory drug*. *Journal of Materials Science: Materials in Medicine*, 1992. **3**(3): p. 160-169.
7. Hunt, J.A., D.G. Vince, and D.F. Williams, *Image analysis in the evaluation of biomaterials*. *Journal of biomedical engineering*, 1993. **15**(1): p. 39-45.
8. Hunt, J.A. and D.F. Williams, *Quantifying the soft tissue response to implanted materials*. *Biomaterials*, 1995. **16**(3): p. 167-170.
9. Peterson, R.A., D.L. Krull, and L. Butler, *Applications of laser scanning cytometry in immunohistochemistry and routine histopathology*. *Toxicologic pathology*, 2008. **36**(1): p. 117.
10. Williams, D.F., *On the mechanisms of biocompatibility*. *Biomaterials*, 2008. **29**(20): p. 2941-2953.
11. Erfle, D.J., J.P. Santerre, and R.S. Labow, *Lysosomal enzyme release from human neutrophils adherent to foreign material surfaces: Enhanced release of elastase activity*. *Cardiovascular Pathology*, 1997. **6**(6): p. 333-340.
12. Labow, R.S., D.J. Erfle, and J.P. Santerre, *Neutrophil-mediated degradation of segmented polyurethanes*. *Biomaterials*, 1995. **16**(1): p. 51-59.
13. Labow, R.S., et al., *Human macrophage-mediated biodegradation of polyurethanes: assessment of candidate enzyme activities*. *Biomaterials*, 2002. **23**(19): p. 3969-3975.
14. Zolnik, B.S. and D.J. Burgess, *Evaluation of in vivo-in vitro release of dexamethasone from PLGA microspheres*. *Journal of controlled release*, 2008. **127**(2): p. 137-145.
15. Wisniewski, N., F. Moussy, and W.M. Reichert, *Characterization of implantable biosensor membrane biofouling*. *Fresenius' Journal of Analytical Chemistry*, 2000. **366**(6): p. 611-621.
16. Lim, F. and A.M. Sun, *Microencapsulated islets as bioartificial endocrine pancreas*. *Science*, 1980. **210**(4472): p. 908.
17. Soon-Shiong, P., et al., *Insulin independence in a type 1 diabetic patient after encapsulated islet transplantation*. *Lancet*, 1994. **343**(8903): p. 950-951.
18. Calafiore, R., et al., *Microencapsulated pancreatic islet allografts into nonimmunosuppressed patients with type 1 diabetes*. *Diabetes Care*, 2006. **29**(1): p. 137.
19. Tuch, B.E., et al., *Safety and viability of microencapsulated human islets transplanted into diabetic humans*. *Diabetes Care*, 2009. **32**(10): p. 1887-1889.
20. Orive, G., et al., *Cell encapsulation: promise and progress*. *Nature medicine*, 2003. **9**: p. 104-107.
21. Bunger, C.M., et al., *Deletion of the tissue response against alginate-pll capsules by temporary release of co-encapsulated steroids*. *Biomaterials*, 2005. **26**(15): p. 2353-2360.
22. Wilson, J.T. and E.L. Chaikof, *Challenges and emerging technologies in the immunoisolation of cells and tissues*. *Advanced drug delivery reviews*, 2008. **60**(2): p. 124-145.
23. Siebers, U., et al., *Time course of the cellular reaction toward microencapsulated xenogeneic islets in the rat*. *Transplantation proceedings*, 1998. **30**(4): p. 494.

24. De Vos, P., et al., *Tissue responses against immunisolating alginate PLL capsules in the immediate posttransplant period*. Journal of Biomedical Materials Research, 2002. **62**(3): p. 430-437.
25. Barshes, N.R., S. Wyllie, and J.A. Goss, *Inflammation-mediated dysfunction and apoptosis in pancreatic islet transplantation: implications for intrahepatic grafts*. Journal of Leukocyte Biology, 2005. **77**(5): p. 587.
26. Cole, D.R., et al., *Microencapsulated islet grafts in the BB/E rat: a possible role for cytokines in graft failure*. Diabetologia, 1992. **35**(3): p. 231-237.
27. Wu, P. and D.W. Grainger, *Drug/device combinations for local drug therapies and infection prophylaxis*. Biomaterials, 2006. **27**(11): p. 2450-2467.
28. Singarayar, S., et al., *A comparative study of the action of dexamethasone sodium phosphate and dexamethasone acetate in steroid-eluting pacemaker leads*. Pacing and Clinical Electrophysiology, 2005. **28**(4): p. 311-315.
29. Ward, W.K. and J.E. Troupe, *Assessment of chronically implanted subcutaneous glucose sensors in dogs: The effect of surrounding fluid masses*. ASAIO journal, 1999. **45**(6): p. 555.
30. Zhong, Y. and R.V. Bellamkonda, *Dexamethasone-coated neural probes elicit attenuated inflammatory response and neuronal loss compared to uncoated neural probes*. Brain research, 2007. **1148**: p. 15-27.
31. Ju, Y.M., et al., *A dexamethasone-loaded PLGA microspheres/collagen scaffold composite for implantable glucose sensors*. Journal of Biomedical Materials Research Part A. **93**(1): p. 200-210.
32. Mond, H., et al., *The porous titanium steroid eluting electrode: a double blind study assessing the stimulation threshold effects of steroid*. Pacing and Clinical Electrophysiology, 1988. **11**(2): p. 214-219.
33. Patil, S.D., F. Papadimitrakopoulos, and D.J. Burgess, *Dexamethasone-loaded poly (lactic-co-glycolic) acid microspheres/poly (vinyl alcohol) hydrogel composite coatings for inflammation control*. Diabetes Technology & Therapeutics, 2004. **6**(6): p. 887-897.
34. Lambillotte, C., P. Gilon, and J.C. Henquin, *Direct glucocorticoid inhibition of insulin secretion. An in vitro study of dexamethasone effects in mouse islets*. Journal of Clinical Investigation, 1997. **99**(3): p. 414.
35. Gummert, J.F., T. Ikonen, and R.E. Morris, *Newer immunosuppressive drugs: a review*. Journal of the American Society of Nephrology, 1999. **10**(6): p. 1366.
36. Halloran, P.F., *Immunosuppressive drugs for kidney transplantation*. New England Journal of Medicine, 2004. **351**(26): p. 2715-2729.
37. Weissleder, R. and M.J. Pittet, *Imaging in the era of molecular oncology*. Nature, 2008. **452**: p. 580-589.
38. Weissleder, R., *Molecular Imaging in Cancer*. Science, 2006. **312**: p. 1168-1171.
39. Ntziachristos, V., et al., *Looking and listening to light: The evolution of whole-body photonic imaging*. Nature Biotechnology, 2005. **23**(3): p. 313-320.
40. Weissleder, R., et al., *In vivo imaging of tumors with protease-activated near-infrared fluorescence probes*. Nature Biotechnology, 1999. **17**: p. 375-378.
41. Helmlinger, G., et al., *Interstitial pH and pO<sub>2</sub> gradients in solid tumors in vivo: High-resolution measurements reveal a lack of correlation*. Nature Medicine, 1997. **3**(2): p. 177-182.
42. Voura, E.B., et al., *Tracking metastatic tumor cell extravasation with quantum dot nanocrystals and fluorescence emission-scanning microscopy*. Nature Medicine, 2004. **10**(9): p. 993-998.
43. Wunder, A., et al., *In vivo imaging of protease activity in arthritis - A novel approach for monitoring treatment response*. Arthritis and Rheumatism, 2004. **50**(8): p. 2459-2465.
44. Hansch, A., et al., *In vivo imaging of experimental arthritis with near-infrared fluorescence*. Arthritis and Rheumatism, 2004. **50**(3): p. 961-967.



45. Schuster, D.P., et al., *Recent advances in imaging the lungs of intact small animals*. American Journal of Respiratory Cell and Molecular Biology, 2004. **30**(2): p. 129-138.
46. Haller, J., et al., *Visualization of pulmonary inflammation using noninvasive fluorescence molecular imaging*. Journal of Applied Physiology, 2008. **104**(3): p. 795-802.
47. Christen, T., et al., *Molecular imaging of innate immune cell function in transplant rejection*. Circulation, 2009. **119**(14): p. 1925-1932.
48. Kumar, V., et al., *Robbins and Cotran Pathologic Basis of Disease*. 8th ed. 2009: Saunders.
49. Kvist, P.H., et al., *Biocompatibility of electrochemical glucose sensors implanted in the subcutis of pigs*. Diabetes Technology & Therapeutics, 2006. **8**(4): p. 463-475.
50. De Vos, P., B.J. Haan, and R. Van Schilfgaarde, *Factors causing failure of islets in nonovergrown capsules*. Transplantation Proceedings, 1998. **30**(2): p. 496-497.
51. Wilflingseder, P., A. Propst, and G. Mikuz, *Constrictive fibrosis following silicone implants in mammary augmentation*. European Journal of Plastic Surgery, 1974. **2**(4): p. 215-229.
52. Anderson, J.M., A. Rodriguez, and D.T. Chang, *Foreign body reaction to biomaterials*. Seminars in Immunology, 2008. **20**(2): p. 86-100.
53. Rihova, B., *Immunocompatibility and biocompatibility of cell delivery systems*. Advanced Drug Delivery Reviews, 2000. **42**: p. 65-80.
54. Faurischou, M. and N. Borregaard, *Neutrophil granules and secretory vesicles in inflammation*. Microbes and Infection, 2003. **5**(14): p. 1317-1327.
55. Lominadze, G., et al., *Proteomic analysis of human neutrophil granules*. Molecular & Cellular Proteomics, 2005. **4**: p. 1503-1521.
56. Duvivier-Kali, V.F., et al., *Survival of microencapsulated adult pig islets in mice in spite of an antibody response*. American Journal of Transplantation, 2004. **4**(12): p. 1991-2000.
57. Duvivier-Kali, V.F., et al., *Complete protection of islets against allojection and autoimmunity by a simple barium-alginate membrane*. Diabetes, 2001. **50**(8): p. 1698-1705.
58. De Vos, P., et al., *Alginate-based microcapsules for immunoisolation of pancreatic islets*. Biomaterials, 2006. **27**: p. 5603-5617.
59. Kendall, W.F., et al., *Effect of alginate composition and purity on alginate microspheres*. Journal of Microencapsulation, 2004. **21**(8): p. 821-828.
60. Choi, Y.S., et al., *Study on gelatin-containing artificial skin: I. Preparation and characteristics of novel gelatin-alginate sponge*. Biomaterials, 1999. **20**(5): p. 409-417.
61. Suzuki, Y., et al., *Evaluation of a novel alginate gel dressing: Cytotoxicity to fibroblasts in vitro and foreign-body reaction in pig skin in vivo*. Journal of Biomedical Materials Research, 1998. **39**(2): p. 317-322.
62. Landa, N., et al., *Effect of injectable alginate implant on cardiac remodeling and function after recent and old infarcts in rat*. Circulation, 2008. **117**: p. 1388-1396.
63. Tsur-Gang, O., et al., *The effects of peptide-based modification of alginate on left ventricular remodeling and function after myocardial infarction*. Biomaterials, 2009. **30**: p. 189-195.
64. Makino, K., et al., *Phagocytic uptake of polystyrene microspheres by alveolar macrophages: Effects of the size and surface properties of the microspheres*. Colloids and Surfaces B: Biointerfaces, 2003. **27**: p. 33-39.
65. Ren, W., et al., *Macrophage depletion diminishes implant-wear-induced inflammatory osteolysis in a mouse model*. Journal of Biomedical Materials Research A, 2007. **85A**(4): p. 1043-1051.
66. Barnett, S.E. and S.J. Varley, *The effects of calcium alginate on wound healing*. Annals of the Royal College of Surgeons of England, 1987. **69**: p. 153-155.
67. Montesano, R. and L. Orci, *Transforming growth factor beta stimulates collagen-matrix contraction by fibroblasts: Implications for wound healing*. PNAS, 1988. **85**: p. 4894-4897.

68. Delves, P., et al., *Roitt's Essential Immunology*. 11th ed. 2006, Malded: Blackwell Publishing.
69. Kaufmann, S.H.E., R. Medzhitov, and S. Gordon, eds. *The Innate Immune Response to Infection*. 2004, ASM Press: Washington, D.C. 465.
70. Takahashi, K., M. Naito, and M. Takeya, *Development and heterogeneity of macrophages and their related cells through their differentiation pathways*. *Pathology International*, 2008. **46**(7): p. 473-485.
71. Houglum, P.A., *Therapeutic Exercise for Musculoskeletal Injuries*. 2nd ed, ed. D.H. Perrin. 2005: Human Kinetics.
72. Sartor, R.B., H. Herfarth, and E.A.F. Van Tol, *Bacterial cell wall polymer-induced granulomatous inflammation*. *Methods: A Companion to Methods in Enzymology*, 1996. **9**: p. 233-247.
73. Hom, D.B., *Growth-factors in wound-healing*. *Otolaryngologic Clinics of North America*, 1995. **28**(5): p. 933-953.
74. Shishatskaya, E.I., et al., *Tissue morphogenesis under the conditions of implantation of polyhydroxybutyrate, a biodegradable polymer*. *Doklady Biological Sciences*, 2001. **383**(1-6): p. 123-126.
75. Wallace, A.M., et al., *Matrix metalloproteinase expression by human alveolar macrophages in relation to emphysema*. *Journal of Chronic Obstructive Pulmonary Disease*, 2008. **5**(1): p. 13-23.
76. Sabaliauskas, N.A., et al., *High-throughput zebrafish histology*. *Methods*, 2006. **39**: p. 246-254.
77. Gerstner, A.O.H., et al., *Quantitative histology by multicolor slide-based cytometry*. *Cytometry Part A*, 2004. **59A**(2): p. 210-219.
78. Park, H. and K. Park, *Biocompatibility issues of implantable drug delivery systems*. *Pharmaceutical research*, 1996. **13**(12): p. 1770-1776.
79. van der Giessen, W.J., et al., *Marked inflammatory sequelae to implantation of biodegradable and nonbiodegradable polymers in porcine coronary arteries*. *Circulation*, 1996. **94**(7): p. 1690.
80. Granchi, D., et al., *Silicone breast implants: The role of immune system on capsular contracture formation*. *Journal of biomedical materials research*, 1995. **29**(2): p. 197-202.
81. Ward, C.R., C. Matthew Peterson, and H.H. Hatasaka, *A hook-traction technique for Norplant removal*. *Obstetrics & Gynecology*, 1995. **86**(5): p. 848-850.
82. Remes, A. and D.F. Williams, *Immune response in biocompatibility*. *Biomaterials*, 1992. **13**(11): p. 731-743.
83. Vinay Kumar, N.F., Abul Abbas, Jon Aster, *Robbins and Cotran Pathologic Basis of Disease Saunders*. 7 ed. 2009.
84. Sharkawy, A.A., et al., *Engineering the tissue which encapsulates subcutaneous implants. I. Diffusion properties*. *Journal of Biomedical Materials Research Part A*, 1997. **37**(3): p. 401-412.
85. Sharkawy, A.A., et al., *Engineering the tissue which encapsulates subcutaneous implants. III. Effective tissue response times*. *Journal of Biomedical Materials Research Part A*, 1998. **40**(4): p. 598-605.
86. Sharkawy, A.A., et al., *Engineering the tissue which encapsulates subcutaneous implants. II. Plasma-tissue exchange properties*. *Journal of Biomedical Materials Research Part A*, 1998. **40**(4): p. 586-597.
87. Moussy, F. *Implantable glucose sensor: progress and problems*. in *IEEE Sensors*. 2002.
88. De Groot, M., T.A. Schuurs, and R. van Schilfgaarde, *Causes of limited survival of microencapsulated pancreatic islet grafts*. *Journal of Surgical Research*, 2004. **121**(1): p. 141-150.
89. De Vos, P., et al., *Improved biocompatibility but limited graft survival after purification of alginate for microencapsulation of pancreatic islets*. *Diabetologia*, 1997. **40**: p. 262-270.
90. Van Schilfgaarde, R. and P. De Vos, *Factors influencing the properties and performance of microcapsules for immunoprotection of pancreatic islets*. *Journal of Molecular Medicine*, 1999. **77**(1): p. 199-205.

91. Dash, A.K. and G.C. Cudworth, "Therapeutic applications of implantable drug delivery systems". *Journal of Pharmacological and Toxicological Methods*. **40**(1): p. 1-12.
92. Labhasetwar, V. and R.J. Levy, *Implants for site-specific drug delivery*. *J Appl Biomater*, 1991. **2**: p. 211-212.
93. Morais, J.M., F. Papadimitrakopoulos, and D.J. Burgess, *Biomaterials/Tissue Interactions: Possible Solutions to Overcome Foreign Body Response*. *The AAPS journal*. **12**(2): p. 188-196.
94. Hickey, T., et al., *Dexamethasone/PLGA microspheres for continuous delivery of an anti-inflammatory drug for implantable medical devices*. *Biomaterials*, 2002. **23**(7): p. 1649-1656.
95. Hickey, T., et al., *In vivo evaluation of a dexamethasone/PLGA microsphere system designed to suppress the inflammatory tissue response to implantable medical devices*. *Journal of Biomedical Materials Research Part A*, 2002. **61**(2): p. 180-187.
96. Galeska, I., et al., *Controlled release of dexamethasone from PLGA microspheres embedded within polyacid-containing PVA hydrogels*. *The AAPS journal*, 2005. **7**(1): p. 231-240.
97. Bhardwaj, U., et al., *Controlling acute inflammation with fast releasing dexamethasone-PLGA microsphere/PVA hydrogel composites for implantable devices*. *Journal of Diabetes science and technology* 2007. **1**(1).
98. Vane, J.R. and R.M. Botting, *Anti-inflammatory drugs and their mechanism of action*. *Inflammation Research*, 1998. **47**(14): p. 78-87.
99. Rhen, T. and J.A. Cidlowski, *Antiinflammatory action of glucocorticoids--new mechanisms for old drugs*. *New England Journal of Medicine*, 2005. **353**(16): p. 1711.
100. Jain, R.A., *The manufacturing techniques of various drug loaded biodegradable poly (lactide-co-glycolide)(PLGA) devices*. *Biomaterials*, 2000. **21**(23): p. 2475-2490.
101. D'Souza, S.S. and P.P. DeLuca, *Methods to assess in vitro drug release from injectable polymeric particulate systems*. *Pharmaceutical research*, 2006. **23**(3): p. 460-474.
102. Golan, D.E., *Principles of pharmacology: the pathophysiologic basis of drug therapy*. 2008: Lippincott Williams & Wilkins.
103. Weissleder, R., et al., *In vivo imaging of tumors with protease-activated near-infrared fluorescent probes*. *Nature Biotechnology*, 1999. **17**: p. 375-378.
104. Bratlie, K.M., et al., *Rapid Biocompatibility Analysis of Materials via In Vivo Fluorescence Imaging of Mouse Models*. *PlosOne*, 2010. **5**(5): p. e10032. doi:10.1371/journal.pone.0010032.
105. Tung, C.H., et al., *In vivo imaging of proteolytic enzyme activity using a novel molecular reporter*. *Cancer research*, 2000. **60**(17): p. 4953-4958.
106. Tuckermann, J.P., et al., *Macrophages and neutrophils are the targets for immune suppression by glucocorticoids in contact allergy*. *Journal of Clinical Investigation*, 2007. **117**(5): p. 1381-1390.
107. Labhasetwar, V. and R.J. Levy, *Clinical Reviews*. *Journal of Applied Biomaterials*, 1991. **2**: p. 211-212.
108. König, K., *Multiphoton microscopy in life sciences*. *Journal of Microscopy*, 2000. **200**(2): p. 83-104.
109. Lominadze, G., et al., *Proteomic analysis of human neutrophil granules*. *Molecular & Cellular Proteomics*, 2005. **4**(10): p. 1503.
110. Goldstein, M. and S. Watkins, *Immunohistochemistry*, in *Current Protocols in Molecular Biology*. 2008, John Wiley & Sons.
111. Chick, W.M.K.R.P.L.W.L., ed. *Cell encapsulation technology and therapeutics*. ed. A. Atala;. 1999, Birkhauser: Boston.
112. Orive, G., et al., *Biocompatibility of alginate-poly-L-lysine microcapsules for cell therapy*. *Biomaterials*, 2006. **27**(20): p. 3691-3700.

113. Soon-Shiong, P., et al., *Successful reversal of spontaneous diabetes in dogs by intraperitoneal microencapsulated islets*. Transplantation, 1992. **54**(5): p. 769.
114. Soon-Shiong, P., et al., *Long-term reversal of diabetes by the injection of immunoprotected islets*. Proceedings of the National Academy of Sciences, 1993. **90**(12): p. 5843.
115. Calafiore, R., et al., *Grafts of microencapsulated pancreatic islet cells for the therapy of diabetes mellitus in non immunosuppressed animals*. Biotechnology and Applied Biochemistry, 2004. **39**(2): p. 159-164.
116. Omer, A., et al., *Long-term normoglycemia in rats receiving transplants with encapsulated islets*. Transplantation, 2005. **79**(1): p. 52.
117. Lalain, S., et al., *In vitro recognition and impairment of pig islet cells by baboon immune cells: Similarity to human cellular reactions*. Transplantation, 2001. **72**(9): p. 1541.
118. Duvivier Kali, V.F., et al., *Survival of microencapsulated adult pig islets in mice in spite of an antibody response*. American Journal of Transplantation, 2004. **4**(12): p. 1991-2000.
119. Kulseng, B., et al., *Alginate polylysine microcapsules as immune barrier: permeability of cytokines and immunoglobulins over the capsule membrane*. Cell transplantation, 1997. **6**(4): p. 387-394.
120. Strand, B.L., et al., *Poly-L-lysine induces fibrosis on alginate microcapsules via the induction of cytokines*. Cell transplantation, 2001. **10**(3): p. 263-275.
121. De Vos, P., et al., *Why do microencapsulated islet grafts fail in the absence of fibrotic overgrowth?* Diabetes, 1999. **48**(7): p. 1381.
122. Palmer, J.P., et al., *Interaction of beta-cell activity and IL-1 concentration and exposure time in isolated rat islets of Langerhans*. Diabetes, 1989. **38**(10): p. 1211-1216.
123. Sandler, S., A. Andersson, and M. Hellerstrom, C., *Inhibitory effects of interleukin 1 on insulin secretion, insulin biosynthesis, and oxidative metabolism of isolated rat pancreatic islets*. Endocrinology, 1987. **121**(4): p. 1424-1431.
124. Campbell, I.L., A. Iscaro, and L.C. Harrison, *IFN-gamma and tumor necrosis factor-alpha. Cytotoxicity to murine islets of Langerhans*. The Journal of Immunology, 1988. **141**(7): p. 2325.
125. De Vos, P., et al., *Association Between Capsule Diameter, Adequacy of Encapsulation, and Survival of Microencapsulated Rat Islet Allografts1*. Transplantation, 1996. **62**(7): p. 893.
126. Fritschy, W.M., et al., *The capsular overgrowth on microencapsulated pancreatic islet grafts in streptozotocin and autoimmune diabetic rats*. Transplant international, 1994. **7**(4): p. 264-271.
127. Labhasetwar, V. and R.J. Levy, *Implants for site-specific drug delivery*. J Appl Biomater, 2004. **2**: p. 211-212.
128. Lemos, P.A., et al., *Unrestricted utilization of sirolimus-eluting stents compared with conventional bare stent implantation in the "real world": the Rapamycin-Eluting Stent Evaluated At Rotterdam Cardiology Hospital (RESEARCH) registry*. Circulation, 2004. **109**(2): p. 190.
129. Stone, G.W., et al., *A polymer-based, paclitaxel-eluting stent in patients with coronary artery disease*. The New England journal of medicine, 2004. **350**(3): p. 221.
130. Rogers, C. and E.R. Edelman, *Pushing drug-eluting stents into uncharted territory: simpler than you think--more complex than you imagine*. Circulation, 2006. **113**(19): p. 2262.
131. Friedl, K.E., *Corticosteroid modulation of tissue responses to implanted sensors*. Diabetes Technology & Therapeutics, 2004. **6**(6): p. 898-901.
132. Schneider, B.L., et al., *Prevention of the initial host immuno-inflammatory response determines the long-term survival of encapsulated myoblasts genetically engineered for erythropoietin delivery*. Molecular Therapy, 2003. **7**(4): p. 506-514.
133. Zhang, W.J., Marx, S.K., et al., *HOE 077 Reduces Fibrotic Overgrowth Around the Barium Alginate Microcapsules*. Transplantation Proceedings, 2000. **32**: p. 206-209.

134. Omer, A., et al., *Macrophage depletion improves survival of porcine neonatal pancreatic cell clusters contained in alginate macrocapsules transplanted into rats*. *Xenotransplantation*, 2003. **10**(3): p. 240-251.
135. Tappy, L., et al., *Mechanisms of dexamethasone-induced insulin resistance in healthy humans*. *Journal of Clinical Endocrinology & Metabolism*, 1994. **79**(4): p. 1063-1069.
136. Beard, J.C., et al., *Dexamethasone-induced insulin resistance enhances B cell responsiveness to glucose level in normal men*. *American Journal of Physiology-Endocrinology And Metabolism*, 1984. **247**(5): p. E592-E596.
137. Ricci, M., et al., *Ketoprofen controlled release from composite microcapsules for cell encapsulation: effect on post-transplant acute inflammation*. *Journal of Controlled Release*, 2005. **107**(3): p. 395-407.
138. Blasi, P., et al., *Preparation and in vitro and in vivo characterization of composite microcapsules for cell encapsulation*. *International Journal of Pharmaceutics*, 2006. **324**(1): p. 27-36.
139. Löwenberg, M., et al., *Novel insights into mechanisms of glucocorticoid action and the development of new glucocorticoid receptor ligands*. *Steroids*, 2008. **73**(9-10): p. 1025-1029.
140. Perretti, M. and A. Ahluwalia, *The microcirculation and inflammation: site of action for glucocorticoids*. *Microcirculation*, 2000. **7**(3): p. 147-161.
141. Attur, M.G., et al., *Differential anti-inflammatory effects of immunosuppressive drugs: cyclosporin, rapamycin and FK-506 on inducible nitric oxide synthase, nitric oxide, cyclooxygenase-2 and PGE 2 production*. *Inflammation Research*, 2000. **49**(1): p. 20-26.
142. Chan, T.A., et al., *Mechanisms underlying nonsteroidal antiinflammatory drug-mediated apoptosis*. *Proceedings of the National Academy of Sciences*, 1998. **95**(2): p. 681.
143. Joe, B., M. Vijaykumar, and B.R. Lokesh, *Biological properties of curcumin-cellular and molecular mechanisms of action*. *Critical reviews in food science and nutrition*, 2004. **44**(2): p. 97-111.
144. Fournier, E., et al., *Biocompatibility of implantable synthetic polymeric drug carriers: focus on brain biocompatibility*. *Biomaterials*, 2003. **24**(19): p. 3311-3331.
145. Dang, T.T., et al., *Spatiotemporal effects of a controlled-release anti-inflammatory drug on the cellular dynamics of host response*. *Biomaterials*, 2011. **32**(19): p. 3364-4470.
146. Ma, M., et al., *Development of Cationic Polymer Coatings to Regulate Foreign Body Responses*. *Advanced Materials*, 2011. **23**: p. H189-H194.
147. Liu, W.F., et al., *Real-time in vivo detection of biomaterial-induced reactive oxygen species*. *Biomaterials*, 2011. **32**(7): p. 1796-1801.
148. Vos, P.D., et al., *Improved biocompatibility but limited graft survival after purification of alginate for microencapsulation of pancreatic islets*. *Diabetologia*, 1997. **40**(3): p. 262-270.
149. Constantinidis, I., et al., *Effects of alginate composition on the metabolic, secretory, and growth characteristics of entrapped [beta] TC3 mouse insulinoma cells*. *Biomaterials*, 1999. **20**(21): p. 2019-2027.
150. Berney, T., et al., *Endotoxin-Mediated Delayed Islet Graft Function Is Associated With Increased Intra-Islet Cytokine Production and Islet Cell Apoptosis*. *Transplantation*, 2001. **71**(1): p. 125.
151. O'Sullivan, E.S., et al., *Rat islet cell aggregates are superior to islets for transplantation in microcapsules*. *Diabetologia*. **53**(5): p. 937-945.
152. Lukic, M.L., S. Stosic-Grujicic, and A. Shahin, *Effector mechanisms in low-dose streptozotocin-induced diabetes*. *Developmental immunology*, 1998. **6**(1-2): p. 119.
153. Buchwald, P., *FEM-based oxygen consumption and cell viability models for avascular pancreatic islets*. *Theoretical Biology and Medical Modelling*, 2009. **6**: p. 5.
154. Ricordi, C., et al., *Islet isolation assessment in man and large animals*. *Acta Diabetologica*, 1990. **27**(3): p. 185-195.

155. Omer, A., et al., *Survival and maturation of microencapsulated porcine neonatal pancreatic cell clusters transplanted into immunocompetent diabetic mice*. *Diabetes*, 2003. **52**(1): p. 69.
156. Mazaheri, R., et al., *Transplantation of encapsulated allogeneic islets into diabetic BB/W rats. Effects of immunosuppression*. *Transplantation*, 1991. **51**(4): p. 750.
157. Vaithilingam, V., et al., *The humanized NOD/SCID mouse as a preclinical model to study the fate of encapsulated human islets*. *The review of diabetic studies: RDS*. **7**(1): p. 62.
158. Barnes, P.J., *Reactive oxygen species and airway inflammation*. *Free Radical Biology and Medicine*, 1990. **9**(3): p. 235-243.
159. Bergamini, C.M., et al., *Oxygen, reactive oxygen species and tissue damage*. *Current pharmaceutical design*, 2004. **10**(14): p. 1611-1626.
160. Thannickal, V.J. and B.L. Fanburg, *Reactive oxygen species in cell signaling*. *American Journal of Physiology-Lung Cellular and Molecular Physiology*, 2000. **279**(6): p. L1005.
161. Virgilio, F.D., *New pathways for reactive oxygen species generation in inflammation and potential novel pharmacological targets*. *Current pharmaceutical design*, 2004. **10**(14): p. 1647-1652.
162. Ali, S.A.M., et al., *Mechanisms of polymer degradation in implantable devices:: I. Poly (caprolactone)*. *Biomaterials*, 1993. **14**(9): p. 648-656.
163. Selvam, S., et al., *Minimally invasive, longitudinal monitoring of biomaterial-associated inflammation by fluorescence imaging*. *Biomaterials*.
164. Nichols, J.A. and S.K. Katiyar, *Skin photoprotection by natural polyphenols: anti-inflammatory, antioxidant and DNA repair mechanisms*. *Archives of dermatological research*. **302**(2): p. 71-83.
165. Udenigwe, C.C., et al., *Potential of resveratrol in anticancer and anti-inflammatory therapy*. *Nutrition reviews*, 2008. **66**(8): p. 445-454.
166. Lontas, A. and H. Yeger, *Curcumin and resveratrol induce apoptosis and nuclear translocation and activation of p53 in human neuroblastoma*. *Anticancer research*, 2004. **24**(2B): p. 987-998.
167. Gonzales, A.M. and R.A. Orlando, *Curcumin and resveratrol inhibit nuclear factor-kappaB-mediated cytokine expression in adipocytes*. *Nutr Metab (Lond)*, 2008. **5**(1): p. 17.
168. Sharma, S., et al., *Resveratrol and curcumin suppress immune response through CD28/CTLA 4 and CD80 co-stimulatory pathway*. *Clinical & Experimental Immunology*, 2007. **147**(1): p. 155-163.
169. Kindt, T.J., et al., *Kuby Immunology*. 6th ed. 2006, New York: W.H. Freeman.
170. Wijisman, J., et al., *Histological and immunopathological analysis of recovered encapsulated allogeneic islets from transplanted diabetic BB/W rats*. *Transplantation*, 1992. **54**(4): p. 588.
171. Vaithilingam, V., et al., *Effect of prolonged gelling time on the intrinsic properties of barium alginate microcapsules and its biocompatibility*. *Journal of microencapsulation*. **28**(6): p. 499-507.
172. Gotfredsen, C.F., et al., *The fate of transplanted encapsulated islets in spontaneously diabetic BB/Wor rats*. *Diabetes research (Edinburgh, Scotland)*, 1990. **15**(4): p. 157.
173. Bouhadir, K.H., et al., *Degradation of partially oxidized alginate and its potential application for tissue engineering*. *Biotechnology progress*, 2001. **17**(5): p. 945-950.
174. Al-Shamkhani, A. and R. Duncan, *Radioiodination of alginate via covalently-bound tyrosinamide allows monitoring of its fate in vivo*. *Journal of bioactive and compatible polymers*, 1995. **10**(1): p. 4-13.
175. Visscher, G.E., et al., *Biodegradation of and tissue reaction to 50: 50 poly (D-lactide-co-glycolide) microcapsules*. *Journal of biomedical materials research*, 1985. **19**(3): p. 349-365.
176. Spenlehauer, G., et al., *In vitro and in vivo degradation of poly (D, L lactide/glycolide) type microspheres made by solvent evaporation method*. *Biomaterials*, 1989. **10**(8): p. 557-563.

177. Vert, M., J. Mauduit, and S. Li, *Biodegradation of PLA/GA polymers: increasing complexity*. *Biomaterials*, 1994. **15**(15): p. 1209-1213.
178. Freiberg, S. and X.X. Zhu, *Polymer microspheres for controlled drug release*. *International Journal of Pharmaceutics*, 2004. **282**(1): p. 1-18.
179. Uhrich, K.E., et al., *Polymeric systems for controlled drug release*. *Chemical Reviews-Columbus*, 1999. **99**(11): p. 3181-3198.
180. Kurien, B.T., et al., *Improving the solubility and pharmacological efficacy of curcumin by heat treatment*. *Assay and drug development technologies*, 2007. **5**(4): p. 567-576.
181. Einmahl, S., et al., *Concomitant and controlled release of dexamethasone and 5-fluorouracil from poly (ortho ester)*. *International Journal of Pharmaceutics*, 1999. **185**(2): p. 189-198.
182. Jaremko, J. and O. Rorstad, *Advances toward the implantable artificial pancreas for treatment of diabetes*. *Diabetes Care*, 1998. **21**(3): p. 444-450.
183. Hovorka, R., *Continuous glucose monitoring and closed loop systems*. *Diabetic medicine*, 2006. **23**(1): p. 1-12.
184. Kanitkar, M., et al., *Novel role of curcumin in the prevention of cytokine induced islet death in vitro and diabetogenesis in vivo*. *British journal of pharmacology*, 2008. **155**(5): p. 702-713.
185. Kanitkar, M. and R.R. Bhonde, *Curcumin treatment enhances islet recovery by induction of heat shock response proteins, Hsp70 and heme oxygenase-1, during cryopreservation*. *Life sciences*, 2008. **82**(3-4): p. 182-189.
186. Read, T.A., et al., *Local endostatin treatment of gliomas administered by microencapsulated producer cells*. *Nature Biotechnology*, 2001. **19**: p. 29-34.
187. Joki, T., et al., *Continuous release of endostatin from microencapsulated engineered cells for tumor therapy*. *Nature Biotechnology*, 2001. **19**: p. 35-39.
188. Chang, T.M.S., *Therapeutic applications of polymeric artificial cells*. *Nature Reviews Drug Discovery*, 2005. **4**(3): p. 221-235.
189. Uludag, H., P. De Vos, and P.A. Tresco, *Technology of mammalian cell encapsulation*. *Advanced drug delivery reviews*, 2000. **42**(1-2): p. 29-64.
190. Lim, F. and A.M. Sun, *Microencapsulated islets as bioartificial endocrine pancreas*. *Science*, 1980. **210**(4472): p. 908-910.
191. Soon-Shiong, P., *Treatment of type I diabetes using encapsulated islets*. *Advanced drug delivery reviews*, 1999. **35**(2-3): p. 259-270.
192. Kizilel, S., M. Garfinkel, and E. Opara, *The bioartificial pancreas: progress and challenges*. *Diabetes Technology & Therapeutics*, 2005. **7**(6): p. 968-985.
193. Elliott, R.B., et al., *Live encapsulated porcine islets from a type 1 diabetic patient 9.5 yr after xenotransplantation*. *Xenotransplantation*, 2007. **14**(2): p. 157-161.
194. Calafiore, R., et al., *Standard technical procedures for microencapsulation of human islets for graft into nonimmunosuppressed patients with type 1 diabetes mellitus*. *Transplantation proceedings*, 2006. **38**: p. 1156-1157.
195. De Vos, P. and P. Marchetti, *Encapsulation of pancreatic islets for transplantation in diabetes: the untouchable islets*. *Trends in Molecular Medicine*, 2002. **8**(8): p. 363-366.
196. Dulieu, C., Poncelet, D., Neufeuld, J.N, *Encapsulation and Immobilization Techniques*, in *Cell encapsulation technology and therapeutics*, W.M. Kühtreiber, R.P. Lanza, and W.L. Chick, Editors. 1999, Birkhauser: Boston, MA, USA. p. 3-17.
197. Serp, D., et al., *Characterization of an encapsulation device for the production of monodisperse alginate beads for cell immobilization*. *Biotechnology and Bioengineering*, 2000. **70**(1): p. 41-53.
198. Wang, T., et al., *An encapsulation system for the immunoisolation of pancreatic islets*. *Nature Biotechnology*, 1997. **15**(4): p. 358-362.

199. Qiu, C., et al., *Generation of uniformly sized alginate microparticles for cell encapsulation by using a soft-lithography approach*. *Adv. Mater*, 2007. **19**: p. 1603–1607.
200. Fukuda, J., et al., *Micromolding of photocrosslinkable chitosan hydrogel for spheroid microarray and co-cultures*. *Biomaterials*, 2006. **27**(30): p. 5259-5267.
201. Yeh, J., et al., *Micromolding of shape-controlled, harvestable cell-laden hydrogels*. *Biomaterials*, 2006. **27**(31): p. 5391-5398.
202. Khademhosseini, A., et al., *Micromolding of photocrosslinkable hyaluronic acid for cell encapsulation and entrapment*. *Journal of Biomedical Materials Research Part A*, 2006. **79A**(3): p. 522 - 532.
203. Franzesi, G.T., et al., *A controlled-release strategy for the generation of cross-linked hydrogel microstructures*. *J Am Chem Soc*, 2006. **128**(47): p. 15064-5.
204. McGuigan, A.P., et al., *Cell Encapsulation in Sub-mm Sized Gel Modules Using Replica Molding*. *PLoS ONE*, 2008. **3**(5).
205. Asfari, M., et al., *Establishment of 2-mercaptoethanol-dependent differentiated insulin-secreting cell lines*. *Endocrinology*, 1992. **130**(1): p. 167-178.
206. Merglen, A., et al., *Glucose sensitivity and metabolism-secretion coupling studied during two-year continuous culture in INS-1E insulinoma cells*. *Endocrinology*, 2004. **145**(2): p. 667-678.
207. Du, Y., et al., *Directed assembly of cell-laden microgels for fabrication of 3D tissue constructs*. *Proceedings of the National Academy of Sciences*, 2008. **105**(28): p. 9522-9527
208. Avgoustiniatos, E.S. and C.K. Colton, *Effect of External Oxygen Mass Transfer Resistances on Viability of Immunoisolated Tissue a*. *Annals of the New York Academy of Sciences*, 1997. **831**(1): p. 145-166.



## **APPENDIX A – ABBREVIATIONS**

<b>ANOVA</b>	Analysis of Variance
<b>DNA</b>	Deoxy-ribonucleic Acid
<b>FDA</b>	Food and Drug Administration
<b>FITC</b>	Fluorescein isothiocyanate
<b>H&amp;E</b>	Hematoxylin and Eosin
<b>HEPES</b>	4-(2-hydroxyethyl)-1-piperazineethanesulfonic acid
<b>HPLC</b>	High-Performance Liquid Chromatography
<b>ID</b>	Inner Diameter
<b>IE</b>	Islet Equivalent
<b>IPGTT</b>	Intra-Peritoneal Glucose Tolerance Test
<b>ISO</b>	International Organization for Standardization
<b>LOQ</b>	Limit of Quantification
<b>LSD</b>	Least Significant Difference
<b>NSAID</b>	Non-steroidal Anti-inflammatory Drug
<b>OD</b>	Outer diameter
<b>PBS</b>	Phosphate buffered saline
<b>PLGA</b>	Poly(lactic- <i>co</i> -glycolic acid)
<b>PMN</b>	Polymorphonuclear
<b>ROI</b>	Region of Interest
<b>ROS</b>	Reactive Oxygen Species
<b>SEM</b>	Scanning Electron Micrograph
<b>STZ</b>	Streptozotocin
<b>Wt%</b>	weight percentage
<b>v/v</b>	volume to volume

## APPENDIX B – CURRICULUM VITAE

### TRAM THUY DANG

Massachusetts Institute of Technology  
Department of Chemical Engineering  
500 Main St, Room 76-687  
Cambridge, MA, 02142 USA

Email : [tramdang@mit.edu](mailto:tramdang@mit.edu)  
Researcher ID : E-7966-2011

### EDUCATION

- 9/2007-7/2012      **Ph.D, Chemical Engineering, Massachusetts Institute of Technology**  
Ph.D Advisors: Professor Robert Langer and Professor Daniel G. Anderson  
**Minor in Business Management, MIT Sloan School of Management**
- 9/2003- 5/2006      **B.Sc, Chemical Engineering (*summa cum laude*),**  
**University of Illinois, Urbana-Champaign**

### RESEARCH APPOINTMENTS

- 10/2007-7/2012      **Graduate Research Assistant**, Department of Chemical Engineering,  
Laboratories of Professor Robert Langer and Professor Daniel Anderson,  
Massachusetts Institute of Technology, Cambridge MA.
- 6/2006- 8/2007      **Research officer**, with Professor Jackie Ying, Pharmaceutical  
Synthesis Group, Institute of Bioengineering and Nanotechnology,  
Singapore
- 8/2005-5/2006      **Undergraduate Research Assistant**,  
Laboratory of Professor Christopher Rao. Department of Chemical  
Engineering, University of Illinois, Urbana-Champaign, IL
- 6/2005-8/2005      **Research intern** with Dr Selvan Subramanian, Quantum Dot Group,  
Institute of Bioengineering and Nanotechnology, Singapore
- 1/2004-8/2004      **Undergraduate Research Assistant**,  
Laboratory of Professor Huimin Zhao. Department of Chemical  
Engineering, University of Illinois, Urbana-Champaign, IL
- 5/2003-8/2003      **Research intern** with Dr Raman Ravishankar, Heterogeneous Catalysis  
Group, Institute of Chemical and Engineering Sciences, Singapore
- 1/2003-5/2003      **Research intern** with Professor Ang How Ghee, High Energy Density  
Materials Research Laboratories, Department of Chemistry, National  
University of Singapore.

## **HONORS and AWARDS**

2012	<b><i>Sung Wan Kim Postdoctoral Fellowship</i></b> awarded by the Controlled Release Society Foundation for excellence in scientific research and strong leadership potential
2010	<b><i>GEMS Travel Grant</i></b> for Graduate Education in Medical Sciences, Harvard-MIT Division of Health Science and Technology
2009	<b><i>A*STAR Conference Travel Grant</i></b> Agency for Science, Technology and Research of Singapore
2007-2008	<b><i>MIT Edward Clark Walsh Presidential Fellowship</i></b> , Massachusetts Institute of Technology
2007-2012	<b><i>A*STAR National Science Graduate Fellowship (PhD)</i></b> , Agency for Science, Technology and Research of Singapore
2006	<b><i>Worth Huff Rodebush Award</i></b> for outstanding senior, Department of Chemical Engineering, University of Illinois, Urbana-Champaign
2006	<b>University Honor</b> with name inscription on University Bronze Tablet, University of Illinois, Urbana-Champaign,
2005	<b><i>Proctor &amp; Gamble Leadership Award</i></b> , University of Illinois, Urbana-Champaign,
2004	<b><i>Alumni Achievement Award</i></b> , Department of Chemical Engineering, University of Illinois, Urbana-Champaign
2003-2006	<b><i>A*STAR National Science Undergraduate Scholarship (B.Sc)</i></b> , Agency for Science, Technology and Research of Singapore

## **PUBLICATIONS**

- Vacanti NM, Hao C, Hill PS, Guerreiro JDT, **Dang TT**, Ma M, Watson S, Hwang NS, Langer R, Anderson DG. "Localized delivery of dexamethasone from electrospun fibers controls the foreign body response" (*submitted*)
- Kastrup CJ, Nahrendorf M, Figueiredo JL, Lee H, Kambhampati S, Lee T, Cho SW, Gorbatov R, Iwamoto Y, **Dang TT**, Dutta P, Yeon JH, Cheng H, Pritchard CD, Vegas AJ, Siegel CD, MacDougall S, Okonkwo M, Stone JR, Coury AJ, Weissleder R, Langer R, Anderson DG. "Painting Blood Vessels and Atherosclerotic Plaques with an Adhesive Drug Depot" (*submitted*)
- **Dang TT**, Bratlie KM, Bogatyrev SR, Chen XY, Langer R, Anderson DG. "Spatiotemporal effects of a controlled release anti-inflammatory drug on the cellular dynamics of host response" **Biomaterials** 2011;32(19):4464-70
- Liu WF, Ma M, Bratlie KM, **Dang TT**, Langer R, Anderson DG. "Real-time *in vivo* detection of biomaterial-induced reactive oxygen species" **Biomaterials** 2011; 32(7):1796-801

- Bratlie KM, **Dang TT**, Lyle S, Nahrendorf M, Weissleder R, Langer R, Anderson DG. “Rapid biocompatibility analysis of materials by *in vivo* fluorescent imaging of inflammatory response”. **PLoS ONE** 2010; 5(4): e10032. doi:10.1371/ journal.pone.0010032
- **Dang TT**, Xu Q, Bratlie KM, O’Sullivan ES, Chen XY, Langer R, Anderson DG. “Microfabrication of Homogeneous, Asymmetric Cell-laden Hydrogel Capsules.” **Biomaterials** 2009; 30(36): 6896-6902
- Xu Q, Hashimoto M, **Dang TT**, Hoare T, Kohane DS, Whitesides GM, Langer R, Anderson DG. “Preparation of Monodisperse Biodegradable Polymer Microcapsules Using a Microfluidic Flow-Focusing Device for Controlled Drug Delivery”. **Small** 2009; 5(13): 1575-1581

### **PATENTS**

- Anderson D.G, Langer R, and **Dang TT**. “Hybrid Microcapsules containing islets and anti-inflammatory drugs for diabetes therapy”. U.S.S.N. 61/444206, filed on Feb. 2011.
- Anderson D.G, Langer R, and **Dang TT**. “Hydrogel-encapsulated cells and anti-inflammatory drugs”. U.S.S.N. 13/400,382 and PCT/US2012/025806, filed on Feb 2012.

### **CONFERENCE PRESENTATIONS AND POSTERS (presenters underlined)**

- **Dang TT**, Bratlie KM, Bogatyrev SR, Chen XY, Langer R, Anderson DG. “Spatiotemporal effects of a controlled release anti-inflammatory drug on the cellular dynamics of host response”. Biomedical Engineering Society Annual Meeting, Hartford, CT, Oct 12<sup>th</sup>-14<sup>th</sup> 2011 (oral presentation)
- **Dang TT**, Bratlie KM, Bogatyrev SR, Chen XY, Langer R, Anderson DG. “Spatiotemporal effects of a controlled release anti-inflammatory drug on the cellular dynamics of host response”. Gordon Research Conference on Biomaterials and Tissue Engineering, Holderness, NH, July 31<sup>st</sup>- Aug 5<sup>th</sup> 2011 (poster presentation)
- **Dang TT**, Bratlie KM, Bogatyrev SR, Chen XY, Langer R and Anderson DG “Investigating the Effect of Anti-Inflammatory Drugs On Material Biocompatibility by In Vivo Fluorescent Imaging”. American Institute of Chemical Engineering Annual Meeting, Salt Lake, Utah, Nov 7<sup>th</sup> -12<sup>th</sup> 2010 (oral presentation)
- **Bratlie KM**, **Dang TT**, Vegas AJ, Vietti TM, Langer R and Anderson DG. “ Determining Biocompatibility of a Chemically Modified Alginate Library through In Vivo Imaging and Histology”. American Institute of Chemical Engineering Annual Meeting, Salt Lake, Utah, Nov 7<sup>th</sup> -12<sup>th</sup> 2010.(oral presentation)
- **Dang TT**, Bratlie KM, Bogatyrev SR, Chen XY, Langer R and Anderson DG “Investigating the Effect of Anti-Inflammatory Drugs On Material Biocompatibility by In Vivo Fluorescent Imaging”. American Chemical Society National Meeting, Boston, Aug 20<sup>th</sup> -26<sup>th</sup> 2010 (oral presentation)

- **Dang TT**, Xu Q, Bratlie KM, O’Sullivan ES, Chen XY, Langer R, Anderson DG. “Microfabrication of Asymmetric, Homogenous Cell-Laden Hydrogel Microcapsule”. The 10<sup>th</sup> US-Japan Drug Delivery Symposium, Hawaii, Dec 16<sup>th</sup> – 20<sup>th</sup> 2009 (poster presentation)
- **Dang TT**, Xu Q, Bratlie KM, O’Sullivan ES, Chen XY, Langer R, Anderson DG. “Microfabrication of Asymmetric, Homogenous Cell-Laden Hydrogel Microcapsule” Material Research Society Meeting, Boston, Nov 30<sup>th</sup> -Dec 2<sup>nd</sup> 2009 (oral presentation)
- Xu Q, Hashimoto M, **Dang TT**, Hoare T, Kohane DS, Whitesides GM, Langer R, Anderson DG. “Preparation of Monodisperse Biodegradable Polymer Microcapsules Using a Microfluidic Flow-Focusing Device for Controlled Drug Delivery”. Material Research Society Meeting, Boston, Nov 30<sup>th</sup> - Dec 2<sup>nd</sup> 2009 (poster presentation)
- **Dang TT**, Gao S, Erathodiyil N, Ying JY. “Hydrogels and nanoparticles for glucose-responsive insulin delivery”. A\*STAR research symposium, Singapore, July 2007 (oral presentation)
- **Dang TT**, Gao S, Erathodiyil N, Ying JY. “Synthesis and characterization of glucose-responsive insulin-delivery hydrogel and nanoparticles for diabetes treatment” International Conference on the Development of Biomedical Engineering, Hanoi, Vietnam, July 2007 (oral presentation)
- **Dang TT**, Chubiz Lon and Rao CV. “Evolution of chemotaxis proteins in proteobacteria” International Conference on the Development of Biomedical Engineering, Hanoi, Vietnam, July 2007 (poster presentation)

### **TEACHING & MENTORING EXPERIENCE**

- |                |  |
|----------------|--|
| 9/2010-present | <b>Research mentor</b> , recruited, trained and supervised two full-time research technicians (B.Sc in Biology and Chemical Engineering) to support a project, funded by the Juvenile Diabetes Research Foundation, to improve immunolocalization of pancreatic islets for diabetes therapy. |
| 1/2008-present | <b>Research mentor</b> , supervised four Undergraduate Research Opportunity Scholars (UROPs) from different departments at MIT : Chemical Engineering, Material Science and Engineering, Biomedical Engineering and Biology  |
| 5/2009-8/2009  | <b>Research mentor</b> , supervised Xiao Chen’s summer research UROP proposal which won the MIT-UROP Howard Hughes Medical Institute summer fellowship to conduct research in the laboratory of Professor Robert Langer  |
| 9/2011-5/2012  | <b>Teaching certificate program participant</b> , attended a series of monthly workshops at MIT on teaching techniques to enhance student-teacher communication.   |
| 9/2009-12/2009 | <b>Graduate Teaching Assistant</b> in the Department of Chemical Engineering, MIT, assisted Prof. Gregory Rutledge and Dr Barry Johnston in an undergraduate course “Introduction to Chemical Engineering”.  |

## **COMMUNITY and OUTREACH ACTIVITIES**

- 3/2012-4/2012     ***Clinical Preceptorship Participant***, shadowed Dr John D'Elia at the Joslin Diabetes Center, Harvard Medical School to observe clinical care of patients with diabetes and kidney failure.
- 9/2011             ***Abstract reviewer***, evaluated student abstracts for the Annual Biomedical Research Conference for Minority Student (ABRCMS) in St Louis, Missouri, 2011
- 10/2011           ***Graduate Career Panelist***, advised undergrad students in the MIT Society of Asian Engineers and Scientists on graduate career paths.
- 2008-2011         ***Volunteer***, contributed to set-up of experiment demonstration and gave lab tours to high school students visiting the laboratory of Professor Langer at MIT.
- 7/2006-7/2007    ***Chemistry teacher/volunteer*** at a Singapore high school, Victoria Junior College